Engineering Journal

Fourth Quarter 2019 | Volume 56, No. 4

Smarter. Stronger. Steel.

187 Simplified Method to Determine the Effect of Detailing on Cross-Frame Forces
Jawad H. Gull and Atorod Azizinamini

201 Simplified Transformative Approaches for Evaluating the Criticality of Fracture in Steel Members
Robert J. Connor

211 Empirical Formulation for Compressive Capacity of Gusset Plates
Meisam Safari Gorji and J.J. Roger Cheng

227 Steel Structures Research Update
Advances in Design with Hollow Structural Steel Members
Judy Liu

Engineering Journal

American Institute of Steel Construction

Dedicated to the development and improvement of steel construction, through the interchange of ideas, experiences and data.

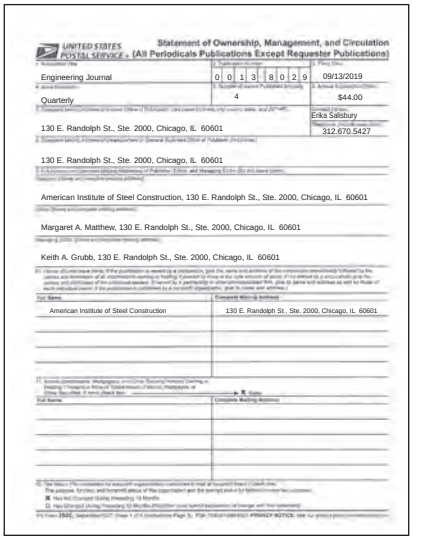

Statement of Ownership, Management, and Circulation
(All Periodicals Publications Except Requester Publications)

Engineering Journal | 0 0 1 3 8 0 2 9 | 09/13/2019
Quarterly | 4 | $44.00
130 E. Randolph St., Ste. 2000, Chicago, IL 60601 | Erika Salisbury | 312.670.5427
130 E. Randolph St., Ste. 2000, Chicago, IL 60601
American Institute of Steel Construction, 130 E. Randolph St., Ste. 2000, Chicago, IL 60601
Margaret A. Matthew, 130 E. Randolph St., Ste. 2000, Chicago, IL 60601
Keith A. Grubb, 130 E. Randolph St., Ste. 2000, Chicago, IL 60601
American Institute of Steel Construction | 130 E. Randolph St., Ste. 2000, Chicago, IL 60601
X None
X Has Not Changed During Preceding 12 Months

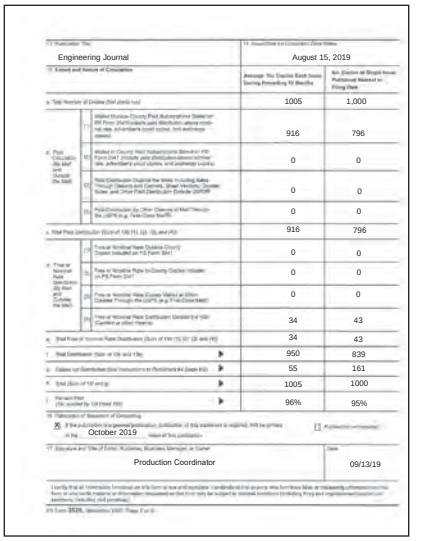

Engineering Journal | August 15, 2019

	Average No. Copies Each Issue During Preceding 12 Months	No. Copies of Single Issue Published Nearest to Filing Date
a. Total Number of Online Copies	1005	1,000
b. Paid Circulation (By Mail and Outside the Mail)	916	796
c. Total Paid Distribution	916	796
d. Free or Nominal Rate Distribution	34	43
e. Total Free or Nominal Rate Distribution	34	43
f. Total Distribution	950	839
g. Copies not Distributed	55	161
h. Total	1005	1000
i. Percent Paid	96%	95%

October 2019

Production Coordinator | 09/13/19

Engineering Journal (ISSN 0013-8029) is published quarterly. Subscriptions: Members: one subscription, $40 per year, included in dues; Additional Member Subscriptions: $40 per year. Non-Members U.S.: $160 per year. Foreign (Canada and Mexico): Members $80 per year. Non-Members $160 per year. Published by the American Institute of Steel Construction at 130 E Randolph Street, Suite 2000, Chicago, IL 60601.

Periodicals postage paid at Chicago, IL and additional mailing offices. **Postmaster:** Send address changes to *Engineering Journal* in care of the American Institute of Steel Construction, 130 E Randolph Street, Suite 2000, Chicago, IL 60601.

Subscriptions: subscriptions@aisc.org, 312.670.2400

Archives: Search at **aisc.org/ej**. Article downloads are free for current members and are avaialable for a nominal fee for non-members.

Simplified Method to Determine the Effect of Detailing on Cross-Frame Forces

JAWAD H. GULL and ATOROD AZIZINAMINI

ABSTRACT

There are several issues that necessitate the use of steel I-girder bridges with skewed supports. Due to skew supports, the axis of rotation of bearing line cross-frames is not in line with the axis of rotation of girders, and connection points of intermediate cross-frames are either at different elevations or undergo different deflections. The consequence of this behavior is that the cross-frames fit between the girders at one loading stage and do not fit between the girders at other loading stages, depending on the detailing method used to detail the cross-frames. Additional structural responses, henceforth called lack-of-fit effects, are developed when cross-frames do not fit between the girders. These lack-of-fit effects can be estimated by different methods of analysis for different detailing methods. In addition to lack-of-fit effects, fit-up forces are required to fit the cross-frames between their connections to the girder during erection, for the total dead load (TDL) fit detailing method. Methods of analysis to estimate fit-up forces are not available.

The objective of this paper is to introduce different methods that can be used to calculate lack-of-fit effects for the steel dead load (SDL) fit detailing method at the TDL stage and the TDL fit detailing method at the SDL stage. A comparison of different methods is done to recommend a single simplified method of analysis that can be used to calculate lack-of-fit effects for both the SDL fit and TDL fit detailing methods with reasonable accuracy. Analysis methods are proposed to estimate the fit-up forces. The main conclusion of this research is that improved 2D grid analysis can be used to estimate lack-of-fit effects for both the TDL fit and SDL fit detailing methods and can also be used to determine fit-up forces for connecting girders and cross-frames detailed with TDL fit.

Keywords: skew, steel bridges, detailing methods, structural response, analysis methods, guidelines.

INTRODUCTION

Although the uses of support lines that are perpendicular to the longitudinal axis of a bridge are highly desirable, there are several issues that necessitate the use of systems with skewed supports, including geometrical constraints of intersecting roadways, geological restrictions of the terrain surrounding the bridge, and other factors. The effects of the skewed supports lead to interactions between adjacent girders and the bracing that can result in significant torsional deformations of steel bridges during construction.

Earlier studies have reported several problems in straight skewed steel bridges during both girder erection and placement of the concrete bridge deck. These problems include excessive twist of the girders, uplift at the support locations, development of flange lateral bending stresses, and difficulty fitting the cross-frames during erection (Grunauer, 2011; Ozgur, 2011; White et al., 2012; Norton et al., 2003; Ahmadi and Henney, 2005). These problems are generally associated with the detailing method used for the girders and cross-frames. In steel dead load (SDL) fit, the cross-frames are detailed to fit to the girders in their ideally plumb, as-deflected positions under the bridge SDL that is load at the completion of the erection. SDL fit is generally used to reduce the forces required to install cross-frames in the field when girders are supported on their self-weight. In total dead load (TDL) fit, the cross-frames are detailed to fit to the girders in their ideally plumb, as-deflected positions under the bridge TDL, that is, dead load at completion of a bridge.

Different methods of analysis that are commonly used for steel bridges with skewed supports include improved 2D grid analysis (GA), traditional 2D GA, and 3D finite element method (FEM) analysis (Grunauer, 2011; Ozgur, 2011; White et al., 2012; AASHTO/NSBA, 2011; Linzell et al., 2010). Currently, 2D GA can be used for the SDL fit detailing method only, and a 3D FEM analysis with initial strains in the cross-frames is required for the TDL fit detailing method.

The objective of this paper is to introduce different methods that can be used to calculate lack-of-fit effect for the SDL fit detailing method at the total dead load stage and the TDL fit detailing method at the steel dead load stage. A comparison of different methods is done to recommend a single simplified method of analysis that can be used to calculate lack-of-fit effects for both the SDL fit and TDL fit

Jawad H. Gull, PhD, PE, Senior Structural Engineer, WSP USA, Lincoln, Neb. Email: jawad.gull@wsp.com

Atorod Azizinamini, PhD, PE, Professor and Chair, Department of Civil and Environmental Engineering, Florida International University, Miami, Fla. Email: aazizina@fiu.edu (corresponding)

Paper No. 2017-20R

detailing methods with reasonable accuracy. The simplified analysis method is further utilized to calculate fit-up forces.

DESCRIPTION OF STRUCTURES USED FOR COMPARISON OF METHODS ANALYSIS

Three straight-skewed, simply supported, I-girder bridges having different levels of skew are selected for consideration in this study. All three bridges have girders and cross-frames designed with Grade 50 steel having a modulus of elasticity of 29,000 ksi.

Bridge A is an extreme case of straight-skew bridges and was used to show extreme skew effects in previous studies (Grunauer, 2011; Ozgur, 2011; White et al., 2012). Bridge A has 300-ft-long by 144-in.-deep girders simply supported on 70.4º skewed supports. The girders of Bridge A are braced with X-type cross-frames containing L6×6×1 angles. The bridge uses staggered cross-frames at 22-ft spacing between nine girders at 9.25 ft center-to-center spacing. Framing plans and sizes of the web and flanges of the bridges studied are shown in Figure 1.

Bridge B is another highly skewed bridge, however

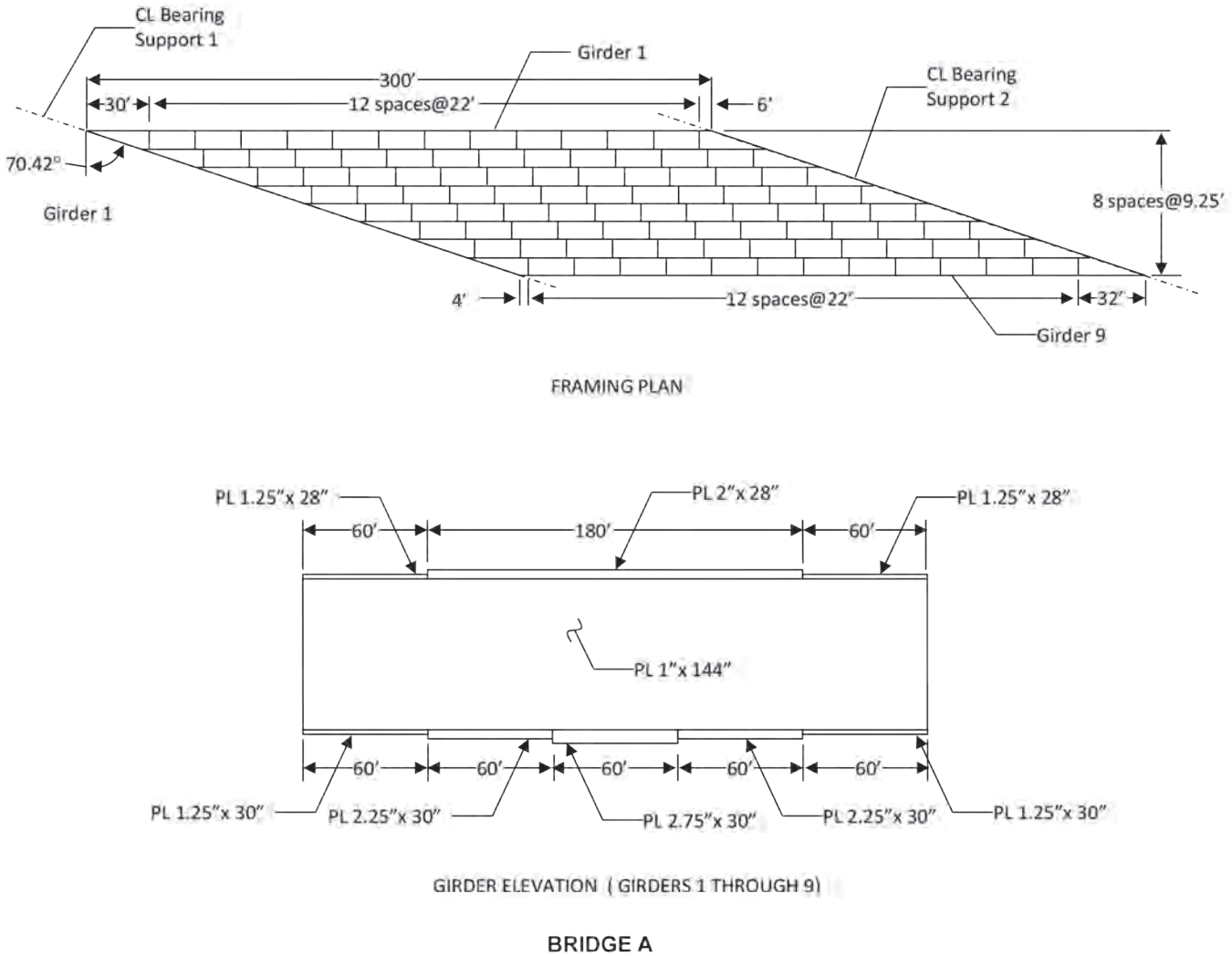

Fig. 1. Framing plan and girder sizes of Bridge A.

the skewed effects in Bridge B are smaller compared to Bridge A. Bridge B has 266-ft-long by 120.5-in.-deep girders simply supported on 62.6º skewed supports. The girders of Bridge B are braced with X-type cross-frames containing L6×6×½ angles. The bridge uses cross-frames at 16-ft spacing between eight girders at 7.26-ft center-to-center spacing. Framing plans and sizes of the web and flanges of the bridges studied are shown in Figure 2.

Bridge C has 150-ft-long by 56.1-in.-deep girders simply supported on 70.0º skewed supports. The girders of Bridge C are braced with X-type cross-frames containing L6×3½×5⁄16 angles. The bridge uses cross-frames at 21-ft spacing between four girders at 8-ft center-to-center spacing. Framing plans and sizes of the web and flanges of the bridges studied are shown in Figure 3.

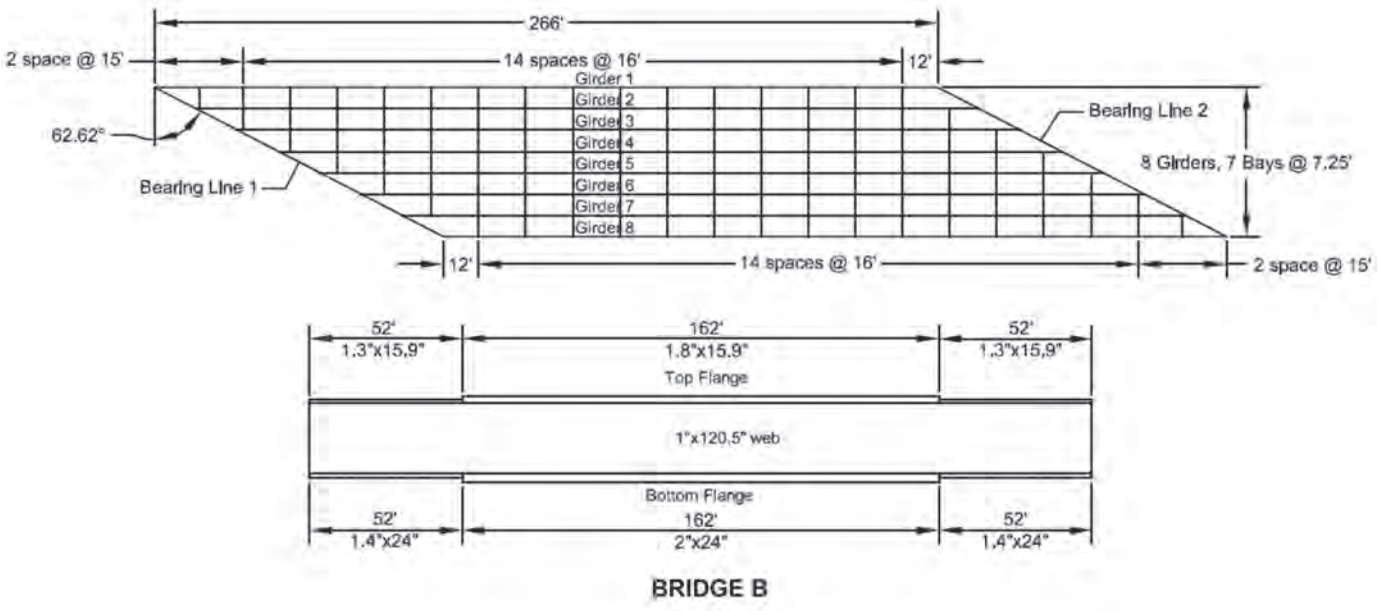

Fig. 2. Framing plan and girder sizes of Bridge B.

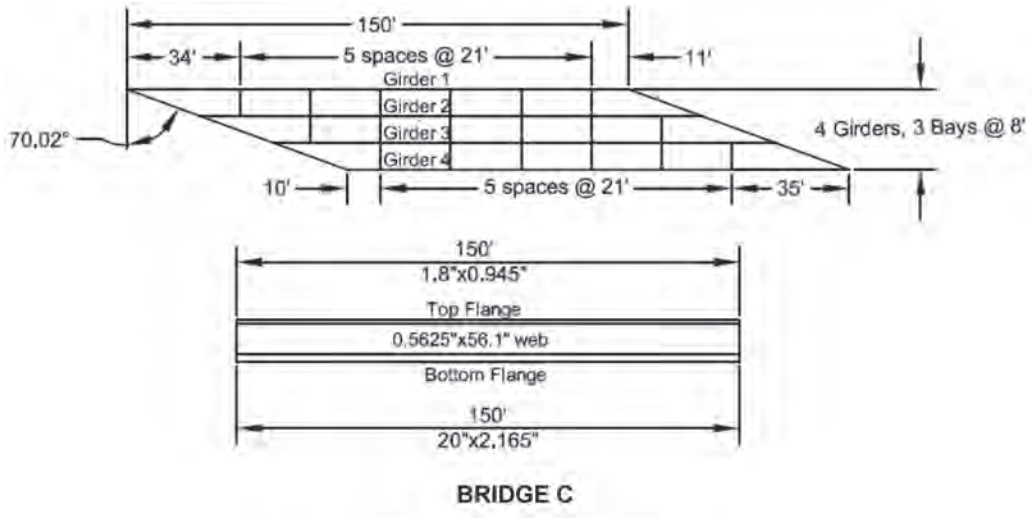

Fig. 3. Framing plan and girder sizes of Bridge C.

SDL FIT DETAILING METHOD

Methods of Analysis

Before discussing different structural responses of skewed steel girder bridges, it is important to discuss different methods of analysis that are used for the calculation of these responses. These methods of analysis are discussed at length in NCHRP 725 (White et al., 2012). A summary is provided here.

1D Line Girder Analysis

In 1D line girder analysis (LGA), the girders are analyzed as line elements without any cross-frame attached to them. In this paper, 1D LGA refers to a line elements model of the bridge girders only.

2D Grid Analysis

In this paper, 2D grid analysis (GA) refers to a modeling technique in which each node has six degrees of freedom (three translations and three rotations), but the entire structural model of the bridge is in a single horizontal plane. This paper uses two types of 2D GA: simplified methods that are used by some commercial programs, hereafter referred at as traditional 2D GA, and an improved 2D GA recommended in (White et al., 2012).

The torsional stiffness of the girders is estimated by the St. Venant term using the torsional constant, J, in traditional 2D GA. In the improved 2D GA, the torsional stiffness of the girder is modeled by using an equivalent torsional constant, J_{eq}, that considers both the St. Venant and warping terms in the calculation of the torsional stiffness. A detailed expression for obtaining J_{eq} for I-sections is given in the literature (Ahmed and Weisberger, 1996) and presented here in Equations 1 and 2. Equation 1 is based upon the assumption that both ends of the unbraced length, L_b, are fixed, while Equation 2 is based upon the assumption that one end of the unbraced length is fixed and the other is pinned.

$$J_{eq(fx-fx)} = J\left\{1-\frac{\sinh(pL_b)}{pL_b}+\frac{[\cosh(pL_b)-1]^2}{pL_b\sinh(pL_b)}\right\}^{-1} \quad (1)$$

$$J_{eq(fx-pin)} = J\left[1-\frac{\sinh(pL_b)}{pL_b\cosh(pL_b)}\right]^{-1} \quad (2)$$

where

$$p=\sqrt{\frac{GJ}{EC_w}}$$

G is the modulus of rigidity and can be approximated by $G=\frac{E}{2(1+\nu)}$, E is the modulus of elasticity, ν is Poisson's ratio, and C_w is the warping constant.

Cross-frames are modeled using a beam element with a moment of inertia, I_{eq}, that matches the flexural stiffness of the truss representation of the cross-frame. The beam also has a cross-sectional area, A_{eq}, that matches the axial stiffness of the cross-frame system. The traditional 2D GA uses the Euler Bernoulli beam stiffness matrix, whereas the improved 2D GA employed here uses an equivalent beam stiffness that matches the stiffness of a truss idealization of the cross-frames exactly within their plane. Detailed derivations and expressions for these stiffness matrices are provided in Grunauer (2011) and White et al. (2012).

It should be noted that in the SDL fit detailing method, the lack-of-fit effects such as layovers, component of deflection due to lack-of-fit, cross-frame forces, component of reactions due to lack of fit, and flange lateral bending stress due to skew effects are of interest after placement of the wet concrete. Therefore, to carry out an SDL fit analysis using the 2D grid analysis, a complete model of the structure is constructed with cross-frames attached to the girders followed by activating the concrete dead load.

3D Finite Element Analysis

At the research stage, different three-dimensional FEM models were analyzed using ANSYS (ANSYS, 2009). Three-dimensional finite element analysis (3D FEM) can be used with different levels of modeling techniques. For example, in a 3D FEM, the flanges can be modeled using either beam elements or shell elements with or without bearing pads. Three-dimensional FEM analyses carried out as a part of NCHRP 725 modeled the flanges using beam elements without bearing pads. In this study, flanges are modeled using shell elements with a bearing pad model. The bearing pads were modeled with solid element of ANSYS (ANSYS, 2009) using an equivalent modulus of elasticity of 10 ksi.

Three-dimensional FEM for the SDL fit detailing method can be accomplished by following the same steps used for 2D GA.

Comparison of Different Methods of Analysis

Different methods of analysis discussed in the preceding sections are used to evaluate lack-of-fit effects for the SDL fit detailing method at the TDL stage. These lack-of-fit effects include layovers, component of deflection due to lack of fit, component of reaction due to lack of fit, flange lateral bending stress, and cross-frame forces. Table 1 shows maximum values of lack-of-fit effects; each lack-of-fit effect is obtained from different methods of analysis and compared to recommend a method of analysis for calculating the lack-of-fit effects. Detailed comparison of the results is provided in research reports by Gull and Azizinamini (2014a, 2014b).

The lack-of-fit effects compared in Table 1 are layovers; component of vertical deflection due to lack of fit, D_{Y2};

Table 1. Comparison of Lack-of-Fit Effects from Different Methods of Analysis—SDL Fit at TDL Stage									
	Absolute Maximum Value of Lack-of-Fit Effect								
	Bridge A			Bridge B			Bridge C		
Lack-of-Fit Effect	3D FEM	2D GA Imp	2D GA Trd	3D FEM	2D GA Imp	2D GA Trd	3D FEM	2D GA Imp	2D GA Trd
Layovers (in.)	2.5	2.3	2.6	1.7	1.8	1.8	1.7	1.8	1.9
D_{Y2} (in.)	2.1	2.4	0.3	0.6	0.7	0.6	1.0	1.0	0.8
R_{Y2} (kips)	278	427	7	56.8	66.5	54.5	17.9	21.6	18.1
f_l (ksi)	14.0	35.9	0.3	2.2	3.6	0.2	2.2	5.1	1.1
Cross-frame forces (kips)	96	193	3	28.9	37.0	36.3	14.9	18.7	17.1
Note: 2D GA Imp = improved 2D grid analysis and 2D GA Trd = traditional 2D grid analysis.									

component of vertical reaction due to lack of fit, R_{Y2}; flange lateral bending stress, f_l; and cross-frame forces. D_{Y2} can computed by subtracting vertical deflection of isolated girder under certain dead load from the vertical deflection of bridge frame (girder and cross-frames connected) under the same dead load. Essentially, D_{Y2} is the component of the deflection caused by interaction of the cross-frames and girder and is directly impacted by the detailing methods. Similarly, R_{Y2} can be computed by subtracting the vertical reaction of the isolated girder under a certain dead load from the vertical reaction of the bridge frame (girder and cross-frames connected) under the same dead load. Essentially, R_{Y2} is the component of the reaction caused by the interaction of the cross-frames and girder and is directly impacted by the detailing methods.

Traditional 2D GA provides poor estimates of lack-of-fit effects for Bridge A and good estimates of lack-of-fit effects for Bridge B, except f_l as shown in Table 1. This is because of the staggered framing used in Bridge A compared to the straight framing used in Bridge B. In staggered framing, a cross-frame connects only two girders and forces in the cross-frame in the adjacent bays must be transferred through the girders. In contiguous framing, forces can be transferred directly from the cross-frames in adjacent bays. Therefore, in staggered framing, lack-of-fit effects are dependent on the torsional stiffness of the independent girders. Because traditional 2D GA does not model the torsional stiffness of the independent girders, in the case of staggered framing Bridge A, the lack-of-fit affects are not estimated correctly by traditional 2D GA. In contiguous framing, cross-frames in a contiguous line can directly transfer the forces among each other without relying on torsional stiffness of the girders. Therefore, lack-of-fit effects (except for f_l) are not affected by torsional stiffness of the independent girders.

Note that Bridge A is a parametric bridge and has been designed to maximize the skew effects. Therefore, the R_{Y2} for Bridge A is exceptionally large along with some other lack-of-fit effects that have unusual values for this bridge.

TDL FIT DETAILING METHOD

Methods of Analysis

Different methods of analysis can be used to calculate lack-of-fit effects for the TDL fit detailing method at the SDL stage. These methods are:

- Reversing 2D GA results for the SDL fit.
- 3D FEM using initial strains.
- 3D FEM using Birth and Death cross-frames.

The following sections provide a discussion on each method.

Reversing 2D GA Results for the SDL Fit

Recent study has shown that the lack-of-fit effects for the TDL fit detailing method at the SDL stage are equal and opposite to the lack-of-fit effects for the SDL fit detailing method at the TDL stage (Gull et al., 2017; Gull, 2014). Lack-of-fit effects for the SDL fit detailing method at the TDL stage can be obtained from grid analysis and reversing their sign shall give the lack-of-fit effects for the TDL fit detailing method at the SDL stage.

3D FEM Using Initial Strains

In this procedure, initial strains are used to model lack of fit at the SDL stage for the TDL fit detailing method. The configurations of cross-frames and girders to calculate the initial strain are shown in Figure 4 for the intermediate cross-frames perpendicular to web and in Figure 5 for the cross-frame parallel to skew. Configuration 1 represents a real situation in which cross-frames do not fit between the girders at the SDL stage for the TDL fit detailing method. Configuration 2 represents an imaginary condition in which cross-frames are deformed to make the connections that were not established in Configuration 1. Configuration 2 is an imaginary high-energy configuration of the system.

Once the system can establish equilibrium it attains its lowest energy state. After equilibrium is established, the system has real configuration of steel framing after attaching the cross-frame for the TDL fit detailing method at the SDL stage.

The initial strain, $\varepsilon_{initial}$, in any cross-frame member can be calculated using the following formula:

$$\varepsilon_{Initial} = \frac{L_1 - L_2}{L_2}$$

where L_1 is the length of the cross-frame member in Configuration 1 and L_2 is the length of the cross-frame member in Configuration 2.

The two configurations of the cross-frames are shown in Figure 4, for the cross-frame that are perpendicular to web and in Figure 5 for the cross-frames parallel to skew. The length of the cross-frame members that are perpendicular to the girder web in Configuration 1 as shown in Figure 4 can be calculated as follows:

$$L_{TC_1} = L_{BC_1} = S$$

$$L_{D1_1} = L_{D2_1} = \sqrt{S^2 + h_b{}^2}$$

where L_{TC_1}, L_{BC_1}, L_{D1_1}, L_{D2_1} are, respectively, lengths of top chord (TC), bottom chord (BC), diagonal 1 (D1), and diagonal 2 (D2) members of the cross-frame in Configuration 1; S is the spacing between the girders; and h_b is the height of bracing.

Similarly, the length of the cross-frame members that are perpendicular to the web in Configuration 2 of Figure 4 can be calculated as follows:

$$L_{TC_2} = L_{BC_2} = \sqrt{S^2 + \Delta^2}$$

$$L_{D1_2} = \sqrt{S^2 + (h_b - \Delta)^2}$$

$$L_{D2_2} = \sqrt{S^2 + (h_b + \Delta)^2}$$

where L_{TC_2}, L_{BC_2}, L_{D1_2}, L_{D2_2} are lengths of TC, BC, D1, and D2 members of the cross-frame in Configuration 2, respectively.

Here, Δ is the difference in elevation of the girders'

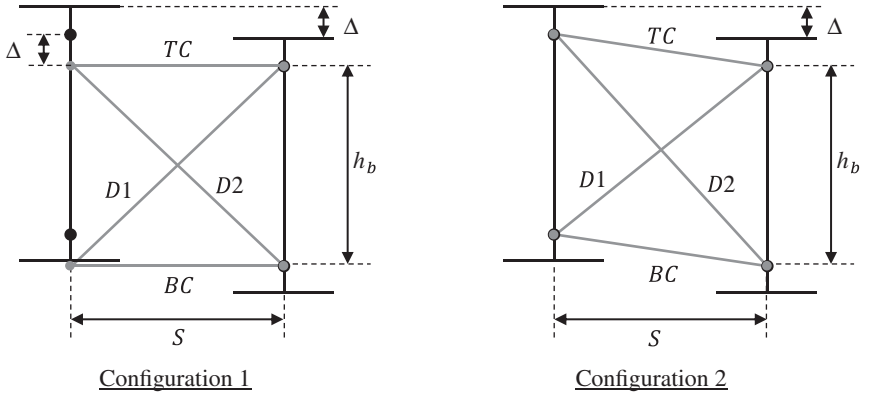

Fig. 4. Configurations to calculate initial strain in the cross-frames that are perpendicular to girder web.

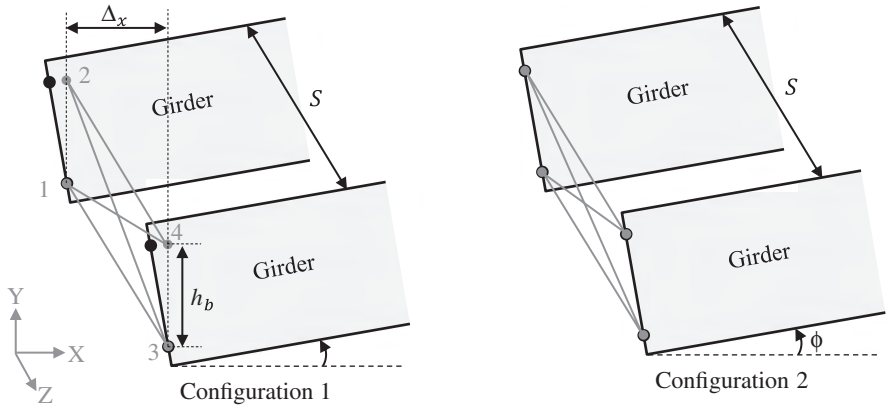

Fig. 5. Configurations to calculate initial strain in the cross-frames that are parallel to skew.

section connected by the cross-frame and can be obtained from the concrete dead load camber calculated from LGA or isolated girder analysis (IGA). It is worth noting that Δ is obtained from the concrete dead load camber calculated from deflection of the system of girders and cross-frames attached together in NCHRP 725 (White et al., 2012). This is an incorrect way of calculating Δ for the TDL fit detailing method at the SDL stage as explained elsewhere (Gull et al., 2017; Gull, 2014).

It should be noted that Δ is the difference in elevation of girders to calculate the initial strains that will simulate lack of fit due to concrete dead load and is different from the real value of Δ that will exist between the girders at the SDL stage.

Lack of fit in the cross-frames that are parallel to the skew supports occurs due to major axis bending rotation of the girder section as shown in Figure 5. Figure 5 illustrates the configuration of the cross-frames parallel to the skewed support at the bearing lines, however, the intermediate cross-frames parallel to skew have similar configurations. Configuration 1 in Figure 5 shows that the cross-frame does not fit between the girders due to major axis bending rotation, ϕ, of their ends. In configuration 2, the cross-frame is deformed to establish the connections as described previously for the cross-frames perpendicular to the girder web.

The length of the cross-frame members that are parallel to the skew supports in Configuration 1 shown in Figure 5 can be calculated as follows:

$$L_{TC_1} = L_{BC_1} = \sqrt{\Delta_x{}^2 + S^2}$$

$$L_{D1_1} = L_{D2_1} = \sqrt{\Delta_x{}^2 + h_b{}^2 + S^2}$$

Neglecting the displacement in the *y*-direction of the connection points and taking $\sin\theta \cong \theta$, the length of the cross-frame members that are parallel to the skew supports in Configuration 2 can be determined as follows:

$$L_{TC_2} = L_{BC_2} = \sqrt{\Delta_x{}^2 + S^2}$$

$$L_{D1_2} = \sqrt{(\Delta_x - \phi.h_b)^2 + h_b{}^2 + S^2}$$

$$L_{D2_2} = \sqrt{(\Delta_x + \phi.h_b)^2 + h_b{}^2 + S^2}$$

and

$$\Delta_x = S \times \tan\theta$$

where, θ is the skew angle and ϕ is the major axis bending rotation due to concrete dead load at the location of the cross-frame; ϕ is positive (counterclockwise) for the bearing line having Girder 1 at the acute corner and is negative (clockwise) for the bearing line having Girder 1 at the obtuse corner.

To get SDL configuration for the TDL fit detailing method, a complete model of the bridge is built with cross-frames attached to the girders. A value of initial strain is assigned to each cross-frame member that can be calculated based on location and orientation of the cross-frame and type of the cross-frame member. Once initial strains are assigned to all the cross-frame members, static analysis is run without applying any external load. In the static analysis, the cross-frame members expand or contract, depending on the initial strain value, and establish equilibrium with the girders. Once equilibrium is established, the steel framing of the bridge achieves its stable lowest possible energy configuration. The geometry of the bridge obtained after the equilibrium is established represents bridge geometry at the SDL stage for the TDL fit detailing method.

3D FEM Using Birth and Death Cross-Frames

Lack of fit at the SDL stage for the TDL fit detailing method can also be simulated by using Birth and Death options for the cross-frame elements.

In the TDL fit detailing method, cross-frames fit between the girders after application of the concrete dead load. Therefore, in this analysis, concrete dead load is applied on the girders to deflect the girders to a position where cross-frames fit between them. Once the girders are deflected by concrete dead load, the cross-frames are made alive. After that, concrete dead load is removed to get the SDL responses for the TDL fit detailing method.

Three-dimensional FEM using Birth and Death cross-frames is a two-step FEM analysis after completing the bridge geometry with cross-frames attached.

Step 1. All the cross-frame elements are killed (using the EKILL command in ANSYS), and the concrete dead load is applied as shown in Figure 6.

Step 2. After the concrete dead load has deflected the girders, all the cross-frame elements are made alive (using EALIVE command in ANSYS), and the concrete dead load is removed (made zero), as shown in Figure 7.

At the completion of step 2, the SDL configuration of bridge framing is obtained for the TDL fit detailing method.

It is worth noting that the Birth and Death method does not involve laborious calculation of initial strain for every single cross-frame member and gives the same results as the method of initial strains.

The next section includes a detailed comparison of different responses obtained from different methods of analysis.

Comparison of Different Methods of Analysis

Different lack-of-fit effects such as layovers; component of deflection due to lack of fit, D_{Y2}; component of reaction due to lack of fit, R_{Y2}; flange lateral bending stress, f_l; and cross-frame forces are compared for different methods of analysis

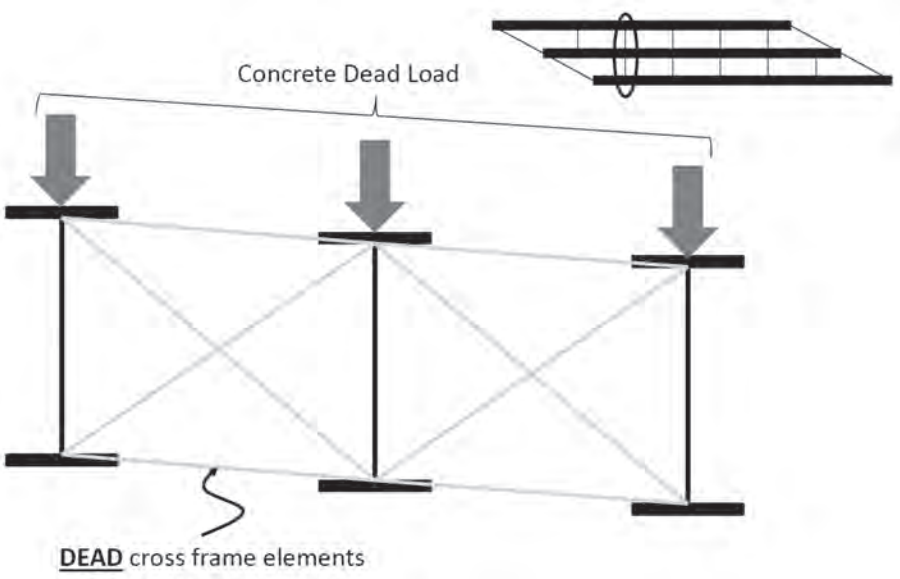

Fig. 6. Application of concrete dead load on girders after killing cross-frame elements.

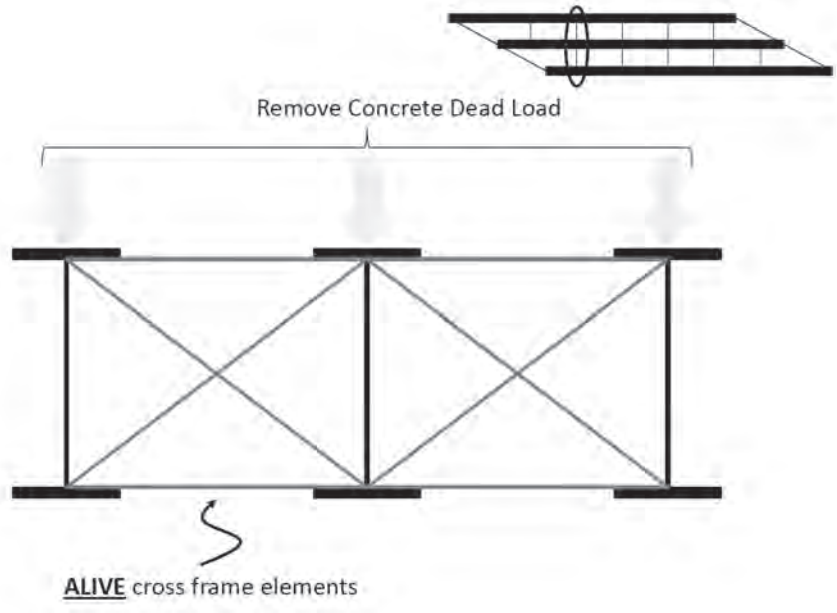

Fig. 7. Removal of concrete dead load from girders after making cross-frame elements alive.

Table 2. Comparison of Lack-of-Fit Effects from Different Methods of Analysis—TDL Fit at SDL Stage									
	Absolute Maximum Value of Lack-of-Fit Effect								
	Bridge A			Bridge B			Bridge C		
Lack-of-Fit Effect	3D FEM InStr	3D FEM B&D	2D GA Rev	3D FEM InStr	3D FEM B&D	2D GA Rev	3D FEM InStr	3D FEM B&D	2D GA Rev
Layovers (in.)	2.5	2.5	2.3	1.7	1.7	1.8	1.6	1.6	1.8
D_{Y2} (in.)	2.1	2.1	2.4	0.6	0.6	0.7	1.0	1.0	1.0
R_{Y2} (kips)	279	279	427	58	57	67	18	18	22
f_l (ksi)	13.9	14.0	35.9	2.2	2.2	3.6	2.1	2.1	5.1
Cross-frame forces (kips)	98	98	193	30	29	37	16	15	19

Notes: 3D FEM InStr = 3D FEM analysis by using initial strains.
3D FEM B&D = 3D FEM analysis using the Birth and Death elements.
2D GA Rev = results obtained by reversing the results of improved 2D grid analysis.

in the TDL fit detailing method at the SDL stage. Three-dimensional FEM analysis using initial strains and 3D FEM analysis using Birth and Death cross-frame element gives almost the same estimates of different lack-of-fit effects for Bridge A and Bridge B as shown in Table 2. Reversing the improved 2D GA results obtained for the SDL fit detailing method at the TDL stage gives conservative estimates of lack-of-fit effects for the TDL fit detailing method at the SDL stage. Bridge A, which has staggered framing, has a higher overestimation of lack-of-fit effects by the improved 2D grid analysis compared to overestimation of the lack-of-fit effects for Bridge B and Bridge C that use contiguous framing. Reasonable estimates of lack-of-fit effects are obtained by reversing the improved 2D GA for Bridge B and Bridge C. Bridge A uses staggered framing with a small stagger distance that results in a small unbraced length and overestimation of torsional stiffness of the girder, which consequently results in overestimation of lack-of-fit effects. Detailed comparison of the results is provided in research reports by Gull and Azizinamini (2014a, 2014b).

Fit-Up Forces

In the TDL fit detailing method, the cross-frames are detailed to fit between the girders at the TDL stage. Therefore, these cross-frames do not fit between the girders at the SDL stage or during the erection of steel framing. To fit the cross-frames detailed with the TDL fit detailing method between the girders at the SDL stage or during erection, a force is required to move the girders into a position where the cross-frames can be attached. The girders are both twisted and moved in a vertical direction to fit the cross-frames between the girders. This is accomplished by the application of horizontal and vertical forces at the top and bottom of the girders, henceforth referred to as fit-up forces. In theory, four fit-up forces are required to move a girder for attaching the cross-frames: two vertical forces acting on the top and bottom of the girder, F_y^T *and* F_y^B, and two lateral forces acting on the top and bottom of the girder, F_z^T *and* F_z^B, as shown in Figure 8.

Knowledge of the fit-up forces allows the bridge steel erector to make arrangements for application of the fit-up force. High fit-up forces are not desirable because these high forces may require special equipment and could slow down construction of the skew bridges.

Proposed Methods of Calculating Fit-Up Forces

Two methods are proposed to calculate the fit-up forces required to fit the cross-frames detailed with the TDL fit detailing method between the girders during erection:

- Cross-frame forces method.
- 3D erection simulation method.

The cross-frame forces method requires less effort and is

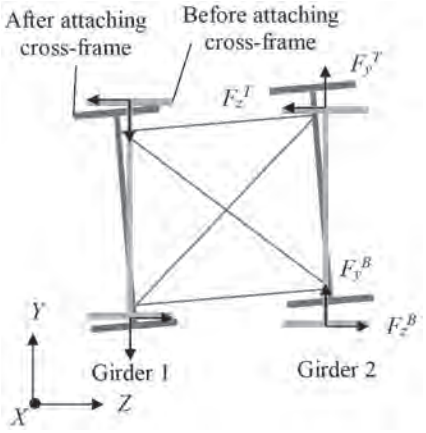

Fig. 8. Fit-up forces required to attach the cross-frames to the girders.

less accurate compared to the 3D erection simulation method, which is more accurate but requires more effort.

The following sections provide details of each method.

Cross-Frame Forces Method

Cross-frame forces at the SDL stage for the TDL fit detailing method are indicative of the fit-up forces. This is because the cross-frames are holding the girders into the twisted positions or are responsible for the lack-of-fit. Recent research (Gull et al., 2017; Gull 2014) has shown that cross-frame forces for the TDL fit detailing method are equal and opposite to the cross-frame forces at the TDL stage for the SDL fit detailing method. Therefore, cross-frame forces for the TDL fit detailing method at the SDL stage can be obtained by reversing the sign of the cross-frame forces for the SDL fit detailing method at the TDL stage. Cross-frame forces for the SDL fit detailing method at the TDL stage can be obtained from improved 2D grid analysis (2D GA), thereby avoiding the use of 3D finite element FEM analysis.

Once cross-frame forces are obtained, they are resolved into vertical and lateral components at the connection points as shown in Figure 9. The fit-up forces in the vertical direction, F_y, and the lateral direction, F_z, at a connection point can be calculated by resolving the cross-frame forces into vertical and lateral components at the connection. For example, Equations 3 and 4 can be used to calculate fit-up forces at the top of Girder 2.

$$F_y^T = -F_{D1}\sin\theta \tag{3}$$

$$F_y^T = -F_{TC} - F_{D1}\cos\theta \tag{4}$$

where, F_{BC}, F_{TC}, F_{D1} and F_{D2} are forces in the bottom chord, top chord, diagonal 1 and diagonal 2 members of the cross-frames, respectively.

Three-Dimensional Erection Simulation Method

Three-dimensional erection simulation attempts to mimic the erection of steel framing in practice. In this simulation, the cross-frames are erected one by one following a particular erection sequence similar to the erection of a real bridge in practice. It is important to note that with the erection of cross-frames detailed with the TDL fit detailing method, both stiffness and geometry of the bridge framing change continually. The change in bridge geometry is considered in erection simulation by updating the geometry after creating each cross-frame element. The change in stiffness of the framing is automatically considered in the erection simulation by the creation of cross-frame elements.

A step-by-step procedure for the erection simulation is described here:

- FEM model of girders cambered using line girder analysis/isolated girder analysis is completed.
- Initial strains (INSTRN) are calculated for a cross-frame to be erected. The initial strains are obtained from the lengths of cross-frame members and the lack-of-fit (the distance between the cross-frame connection holes and girder connection holes). Each cross-frame member is assigned a value of INSTRN as shown in Figure 10.
- After assigning INSTRN to each cross-frame member, static analysis is run to get the cross-frame forces in the erected cross-frame. Fit-up forces are obtained from the cross-frame forces obtained as explained earlier.
- Once the fit-up forces are obtained for the erected cross-frame, the initial strains in the next cross-frame are calculated based on updated geometry of the bridge. The procedure is repeated until all cross-frames are erected.

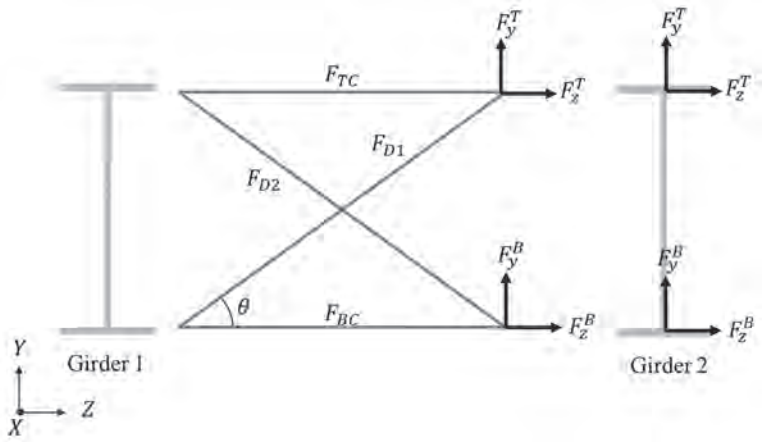

Fig. 9. Fit-up forces by resolving cross-frame forces at connection points.

Bridge girders are generally elastic during the erection of steel framing. The final deflected geometry of elastic girders is not affected by attaching cross-frames one by one or by attaching all of the cross-frames at once. Therefore, the geometry of girders at the end of erection simulation (attaching cross-frames one by one) should be same as the geometry of girders attaching cross-frames all at once. Comparison of the geometry of the girders (layovers and girder elevations) at the end of the erection simulation (attaching cross-frames one by one) to the geometry of the girders attaching cross-frames all at once is shown in Figure 11 for Girder 4 of Bridge C. As indicated by Figure 11, attaching the cross-frames either all at once or one by one results in the identical final geometry (layovers and girder elevations) of Girder 4 of Bridge C. Results shown in Figure 11 provide evidence that erection simulation is working properly. Similar results were obtained for other girders of Bridge C, as well as Bridge A and Bridge B.

An alternative approach to 3D erection simulation can be to use the Birth and Death option with cross-frame elements and evaluate cross-frame forces for the TDL fit detailing method at the SDL stage. The details for carrying out analysis using the Birth and Death option with cross-frame elements were provided earlier. Once the cross-frame forces are obtained, the fit-up forces can be calculated by resolving the cross-frame forces in the horizontal and vertical

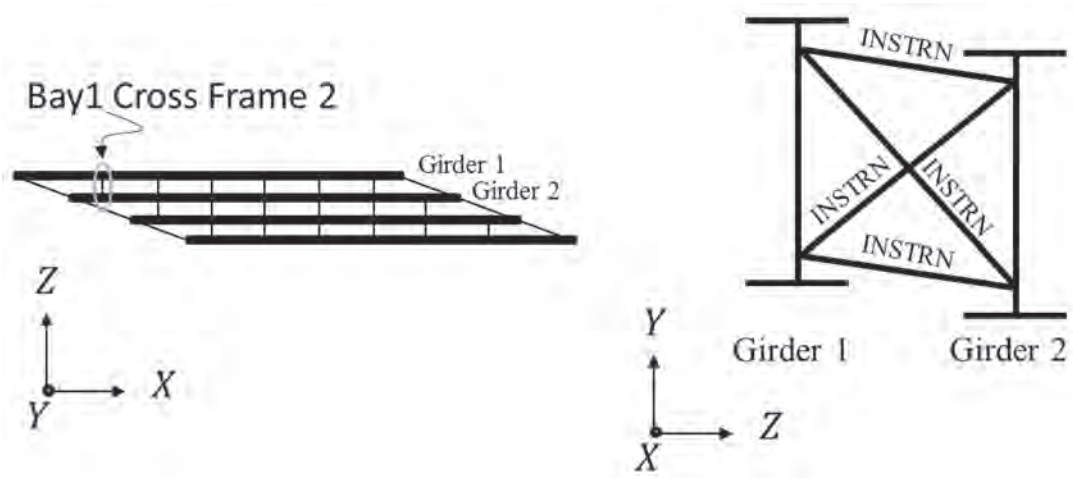

Fig. 10. Steps followed to calculate fit-up forces in erection simulation.

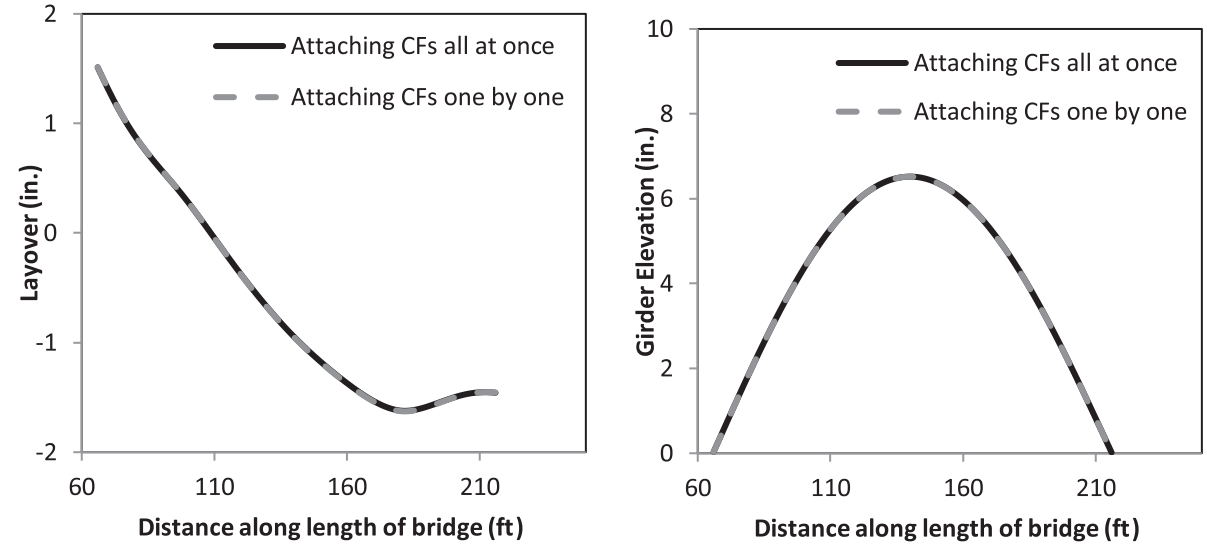

Note: CFs = cross-frames.

Fig. 11. Geometry of Girder 4 of Bridge C after completion of erection.

direction as explained earlier. However, in this case, all the cross-frames are erected at once, and an erection sequence cannot be followed for erecting cross-frames one by one.

Discussion and Comparison of Fit-Up Forces

As discussed earlier, erection of a cross-frame requires both lateral and vertical forces at the top and bottom (F_z^T, F_z^B, F_y^T, F_y^B) to move the girders into a position where connections can be made between the cross-frame and the girders. Comparison of these fit-up forces obtained from the cross-frame force method and the erection simulation method is shown in Figures 12 and 13 for Girder 3 of Bridge C for erecting cross-frames in Bay 3. The results of the erection simulation method discussed in this section are obtained following Erection Sequence 1. The following observation can be made from by inspecting the data presented in Figures 12 and 13.

- Lateral fit-up forces at the top and bottom are in opposite directions, indicating that the girder is required to be twisted to make the connections between a cross-frame and the girders.
- Vertical fit-up forces for the top and bottom are generally in the same direction, indicating that the girder needs to be moved up or down to make a connection between a cross-frame and the girders.
- Both lateral and vertical fit-up forces are relatively high for the first intermediate cross-frame because (1) the distance between the cross-frame and the connection point is largest for this cross-frame, and (2) the girders are very stiff near the supports and require more force for deflection and twisting.
- The highest fit-up force calculated from the cross-frame force method is in good agreement with the highest fit-up force calculated from the erection simulation method.

Typically, the erector is interested in knowing the maximum level of fit-up force required to fit the cross-frames detailed with the TDL fit detailing method between the girders during the erection of a steel bridge. Therefore, the absolute maximum fit-up force in both the vertical and lateral directions is obtained from different methods of analysis for Bridge A, Bridge B, and Bridge C as shown in Table 3. The fit-up forces calculated from cross-frame forces method (obtained from improved 2D GA) are in close agreement with the fit-up forces obtained from the erection simulation method, except for Bridge A. For Bridge A, the cross-frame forces method overestimates the fit-up forces because the cross-frame forces are overestimated by improved 2D GA for this bridge. The overestimation of cross-frame forces by improved 2D GA for Bridge A was discussed earlier. It is also worth noting from Table 3 that Bridge A has a very large magnitude of fit-up forces that will require significant amount of jacking of girders in the field to install the cross-frame; therefore, this bridge should be detailed for SDL fit.

In summary, cross-frame forces obtained from improved 2D GA can be used to estimate fit-up forces required for the TDL fit detailing method at the erection stage.

SUMMARY AND CONCLUSIONS

For the SDL fit detailing method, performance of improved and traditional 2D GA is different for different framing options as follows:

- For bridges with contiguous cross-frames, traditional 2D GA gives reasonable estimates of all responses, except for flange lateral bending stress, and improved 2D GA gives reasonable estimates of all responses.
- For bridges with staggered cross-frames, traditional 2D GA gives erroneous estimates of all the responses, and improved 2D GA gives reasonable estimates of all responses. However, when the stagger distance is small, J_{eq} in improved 2D GA has a very high value, resulting in overestimation of lack-of-fit effects.

Lack-of-fit effects for the TDL fit detailing method at the SDL stage obtained from a method of initial strain shows a very good agreement with the lack-of-fit effects obtained from the method of Birth and Death cross-frames elements. Reversing improved 2D GA results for the SDL fit detailing method at the TDL stage also gives reasonable estimates of the lack-of-fit effects for the TDL fit detailing method at the SDL stage.

The fit-up forces should be considered by the designer as required in the AASHTO LRFD design specification. Designers need to specify the load stage for which the cross-frames should be detailed. The designer needs to consider the effect of the fit and specify the maximum fit-up required in the field to install cross-frames for TDL fit. This paper provides a simplified method to estimate the maximum fit-up forces.

Although layovers do not have any known effect on the strength of girders, they cause additional rotation in the girders and should be considered in the bearing design for SDL fit. For TDL fit, the layovers appear only at the temporary SDL stage and are not significant at the TDL stage.

Two different methods are introduced to evaluate the fit-up forces that are required to erect the framing of a skew bridge: cross-frame forces method and 3D erection simulation method.

It has been shown that cross-frame forces evaluated from improved 2D GA can be used to estimate the fit-up forces required to fit the cross-frames, detailed with the TDL fit detailing method between the girders during erection of a steel bridge.

Table 3. Absolute Maximum Fit-Up Force from Different Methods				
	Absolute Maximum Fit-Up Force (kips)			
	Lateral		Vertical	
Bridges	CF Forces	Erection Simulation	CF Forces	Erection Simulation
Bridge A	230	180	104	131
Bridge B	41	38	28	30
Bridge C	25	29	7	10

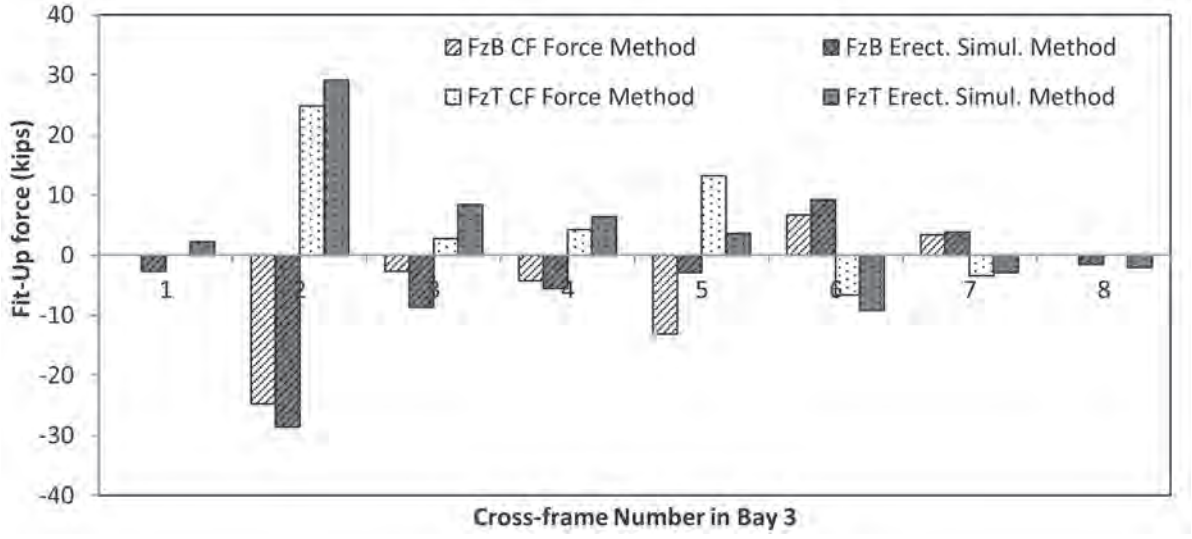

Fig. 12. Lateral fit-up forces applied on Girder 3 of Bridge C for erecting cross-frames in Bay 3.

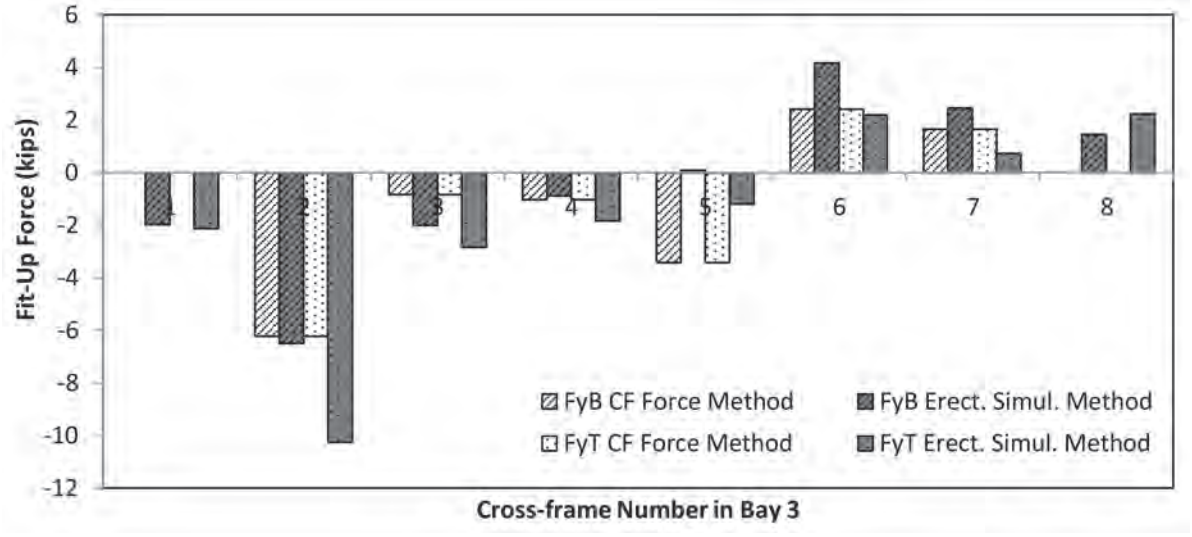

Fig. 13. Vertical fit-up forces applied on Girder 3 of Bridge C for erecting cross-frames in Bay 3.

Improved 2D GA can be used to estimate the lack-of-fit effects for both the TDL fit and the SDL fit detailing methods.

ACKNOWLEDGMENTS

The authors would like to acknowledge the support of the Florida Department of Transportation (FDOT) for providing funding and holding technical discussions on various issues related to skewed bridges. The authors would like to thank Dennis Golabek, Jerry Hocking, Ben Goldsberry, Robert Robertson, and Sam Fallaha for their input. The project was led by the second author.

The recommendations made in this paper reflect the opinions of the authors and do not necessarily reflect those of the sponsor.

REFERENCES

AASHTO/NSBA (2011), *G 13.1 Guidelines for Steel Girder Bridge Analysis*, AASHTO/NSBA Steel Bridge Collaboration.

Ahmadi, A.K. and Henney, R. (2005), "Lessons Learned from the Construction of a Sharply Skewed, Two-Span, Steel Multi-Girder Bridge," *Proceedings of the International Bridge Conference,* International Bridge Conference, Pittsburgh, Pa., pp. 8–13.

Ahmed, M. and Weisberger, F. (1996), "Torsion Constant for Matrix Analysis of Structures Including Warping Effect," *International Journal of Solids and Structures*, Vol. 33, No. 3, pp. 361–374.

ANSYS (2009), "ANSYS Release 12.1 UP20091102," *Analysis Software*. Copyright 2009 SAS IP, ANSYS Inc.

Gull, J.H., (2014), *Comprehending Performance of Cross-Frames in Skewed Straight Steel I-Girder Bridges,* Doctoral Thesis, Florida International University, Miami, Fla.

Gull, J.H. and Azizinamini, A. (2014a), *Steel Framing Strategies for Highly Skewed Bridges to Reduce/Eliminate Distortion Near Skewed Supports*, Final Research Report, Florida Department of Transportation, Tallahassee, Fla.

Gull, J.H. and Azizinamini, A. (2014b), *Steel Plate Girder Diaphragm and Cross Bracing Loads*, Final Research Report, Florida Department of Transportation, Tallahassee, Fla.

Gull, J.H., Azizinamini, A., and Helwig, T.A. (2017), "Comparison of Detailing Methods for Straight Skewed Steel I-Girder Bridges," *Journal of Constructional Steel Research*, Vol. 136, pp. 24–34.

Grunauer, T.A. (2011), *Influence of Bracing Systems on the Behavior of Curved and Skewed Steel I-Girder Bridges during Construction*, Doctoral Thesis, Georgia Institute of Technology, Atlanta, Ga.

Linzell, D., Chen, C., Sharafbayani, M., Seo, J., Nevling, D., Jaissa-Ard, T. (2010), *Guidelines for Analyzing Curved and Skewed Bridges and Designing Them for Construction*, Research Report, Pennsylvania Department of Transportation, Harrisburg, Pa.

Norton, E., Linzell, D., and Laman, J. (2003), "Examination of the Response of a Skewed Steel Bridge Superstructure during Deck Placement," *Journal of the Transportation Research Board,* Vol. 1,845, pp. 66–75.

Ozgur, C. (2011), *Influence of Cross-Frame Detailing on Curved and Skewed Steel I-Girder Bridges,* Doctoral Thesis, Georgia Institute of Technology, Atlanta, Ga.

White, D.W., Coletti, D., Chavel, B.W., Sanchez, A., Ozgur, C., Chong, J.M. (2012), *NCHRP 725: Guidelines for Analysis Methods and Construction Engineering of Curved and Skewed Steel Girder Bridges*, NCHRP and NSBA.

Transformative Approaches for Evaluating the Criticality of Fracture in Steel Members

ROBERT J. CONNOR

ABSTRACT

There has been considerable research and interest in the topic of fracture-critical members (FCM) during the past decade. As a result, the entire concept of what constitutes an FCM is being revisited, and many long-standing ideas and opinions related to this classification of members are being shown to be overly conservative. Significant advances in the understanding of fracture mechanics, material and structural behavior, fatigue crack initiation, fatigue crack growth, fabrication technology, and inspection technology have allowed other industries to address fracture—or, more importantly, control of fracture—in a more integrated manner. After years of research, new stand-alone AASHTO guide specifications that give codified direction on how to perform 3D system analysis to verify system redundancy, as well as guide specifications to evaluate internal member-level redundancy of mechanically fastened built-up members for both new and old bridges, have been proposed. Additional research demonstrating the benefits of exploiting the improved toughness of modern high-performance steel (HPS) grades has been completed. Through these advances, it is now possible to create an integrated fracture control plan (FCP) combining the original intent of the 1978 FCP with modern materials, design, fabrication, and inspection methodologies. Further, an integrated FCP provides economic benefits and improved safety to owners by allowing for a better allocation of resources by setting inspection intervals and scope based on sound engineering rather than based simply on the calendar. In summary, an integrated FCP encompassing material, design, fabrication, and inspection can ensure fracture is no more likely than any other limit state, ultimately allowing for a better allocation of owner resources and increased steel bridge safety. This paper summarizes some of the recent advancements related to the topic of the FCM and provides a suggested approach to providing more rational treatment of such members without compromising reliability.

Keywords: fracture critical members, steel bridges.

INTRODUCTION

Despite the perception surrounding bridges classified as having fracture critical members (FCM), there is actually very little evidence that would suggest such bridges have been more unreliable than other types of steel bridges. In fact, the term *fracture critical* conjures up images of certain failure to many. In contrast, truss bridges, which are classified as having FCM, also have what the author refers to as BCM, or "buckling critical members." However, nonredundant compression members in trusses exist without any additional concern regarding their criticality, nor do they require any special fabrication or in-service inspection. What is interesting is that it is often much more difficult to redistribute compression forces into other members. For example, a compression member, when subject to tension, will generally be able to carry such forces without becoming unstable, presuming there is enough steel in the cross section. However, a slender tension member will likely buckle should compression forces be applied following failure of a nearby compression member.

Nevertheless, as an industry, there is little concern that nonredundant compression members will suddenly fail in an unstable buckling mode. The reason is simple: The bridge engineering community as a whole believes the results of many years of experimental research and analysis. Thus, such members are not treated differently in design or during in-service inspection whether they are redundant or not. For some reason, the same is not true for tension members. While isolated failures of tension members have occurred, the bridge engineering community is very reluctant to accept the decades of research and advancements that have been made in the understanding of fracture mechanics, the availability of steels with superior toughness, advances in fabrication methods, and nondestructive testing. This paper attempts to demonstrate that it is time to move forward and accept integrated fracture control plan concepts that have been widely accepted and proven to be reliable in the aerospace and pipeline industries.

CURRENT VIEWS ON FCM

It is the observation of the author that the majority of the papers published since 2007 that are related to fatigue and fractures issues or structural health monitoring (SHM) in highway bridges begin by citing the I-35W collapse, which

Robert J. Connor, Professor of Civil Engineering and Director S-BRITE Center, Lyles School of Civil Engineering, Purdue University, West Lafayette, Ind. Email: rconnor@purdue.edu

Paper No. 2018-12

occurred in August 2007. The papers typically go on to recite how the I-35W bridge was a "fracture critical bridge." (*It is noted that there is no such thing as a fracture critical bridge per the AASHTO Specifications, but only fracture-critical members.*) The obvious problem with such papers is that the failure of the I-35W bridge had nothing to do with the fact that the bridge had members classified as FCM (NTSB, 2008). Rather, the failure was due to a serious error that occurred during design that resulted in undersized gusset plates at several locations on the trusses. It is also worth noting that the bridge was built circa 1967, long before (1) the implementation of the modern fatigue design provisions for highway bridges and (2) the implementation of the AASHTO/AWS D1.5 fracture control plan (FCP).

Another common failure cited in papers is of course the Silver Bridge (aka the Point Pleasant Bridge). This bridge opened in 1928 and collapsed in 1967 (NTSB, 1968). Despite the fact the bridge carried traffic for nearly 40 years, the sudden failure of one of the eyebars led to a sudden catastrophic failure of the bridge, resulting in the loss of 46 lives. While it is true that the failure of the Silver Bridge was due to brittle fracture of a nonredundant eyebar, it cannot be overlooked that the circa 1928 high-strength steel used in the eyebar was extremely brittle and would never be permitted for use in highway bridges built since at least the mid-1980s.

In fact, a brief literature review will quickly reveal that the "classic" brittle fractures often cited have two things in common. First, they have only occurred in bridges designed and fabricated prior to the implementation of the AASHTO/AWS D1.5 FCP and modern AASHTO fatigue design provisions (AWS, 2015; AASHTO, 2017). Second, with the exception of the Silver Bridge (eyebar failure) and Mianus River Bridge (pin/hanger failure) (NTSB, 1968, 1984), which both utilized fundamental design approaches that have been completely abandoned by the U.S. bridge industry, all other cases where an FCM has fractured have not resulted in catastrophic collapse. Interestingly, the obvious implication of the first point is that bridges designed and fabricated *after* the implementation of these provisions are highly unlikely to experience a brittle fracture. Considering the FCP and modern fatigue provisions have been in place for more than 40 years with no noted failures suggests they are working quite well. The second point also illustrates that although failure of an FCM would be expected to possibly result in collapse of a portion of or the entire structure, history seems to prove otherwise in all but those systems that are truly nonredundant and, as stated, no longer utilized.

The preceding statement—that the lack of observed failures is due to the improvements in design, materials, and fabrication—is often questioned. Some believe that the lack of in-service fractures is primarily due to significant efforts spent on in-service inspections. While inspections are certainly important, the evidence does not suggest this is the primary reason for the lack of failures. In fact, with the exception of the Mianus River Bridge, fractures are almost always traced back to a flaw that could not be detected with the naked eye. For example, the fracture in the Silver Bridge was triggered by a small crack in the eyebar that could never be detected visually (NTSB, 1968). Other fractures, such as those observed in the Hoan Bridge, U.S. 422 Bridge, and others deemed to be due to so-called constraint induced fracture (CIF), were all triggered in the absence of any detectible fatigue crack (Fisher et al., 2001; Kaufman et al., 2004; Ellis and Connor, 2013). Hence, the evidence suggests that the improved performance is primarily due to the efforts of the FCP, better detailing, and better design rather than hands-on inspection. This is not to say inspection is not needed nor that it has not prevented failures in general. Rather, the role of inspection as the major preventer of sudden brittle fractures (in contrast with failures say due to corrosion) appears to be questionable.

Unfortunately, despite the excellent service record of FCM, even those designed and fabricated *prior* to the modern FCP and fatigue design provisions, many in the bridge industry seem to be of the opinion we are still building steel bridges no differently than we did in, say, the 1950s or even earlier. In effect, the perception is when the "FCM" term is evoked, it is thought that somehow, although the structure was designed and built in 2018, it is no less likely to experience a brittle fracture than a bridge built in, say, 1958, and it will, in fact, most likely experience a brittle fracture during its service life.

WHAT HAS CHANGED SINCE THE INTRODUCTION OF THE FCP?

Table 1 presents a short summary of a few high-profile examples where brittle fractures have been observed due to a variety of issues. These specific structures highlight some of the more common reasons fractures have been observed. (For example, poor weld quality, either during fabrication or during repair of a weld, is often a concern.) The use of plug welds or other fracture susceptible details (e.g., CIF details) has been identified to be the cause of several brittle fractures.

Table 1 clearly illustrates several important points. The most obvious is that all of the bridges were designed and fabricated prior to the introduction of the AASHTO/AWS D1.5 FCP introduced in the mid-1980s and the modern fatigue design specifications introduced about 1974. (It is noted that the FCP was first introduced in 1978 as an AASHTO Guide Specification, and many bridges were built to these provisions as early as this.) The details or materials that were utilized in these bridges are no longer permitted, as noted in Table 1. Another observation is related to all the bridges with FCMs that are *not* listed in the table—in other

Table 1. Summary of High-Profile Cases of Brittle Fractures							
Bridge	**Cause**	**Approximate Year of Destruction or Construction**	**Fabricated to FCP?**	**Designed for Fatigue?**	**Are these Details or Materials Permitted Today?**	**Would Field Inspection Have Prevented?**	**Did the Bridge Collapse?**
Silver Bridge (W. Va.)	Brittle high-strength steel	1928	No	No	No	No	Yes
Neville Island I-79 (Pa.)	Poor repair weld procedures	1970	No	No	No	No	No
Lafayette St. (Minn.)	Poor quality intersecting weld	1966	No	No	No	Maybe	No
Hoan Bridge (Wis.)	Constraint-induced fracture (CIF)	1968	No	No	No	No	No
Delaware River Truss (Pa.)	Misdrilled holes filled with weld	1954	No	No	No	No	No

words, those in which a failure has not occurred. The majority of these bridges were put into service before the profession considered the fatigue or fracture limit states in design, prior to mandatory Charpy V-notch (CVN) requirements, and prior to the introduction of much more stringent shop welding procedures. These bridges, which by far exceed the number in which individual problems have been observed, have been carrying traffic safely for decades. As such, this again emphasizes that the overall historical performance of steel bridges with FCMs has been excellent, despite a few isolated failures. Also as stated, when failures have occurred, the outcome has rarely been catastrophic.

PERFORMANCE OF THE "MODERN" STEEL BRIDGE

Prior to discussing how modern steel bridges have performed over the years, one must first define what is meant by the term *modern* steel bridge. In the context of this paper, the author refers to modern steel bridges as those that were designed and fabricated after certain criteria were in place. In the context of FCM, those built after this date will typically possess the following characteristics:

1. Meet modern CVN requirements.
2. Be fabricated to the AASHTO/AWS D1.5 FCP.
3. Be designed using the nominal stress range approach for fatigue.
4. Are unlikely to possess details susceptible to distortion-induced fatigue cracking, which is responsible for most cracking observed in highway bridges.

In general, bridges built after about 1985 meet all of the above criteria, while none of the bridges listed in Table 1 do. More recent work related to CIF would add a fifth criterion to the list. Around 2012, requirements were added to the AASHTO LRFD Bridge Design Specifications to prevent the use of details susceptible to this form of fracture. Fortunately, most if not all girder bridges in the United States that possess CIF susceptible details on FCM designed prior to this date have been retrofit in order to prevent this form of fracture. Thus, this fifth criterion is met by most welded FCM.

History has shown that steel bridges that meet these criteria are extremely unlikely to be susceptible to brittle fracture. In fact, the author has not been able to identify any FCM that have met the preceding criteria in which a brittle fracture has occurred. Thus, the improvements made in the design and fabrication of FCM have resulted in steel members that are highly reliable in terms of the fatigue and fracture limit state.

Despite these major improvements, there has been no relief regarding the 24-month hands-on in-service inspection of bridges that contain FCM. As is well known, these inspections consume considerable resources and place risk on both the inspectors and the public. What this means is that an FCM built in 1955 is treated identically to one in a bridge built in 2015 when it comes to in-service inspection. Obviously, this makes little sense. If a member is deemed to be an FCM, then it shall be inspected every 24 months regardless of any other criteria, period. Shorter intervals are sometimes introduced due to concerns over the condition of the member, but again, these are arbitrary. In some ways, it is not surprising that the inspection interval has not changed

as improvements have been made because the current maximum 24-month interval for FCM inspection was not based on engineering. In other words, improvements in fabrication, material, design, and so forth cannot easily be used to justify a change in the interval because these were not the criteria used to set the original interval in the first place.

The one-size-fits-all approach may also have been somewhat reasonable nearly 50 years ago when the National Bridge Inspection Standards (NBIS) were introduced because the average age of many of the bridges in the United States was much younger. Consider that since the U.S. Interstate system was initiated in 1956, most bridges were still relatively new in the early to mid-1970s. Hence, inspections that were calendar based could be justified in a way that is similar to what is done in the health care industry. For example, younger individuals visit the doctor for brief routine checkups at calendar-based intervals of, say, every 12 months or longer. However, for older individuals, say, 70 years or older, routine checkups are often much more frequent, and in most cases, there are specific health issues that require special attention and time. In fact, the suggestion that an 18-year-old should require or *be required* to receive the same health care as a 70-year-old illustrates the error in the current approaches to bridge inspection.

Another very important issue that is commonly overlooked is related to the fact that other countries also have bridges that contain members that would be classified as FCM in the United States. However, international scanning tours for bridge management and fabrication have noted that Europe does not have special policies for FCM with regard to how such members are inspected in service (Connor et al., 2005; Verma, 2003). While other countries inspect their inventory, they do not impose additional and arbitrary inspection criteria on such members. Interestingly, the failure rate of these members is no greater than that observed in the United States from the data that can be found (Verma, 2003). In other words, it appears that the extra in-service inspection efforts mandated by law in the United States for FCM have not resulted in any significant improvement in reliability in modern steel bridges.

Finally, when performing any type of inspection, one must consider the concept of probability of detection (POD). POD studies are used to determine the probability of detecting a defect in a specified component under the inspection conditions and procedures provided or commonly used. In the case of highway bridges, this is almost always performed through a visual inspection. POD is typically expressed as a function of a quantifiable target parameter associated with the given flaw (e.g., length). While the target parameter is the single most influential factor in determining the probability of detection, it is also a function of many other physical and operational factors, including the material, geometry, flaw type, nondestructive testing (NDT) method, testing conditions, as well as the inspector and his or her certification, education, and experience (Georgio, 2006).

Probability of detection data can be analyzed as discrete data, where the response is binary (either a hit or a miss), or as continuous data, which is a signal response (tracking how close the noted size of the defect is to the actual size). Hit/miss data produces qualitative information indicating whether a flaw is present or absent.

To investigate the likelihood of detecting a fatigue crack in a steel member, a large-scale POD study was performed at Purdue University (Snyder et al., 2015). This study, believed to be the first statistically significant study of its kind focused on fatigue cracks in bridge members, revealed that the 50-50 crack length (i.e., that length with a 50% probability of an inspector hitting or missing) is on the order of 1 in. using visual inspection. Further, to achieve a POD of 90% requires cracks to be in the range of 5 in. in length. Other studies have shown similar results in terms of the overall low POD associated with visual inspection (Moore et al., 2001; Washer et al., 2014). This is not to criticize the inspection community but is simply pointing out that with limited inspection budgets, coupled with the time constraints placed on inspectors, quality will suffer. This suggests that the inspections being performed may have limited value regarding the detection of a crack that could lead to brittle fracture because it is clear that many cracks are missed. Again, the inference is that the excellent service record of modern FCM is primarily based on the improvements that have greatly decreased the likelihood of cracking and is not due to in-service inspections finding such cracks before they reach some critical size.

DEVELOPMENT OF AN INTEGRATED FRACTURE CONTROL PLAN

Considering the preceding data, it would seem that existing state-of-the-practice engineering concepts could be used to develop a strategy toward inspecting members traditionally classified as FCMs that are based on quantitative engineering principles rather than simply relying upon calendar-based approaches. Ideally, the approach would link the capability of the inspector, the strength or performance of the member, and the interval of the inspection. This would result in what is referred to as an *integrated fracture control plan*. In such an approach, the desired reliability is achieved, and deficiencies in one area (e.g., the inability to reliably find small fatigue cracks) is made up through the design of the member and/or inspection interval. Interestingly, this approach is commonly utilized in other industries, such as oil and gas and aerospace, and is a proven and effective strategy. A few examples of how an integrated fracture control plan can be achieved using different, but rational strategies follow.

Through Internal Redundancy

Mechanically fastened built-up steel members have long been perceived to be highly resistant to complete and sudden catastrophic failure due to brittle fracture. In fact, the AASHTO *Manual for Bridge Evaluation* states in the commentary for Article 7.2.1 that for evaluation of riveted members and connections, Category C, rather than Category D (which is used for design as it represents first cracking) is appropriate since "Category C more accurately represents cracking that has propagated to a critical size. This increase in fatigue life for evaluation purposes is appropriate due to the redundancy of riveted members" (AASHTO, 2016) Thus, AASHTO recognizes that the redundancy within an individual member built-up from multiple components, which provides mechanical separation of elements, can limit crack propagation across the entire member cross-section as compared to an all welded member.

While this type of redundancy was typically known to be present through anecdotal evidence, no guidance existed on how to establish if *adequate and reliable* internal redundancy is present in a given mechanically fastened built-up steel member. Due to a lack of experimental evidence or existing standards, the Federal Highway Administration (FHWA) was not able to recognize mechanically fastened built-up members as having adequate redundancy to alter the inspection rigor from that of a fracture critical inspection associated with, say, a welded member (Lwin, 2012).

Transportation Pooled Fund Project TPF-5(253), "Evaluation of Member Level Redundancy in Built-up Steel Members," was conceived and completed to address all of the critical issues related to performing a "credible" analysis to identify built-up members that have adequate internal redundancy to resist complete failure of the cross-section should one component suddenly fail (Hebdon et al., 2017a, 2017b; Lloyd, 2018). The resistance to such a failure mode is referred to as cross-boundary fracture resistance (CBFR). Through full-scale experimental testing performed in the research, it was shown that brittle fracture in one component does not propagate into the adjacent component if certain conditions are met. The member is then checked to establish if there is sufficient strength in the faulted condition under prescribed load combinations. The experimental work was furthered through fatigue testing to establish how long a member in the faulted state could survive in this damaged condition (i.e., with one component completed failed). Using this information, conservative estimates could then be made to set an appropriate inspection interval and scope to ensure a second component will not fail prior to the next inspection. The research showed that members meeting specific proportion and condition requirements can be designated as internally redundant members (IRM) that do not need to be subjected to the traditional arms-length inspection associated with FCMs. The research was recently incorporated into the AASHTO *Guide Specifications for Internal Redundancy of Mechanically-fastened Built-up Steel Members*, which was approved by the AASHTO Subcommittee on Bridges and Structures in June 2018 (AASHTO, 2018a). These specifications are applicable to both new and old steel bridge structures.

It is also important to note that the primary objective of the in-service special inspections of an IRM is to detect fully severed components and *not* to find very small fatigue cracks emanating from any one of thousands of fastener holes. Conceptually, this is illustrated in Figure 1. (It is noted that the crack must extend beyond the rivet head in order to be detected in the first place. Hence, it is implied in the current inspection strategies that the member can at least tolerate cracks on the order of a few tenths of an inch before

Fig. 1. Photographs of two different cracks in built-up members contrasting the differences in cracks that need to be detected in a traditional FCM inspection vs. those associated with an IRM.

they are detected.) The POD study cited earlier showed that it is unrealistic to assume that small cracks can be identified with a high level of reliability using traditional visual inspection techniques. In contrast, the likelihood of detecting a severed component in a built-up member, on the order of 10 in. long or more, is obviously much higher. Using the experimental data from the member testing and the data from the POD study, an integrated fracture control plan was developed for IRM as follows:

- Through rational evaluation procedures, the member can be shown to be capable of tolerating the assumed damage (i.e., an entirely failed component).
- The inspection interval is based on experimental data derived from fatigue testing of damaged girders with a safety factor incorporated in order to set a rational inspection interval based on the time required to fail a second component.
- The damage is large enough to be detected with a high level of reliability. For example, rather than trying to find a ½-in. crack emanating from any one of thousands of rivets, the inspector need only find an entirely broken component. As stated, the POD for such damage is high.

In this way, the fracture control plan is "integrated" in that the inspection interval and capability of the inspector is linked to the tolerance of the member as a function of time. The entire methodology is based on quantitative engineering and not simply a calendar-based approach. The converse is what is being done today; inspectors look for cracks that they are unlikely to find and that are not likely to be critical in the first place at an interval that is entirely arbitrary. For example, there is no calculation that shows the 24-month interval is the appropriate duration to ensure cracks are reliably found before they become critical. Obviously, the integrated FCP is a major departure from the current calendar-based approach to setting inspection intervals.

A subtle, but very important difference in the preceding approach is that the damage that is deemed critical is assumed to have occurred (i.e., fracture of a component is assumed to have occurred immediately following the previous inspection). In other words, inspectors are not randomly looking for small fatigue cracks or other damage that may not be critical, which could be located almost anywhere on the member. Rather they are searching for a specific form of damage that has been shown to be of importance based on engineering; hence, they can focus on looking for what is important.

Through System Analysis

Another form of redundancy can be exploited through the use of advanced analytical tools. In such an approach, analysis is performed in which entire FCM are assumed to have failed and the structure analyzed to establish the consequence of the failure. By definition, failure of an FCM is generally presumed to probably result in collapse of the structure or a portion thereof. However, as shown in Table 1, and based on historical experience, in the rare instances an FCM has failed, catastrophic collapse did not result. Thus, what if it could be shown that even in such a faulted condition, the structure possesses sufficient reserve capacity that it can carry some appropriate level of live load? To develop and codify the procedures to evaluate the redundancy of bridges with members traditionally designated as FCMs through 3D system analysis, NCHRP Project 12-87a was conducted (Connor et al., 2018).

While guidance on the required level of analysis is essential (e.g., nonlinear vs. linear analysis, etc.), other very important criteria must be established in order to ensure uniform evaluation procedures. For example, some critical questions arise, such as:

- What is an acceptable target reliability for a damaged structure?
- What level of live load should a faulted structure be capable of carrying?
- How should live load be positioned on the bridge?
- What criteria (service and strength) should be used to define failure?
- What is the exposure period during which the bridge should be assumed to be in the faulted state, and how does this tie into future inspection needs?

The NCHRP 12-87a project attempted to answer all of these questions. The research resulted in the AASHTO *Guide Specifications for Analysis and Identification of Fracture Critical Members and System Redundant Members*, which was approved by the AASHTO Subcommittee on Bridges and Structures in June 2018 (AASHTO, 2018b). This *Guide Specification* provides owners and engineers with a robust benchmarked analysis methodology that can be used to increase the effectiveness and efficiency of inspection in steel bridges with members traditionally classified as an FCM. These specifications are also applicable to both new and old steel bridge structures.

One significant aspect of the *Guide Specifications* is the development of new load combinations specifically intended for evaluating the performance of a steel bridge in which an FCM is assumed to be completely failed. The reliability principles used in current design and evaluation specifications were utilized to develop load combinations that capture uncertainty in load and resistance. Two new load combinations, referred to as Redundancy I and Redundancy II, were developed. Redundancy I characterizes the instant when a

primary steel tension member fails, in which the dynamic amplification of load is considered. As has been discussed, most bridges in which a brittle fracture of an FCM has occurred carried live load for some extended period of time,—in some cases, up to a few months. This observation resulted in the development of the Redundancy II load combination. This load combination characterizes the loading during an extended period of service between the occurrence of the failure and the discovery of the failure.

Other strength and serviceability requirements were also developed. If the bridge is able to satisfy these strength and serviceability requirements when subjected to the redundancy load combinations after the failure of a member previously designated as an FCM, such a member can be redesignated as a system redundant member (SRM). An SRM must still be fabricated to AASHTO/AWS D1.5, clause 12, but does not need to be subjected to hands-on inspections every 24 months.

While the level of analytical effort is admittedly considerable in some cases, one must also consider the objective of the analysis. Specifically, an engineer who performs such an evaluation is attempting to establish that if a primary tension member were to fail, the bridge either is or is not capable of (1) surviving the event while subjected to some level of live load and dynamic amplification and (2) carrying the traveling public for some extended but undefined interval. One must also recognize that for bridges satisfying the requirements of the evaluation, future hands-on inspections will not be required by law and, hence, may not be performed for quite some time. Clearly, this is a weighty responsibility and an area of bridge engineering in which the profession has virtually no experience. Thus, it is not an unreasonable request that the engineer perform some rather rigorous analysis.

However, as with any methodology, experience is gained with time, and the author believes the same will eventually be true regarding this type of system analysis. As more and more structure types are analyzed using the *Guide Specifications* described herein, the industry as a whole will begin to identify structural configurations that inherently possess considerable reserve strength, even in a severely faulted state (i.e., with one girder or tension member completely failed). Such appears to be the case with continuous-span twin tub girder bridges. Ongoing work suggests that such bridge types can be very robust when certain basic design and detailing criteria are utilized (e.g., curvature limits, span limits, required details, etc.). For example, full-depth full-width diaphragms between girders and the use of shear studs that extend above the bottom layer of deck reinforcement provide significant load redistribution capabilities when one of the tubs is assumed to have completely failed at some critical cross section. The author believes that, very soon, the industry will be able to develop simple guidelines that can be used to "prequalify" the girders of certain continuous twin tub-girder bridges as SRM and eliminate the need for complex 3D FEA.

Through Design and Material Selection

Another, possibly more forward-thinking approach to addressing the concerns associated with FCM is related to reducing the likelihood of the fracture to an extremely low level. As has been stated, for bridges fabricated after the introduction of the AASHTO/AWS FCP nearly 40 years ago, there have been no brittle fractures observed in the field. However, one must also recognize that in the past 40 years, there have been major improvements in design, understanding of fatigue and fracture, and fabrication. Further, with the introduction of HPS grades, modern steels can be economically produced that possess toughness levels much higher than the current specified minimums. Thus, it does not seem out of the question to begin to treat failure due to fracture like any other failure mode, such as ultimate strength or buckling. As discussed, bridge engineers do not become overly concerned with nonredundant compression members and identify them as BCM on plans. Such members are not required to meet more stringent out-of-straightness tolerances during fabrication, nor are they treated differently during design by using lower nominal compressive resistance than that specified. Special measurements are not required for such members during in-service inspections to establish if they have deviated from the as-built out-of-straightness or if corrosion has resulted in some minor change of the cross-section. While failure of a compression member is likely more critical than a tension member, engineers are not overly concerned with possible failure of these members when they are deemed non-redundant. The reason is simple: The bridge engineering community as a whole believes the results of many years of experimental research and analysis. There is a considerable body of work that documents the effects of geometric imperfections, residual stresses, fabrication tolerances, etc., on the behavior of compression members (Ziemian, 2010). This work has resulted in conservative approaches to economical design of such members that are also very reliable.

While isolated failures of tension members have occurred in the past, the bridge engineering community is very reluctant to accept the decades of research and advancements that have been made in the understanding of fracture mechanics, the availability of steels with superior toughness, and advances in fabrication methods and NDT. Other industries, however, have not taken the same view. For example, the aircraft industry routinely designs components using state-of-the-practice fitness-for-service (FFS) principles in which in-service inspection strategies, inspection intervals, material selection, and design are all linked to ensure a target reliability against failure/fracture. Again, that industry is utilizing an integrated approach to fracture control that has resulted in a high level of reliability associated with

air travel. The author believes that these methods are easily extended to bridge structures and, with relatively little effort, could be used to show that the fracture limit state can be treated like any other failure mode, as is routinely done for ultimate strength, buckling, etc.

As an example, consider a truss bridge in which all the connections are bolted and the lowest fatigue detail is Category B. Suppose also that the steel possesses toughness much greater than the current minimums required by ASTM A709, possibly as high as 100 ft-lb at the lowest anticipated service temperature (ASTM, 2017). Finally, assumed that during design, the members were all sized to ensure infinite fatigue life. Using basic FFS principles, it could be shown that if one were to assume some reasonable initial defect, sudden brittle fracture is less likely to occur than failure due to some other limit state, such as strength. Further, one could design the member such that the critical defect is of a size that could be reliably found during inspection. With reasonable estimates of the in-service stress range and number of cycles applied per day, one could estimate the time needed for a small initial defect to become critical. During design, it could be ensured that the time needed for such a defect to become critical is 20 to 30 years, or even more. If one were to apply a safety factor of 2, hands-on inspection would be required only every 10 to 15 years. These inspections would be based on engineering principles because the scope, depth, and interval would be based on FFS and not the calendar. These approaches are not new and have been well-vetted in other industries. Thus, it seems that applying them to certain bridge structures during design could be done to more effectively manage the inspection needs of the inventory and result in lower life-cycle costs.

SUMMARY

Over the past 40 years, the steel bridge industry has seen many improvements and changes in materials, analytical tools, design methods, and fabrication. However, the fundamental assumptions regarding the likelihood of failure and the associated consequences specifically associated with FCM have not kept up with these advancements. For example, there are basically two distinct families of FCM: those built to the modern FCP and those that are not. However, these are both treated the same regarding in-service inspection. Further, welded FCM are treated the same as those that are built up from multiple components mechanically fastened together, again with no delineation between bolted or riveted members. Finally, regardless of the overall configuration of the structure, failure of an FCM is presumed to probably result in collapse of a portion of or the entire bridge. As a result, the overall risk associated with an FCM is always high in that it is assumed they will very likely fail sometime during the life of the structure, and the consequence of the failure is high.

This paper has presented a number of significant advancements that have been made in recent decades that can be used to more rationally treat members traditionally classified as FCM and lower the perceived and actual risk associated with such members. Despite these advances and the overall excellent service record of members classified as FCM, the profession still holds an unsubstantiated perception associated with their performance. The reality is that steps that have been taken to reduce the likelihood of fracture, such as the introduction of the AASHTO/AWS FCP, have been shown to be highly effective. Other strategies can be used to show the consequence associated with a partial or complete member fracture, though highly unlikely, is also low. Lowering the likelihood of failure and/or consequence will reduce the risk associated with FCM. Using state-of-the-practice approaches—such as system analysis or exploiting internal redundancy combined with the advancements in design, fabrication, and material—the risk associated with brittle fracture can be as low or lower than failure due to other limit states. Further, explicitly considering the fracture limit state in such a way allows for the development of an integrated fracture control plan in which the inspection interval, scope, and capability of the inspector are linked to the tolerance of the member or structure as a function of time. Moving forward with an integrated fracture control plan would allow a more rational treatment of these members that is based on engineering principles rather than perception and feeling.

ACKNOWLEDGMENTS

The author is truly indebted to his colleagues and students, without whose hard work and support, he would never have had the opportunity to contribute to advancing the topic presented in this paper. More than just “colleagues and students”, he is honored to call them his “friends,” as that is what they have been to him for many, many years.

REFERENCES

AASHTO (2016), *AASHTO Manual for Bridge Evaluation*, 2nd Ed., American Associations of State Highway and Transportation Officials, Washington, D.C.

AASHTO (2017), *AASHTO LRFD Bridge Design Specifications. Transportation*, 8th Ed., American Associations of State Highway and Transportation Officials, Washington, D.C.

AASHTO (2018a), *AASHTO Guide Specifications for Internal Redundancy of Mechanically-Fastened Built-up Steel Members*, 1st Ed., American Associations of State Highway and Transportation Officials, Washington, D.C.

AASHTO (2018b), *AASHTO Guide Specifications for Analysis and Identification of Fracture Critical Members and System Redundant Members*, 1st Ed., American Associations of State Highway and Transportation Officials, Washington, D.C.

AWS (2015), *Bridge Welding Code*, AWS D1.5:2015, Miami, Fla.

ASTM (2017), "Standard Specification for Structural Steel for Bridges," ASTM A709/ A709M-17, ASTM, International, Philadelphia, Pa.

Connor, R. J., Bonachera Martin, F.J., Varma, A.H., Lai. Z., and Korkmaz, C. (2018), "Fracture-Critical System Analysis for Steel Bridges," NCHRP Report 883, National Cooperative Highway Research Program (NCHRP), Washington, D.C.

Connor, R. J., Dexter, R., and Mahmoud, H. (2005), "NCHRP Synthesis 354: Inspection and Management of Bridges with Fracture-Critical Details," Washington D.C., p. 84.

Ellis, R.M. and Connor, R.J. (2013), "Investigation and Repair of the Diefenbaker Bridge Fracture in Prince Albert, Saskatchewan," IBC Paper 13–20, *Proceedings of the 29th Annual International Bridge Conference*, Pittsburgh, Pa., June, pp. 214–224.

Fisher, J.W., Kaufmann, E.J., Wright, W., Xi, Z., Tjiang, H., Sivakumar, B., and Edberg, W. (2001), "Hoan Bridge Forensic Investigation Failure Analysis Final Report," Bethlehem, Pa.

Georgio, G.A. (2006), "Probability of Detection (PoD) Curves: Derivation, Applications and Limitations," *Health and Safety Executive*, Research Report 454.

Hebdon, M.H., Bonachera Martin, F.J., Korkmaz, C., and Connor, R.J. (2017a), Fracture Resilience of Steel Built-up Members Subjected to Flexure," *Journal of Bridge Engineering*, ASCE. doi: 10.1061/(ASCE) BE.1943-5592.0001059.

Hebdon, M.H., Bonachera Martin, F.J., Korkmaz, C., and Connor, R.J. (2017b), "Load Redistribution and Remaining Fatigue Life of Steel Built-up Members Subjected to Flexure Following a Component Failure," *Journal of Bridge Engineering*, ASCE. doi: 10.1061/(ASCE) BE.1943-5592.0001087.

Kaufman, E.J., Connor, R.J., and Fisher, J.W. (2004), "Failure Analysis of the US 422 Girder Fracture—Final Report," ATLSS Report No. 04-21, Center for Advanced Technology for Large Structural Systems, Lehigh University, Bethlehem, Pa., October.

Lloyd, J.B. (2018), "Internal Redundancy of Mechanically-Fastened Steel Built-up Axially-Loaded Members," Dissertation, Purdue University, West Lafayette, Ind.

Lwin, M. (2012), "Memorandum: Clarification of Requirements for Fracture Critical Members," Washington, D.C.

Moore, M., Phares, B., Graybeal, B., Rolander, D., and Washer, G. (2001), "Reliability of Visual Inspection for Highway Bridges," FHWA-RD-01-020, Federal Highway Administration, McLean, Va.

NTSB (1968), "Collapse of US 35 Highway Bridge Point Pleasant, West Virginia December 15, 1967," Highway Accident Report, National Transportation Safety Board, Department of Transportation, Washington, D,C.

NTSB (1984), "Collapse of a Suspend Span of Interstate Route 95 Highway Bridge over the Mianus River Greenwich Connecticut, June 28, 1983," Highway Accident Report PB84-916203, National Transportation Safety Board, Department of Transportation, Washington, D.C.

NTSB (2008), "National Transportation Safety Board. 2008. Collapse of I-35W Highway Bridge, Minneapolis, Minnesota, August 1, 2007," Highway Accident Report NTSB/ HAR-08/03, Washington, D.C.

Snyder, L.R., Whitehead, J., Connor, R.J., Lloyd, J.B. (2015), "Probability of Detection Study for Visual Inspection of Steel Bridges Volume II—Full Project Final Report SPR 3820," Joint Transportation Research Program, Indiana Department of Transportation, West Lafayette, Ind., May.

Verma, K. (2003), *Steel Bridge Fabrication Technologies in Europe and Japan,* Report FHWA-PL-01-018, Federal Highway Administration, Washington, D.C., March.

Washer, G.A., Connor, R.J., and Looton, D.W. (2014), "Performance Testing of Inspectors Implementing NDT Technologies," *Journal of the Transportation Research Record*, Vol. 2,048, pp. 107–113.

Ziemian, R.D. (2010), *Guide to Stability Design Criteria for Metal Structures*, 6th Ed., Wiley, Hoboken, N.J.

Empirical Formulation for Compressive Capacity of Gusset Plates

MEISAM SAFARI GORJI and J.J. ROGER CHENG

ABSTRACT

Gusset plates play a critical role in the behavior and stability of bracing systems and truss bridges. While the behavioral characteristics of gusset plates have been widely investigated and analysis procedures have been developed, considerable uncertainty exists in the design equations, due primarily to the complexity of stress distribution in the connection area. Current design procedures rely heavily on highly simplified approaches, which typically result in inconsistent design factor of safety for various gusset configurations and boundary conditions. In this research, a powerful genetic programming (GP) tool is employed to develop an empirical formulation for compressive capacity of corner gusset plates using a comprehensive database collected from previously published test results and test-validated finite element models. The predictive model correlates the ultimate compressive strength of gusset plates with their mechanical and geometrical properties. A comparative study is performed to evaluate the performance of the derived expression compared to the results of the well-known effective length factor method. The results indicate that the GP-based equation accurately estimates the compressive capacity of gusset plates and its prediction performance is significantly better than that of the current procedures.

Keywords: gusset plate, compressive strength, buckling.

INTRODUCTION

The behavior of gusset plates in concentrically braced frames is quite complex, especially under compression, where the ultimate capacity depends largely on the boundary conditions and plate geometry. For this reason, it is difficult to evaluate the internal stress distribution in the gusset plates and determine their compressive strength. As such, in order to analyze and design these connections, designers have conventionally employed highly simplified approaches, which typically result in inconsistent reliability for various gusset configurations and boundary conditions. Current procedures to predict the buckling capacity of gusset plates are generally based on the column analogy method, also called effective length factor method, originally proposed by Thornton (1984). According to this method, it is assumed that the compressive capacity of the gusset plate is equal to that of an imaginary rectangular column below the effective width established by a 30° stress dispersion angle (Whitmore, 1952) and an average buckling length (Figure 1). The compressive strength of this imaginary column is then determined using the column curves available in the codes assuming an effective length factor of $K = 0.65$, which corresponds to the fixed-fixed boundary condition (Thornton, 1984). While the Thornton method is based on a rational approach, several previous experimental and analytical studies have shown that this method can be conservative and inaccurate in many cases for a variety of reasons, including the following: (1) The column curves in the codes may not be appropriate for plates, (2) the out-of-plane restraint provided by the material outside the Whitmore width is neglected, (3) uncertainties exist in the value of K factor used for various gusset plate configurations and boundary conditions, and (4) the effect stress redistribution due to yielding prior to plate buckling is not appropriately captured (Dowswell, 2006). To account for the latter, Yam and Cheng (2002) proposed a modified Thornton method in which it was suggested that the effective width can be determined with a 45° stress trajectory angle instead of 30° angle.

Dowswell (2006) classified corner gusset plates into three types based on shapes and compactness and suggested an effective length factor for each category. While the suggested K values improved the estimations of compressive strength in many cases, the method still underestimates the buckling capacity of the gusset plates, especially for noncompact ones, where the mean value of test-to-predicted ratio was 3.08.

In 2009, the Federal Highway Administration (FHWA) issued a design guide for bolted and riveted gusset plates in truss bridges, where the compressive capacity of the gusset plates is determined using the early Thornton method (FHWA, 2009.) The guideline suggests several effective length factors ranging from 0.65 to 2 for various assumed

Meisam Safari Gorji, Postdoctoral Fellow, Department of Civil and Environmental Engineering, University of Alberta, Edmonton, Canada. Email: meisam.safari@ualberta.ca (corresponding)

J.J. Roger Cheng, Professor and C.W. Carry Chair in Steel Structures, Department of Civil and Environmental Engineering, University of Alberta, Edmonton, Canada. Email: roger.cheng@ualberta.ca

Paper No. 2018-14

buckling shapes and boundary conditions. However, since the ultimate compressive strength calculated using this method depends significantly on the selection of the *K* factor based on the buckling shape of the gusset, which is unknown in most cases, the estimated value is highly influenced by the engineer's judgement. While this design approach has served the profession rather well in the past, innovative solutions and design tools to achieve a more consistent factor of safety would be extremely beneficial to help facilitate the design process and possibly improve design economy.

The compressive behavior of gusset plate connections has been widely investigated by researchers in the past four decades, and a number of experimental and analytical databases were published by several researchers. These databases not only helped verify the validity of current design procedures, but also can serve as a basis for the development of new design methods in the future. A robust empirical model based on a reliable database can eliminate the highly simplified design assumptions and reduce errors in the prediction values. Such a predictive tool can be very useful as a cross check on the results of the existing methods, particularly, to examine if the new designs are consistent with the published test data. One such efficient tool is developed in this research using an advanced data mining technique called gene expression programming (GEP) (Ferreira, 2006).

RESEARCH OBJECTIVE

As mentioned previously, the primary objective of this research is to develop empirical formulations for predicting the compressive strength of corner gusset plate connections using an evolutionary computing approach. The predictive model, which is developed based on a comprehensive database collected from the available literature, is expected to provide a valuable tool for design engineers and researchers.

DATA COLLECTION

Developing a reliable empirical model requires a comprehensive database that covers most important variables and key parameters affecting the compressive strength of gusset plate connections. A large database containing 41 experimental results and 164 test-validated finite element models covering a reasonably wide range of gusset plate geometries and mechanical properties was collected from a survey of past research conducted on the subject. The majority of experimental data used in this research were the results of a comprehensive testing program carried out by the senior author and his associates at the University of Alberta (Cheng and Hu, 1987; Yam and Cheng, 1993; Rabinovitch and Cheng, 1993; Cheng et al., 1994; Nast et al., 1999). The finite element data were adopted from several previously published analytical research on gusset plates in compression. Many of the aforementioned studies have been collected in previous research (Dowswell, 2006). It should be recalled that the primary focus herein is to investigate the ultimate strength of gusset plates in which the plate buckling is the governing failure mode. Although the total number of experimental and numerical data available on the subject was larger than that considered in this research, a number of gusset plates were excluded from the database, including the finite element (FE) models with purely elastic material models and

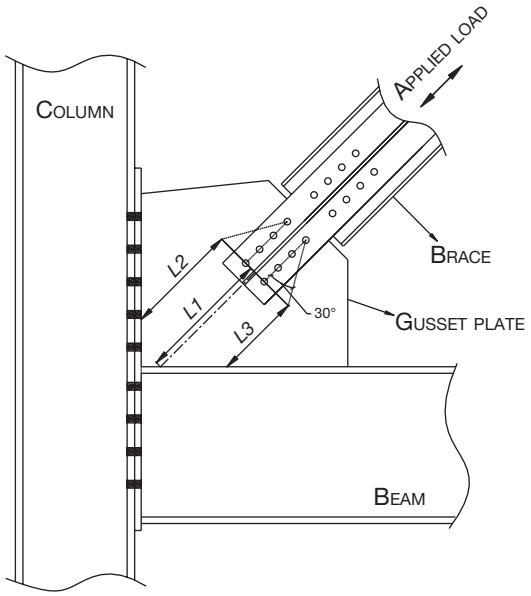

Fig. 1. Geometrical variables and effective width.

the specimens that did not fail by gusset plate buckling, as well as those with unrealistic boundary conditions. Also, specimens with loading eccentricity and stiffened gusset plates were not considered in this study. A summary of the experimental and numerical research used in this paper are described in the next sections, and the details of database are presented in the Appendix.

Experimental Data

Cheng and Hu (1987) conducted 14 experimental tests on six full-scale corner gusset plate connections to investigate their compressive behavior and buckling capacity. The main parameters studied included geometric configuration, plate thickness, eccentricity, boundary conditions, and plate reinforcement. The test specimen consisted of two plate sizes (33.5 in. by 21.7 in. and 33.5 in. by 27.6 in.) and two plate thicknesses (approximately ⅛ in. and ¼ in.) To evaluate the effects of eccentricity, additional specimens were considered in which gusset plates were attached to the brace using a single 5⁄16-in.-thick splice. All specimens were tested in compression for two separate boundary conditions, namely (1) fixed-fixed, where both the test frame and the bracing member were fixed laterally and rotationally, and (2) fixed-roller, where the brace was fixed and the test frame was allowed to move out-of-plane by using roller support. By comparing the compressive capacity of the test specimens with those calculated with Whitmore method, the authors reported that this method significantly overestimated the gusset plate ultimate strengths. This was primarily due to the fact that the governing failure mode was elastic bucking of the gusset plates.

Gross and Cheok (1988) tested three vertical brace subassemblies where the braces, columns, and connecting beam were pinned at the ends. The gusset plates' dimensions were 23 in. by 11 in. with a thickness of ¼ in. The research objectives were to study the connection behavior, the effect of eccentricity of the forces in the connection, and the influence of column orientation. All specimens experienced yielding prior to ultimate loads and failed by buckling, except one specimen that failed by tearing of the gusset plate. The researchers reported that the Thornton method with K factor of 0.65 significantly underestimated the ultimate capacity of the gusset plates achieved in the tests.

Brown (1988) experimentally tested 24 half-scale corner gusset plate connections with the main variables of study being gusset plate thickness, geometry, type, and orientation angles of bracing member. Three different gusset plate thicknesses were used with two types of bracing members, which had five different inclination angles ranging from 26° to 55°. It was reported that the majority of specimens failed by buckling of the longer free edge of the gusset plates, followed by large deflections that occurred out-of-plane.

Yam and Cheng (1993) conducted experimental tests on 19 gusset plates in compression. The primary objective was to investigate the compressive behavior and ultimate capacity of the gusset plates, where the effects of several parameters were studied, including gusset geometry, plate thickness, brace angle, and out-of-plane boundary conditions. The governing failure mode for most of the specimens was sway buckling of the gusset plate. Three of the specimens were intended to study the effects of out-of-plane loading eccentricity. The researchers also studied the effects of frame actions and reported that the presence of moments on the beam and columns had negligible effect on the buckling capacity of the gusset plates. The gusset plates generally experienced significant yielding prior to the ultimate capacity even at a load level considerably lower than that calculated using the Whitmore method. The compressive strength of the specimens was almost directly proportional to the thickness of their gusset plates.

Rabinovich and Cheng (1993) cyclically tested five full-scale corner gusset plate connections. The specimens were designed based on the concept of weak gusset plate–strong bracing members proposed by the authors, such that the input energy would be dissipated by the gusset plate rather than the bracing member itself. The study parameters included gusset plate thickness, geometry, bolt slip, and adding a free edge stiffener. The main objective was to investigate the effects of these parameters and to examine if the cyclic loading would affect the ultimate capacity of the connections. The results indicated that while the tensile capacities of the specimens were not considerably affected by the cyclic loading, the compressive capacities were significantly reduced due to load reversals. It was reported that the Thornton method conservatively estimated the compressive capacity of the unstiffened gusset plates.

Nast et al. (1999) conducted cyclic tests on four full-scale corner gusset plate specimens, two of which had free-edge stiffeners. Only one of the unstiffened gusset plates was designed to buckle under compression. The intention of the research was to study the effects of free-edge stiffeners as well as bracing member-gusset plate interaction on the cyclic behavior of gusset plates.

Chen and Chang (2012) cyclically tested six low-yield point (LYP) steel gusset plate connections that were designed following the weak gusset–strong brace concept. The researchers used free-edge stiffeners and slot-type restrainers (STR) to prevent early bucking of the gusset plates. It was shown that the gusset plates with STR exhibited similar strength in tension and compression and that adding STR resulted in improved energy dissipation capacity of the connection.

Naghipour et al. (2013) tested a single corner gusset plate with a W-shape bracing member. The thickness and dimensions of the gusset plate were 5⁄16 in. by 19.7 in. by 19.7 in., respectively. The specimen failed due to buckling of the gusset plate.

Finite Element Data

Chakrabarti (1987) used linear and nonlinear finite element models to evaluate the compressive behavior and buckling strength of eight gusset plate connections previously tested by other researchers. Of the eight specimens, only three were corner brace connections and thus are considered in this research. It was shown that the inelastic finite element models accurately captured the behavior of the specimens and that the failure was due to the inelastic buckling of the gusset plates.

Cheng et al. (1994) developed finite element models of the gusset plate specimens tested by Cheng and Hu (1987) and showed that the models could reasonably predict the buckling load of the gusset plates observed during the tests. A parametric study was then conducted to investigate the effect of a number of parameters on the compressive capacity of the gusset plates such as length and thickness of the splicing member. It was found that extending the splicing member toward the beam and column would increase the bucking capacity of the gusset plates. Also, an increase in the thickness of the splice plate would result in increased buckling strength of the gusset plate.

Walbridge et al. (1998) used the finite element method to capture the compressive behavior of the gusset plates previously tested by Yam and Cheng (1993) and Rabinovitch and Cheng (1993), followed by a comprehensive parametric study investigating several parameters, including the effects of interaction between the gusset plate and bracing member and the effects of load sequence as well as the potential of the concept of weak gusset plate–strong brace proposed by Rabinovitch and Cheng (1993).

Sheng et al. (2002) conducted a comprehensive parametric study on the compressive strength of gusset plate connections using nonlinear finite element models. The study parameters included gusset plate geometry, thickness, splice length, and connection type between splice member and the gusset plate (i.e., welded versus bolted). It was recommended that the splice member should be welded to the gusset plate rather than bolted. Also, the authors suggested that the gusset plate can be shaped according to the 30° dispersion angle so that the length of the connection between the gusset plate and the supporting members can be reduced.

Naghipour et al. (2013) studied the compressive behavior of gusset plates with test-verified FE models. The researchers attempted to capture the compressive behavior of the corner gusset plate in the buckling restrained braced (BRB) frame by incorporating a large brace section into the models such that the buckling occurred in the gusset plates. A numerical investigation was carried out that studied several key design parameters such as plate thickness, plate geometry, and connection length.

Fang et al. (2015) conducted a comprehensive numerical investigation on the compressive behavior of gusset plate connections with an emphasis on the post-buckling resistance. The primary objective of that research was to study the strength of relatively slender gusset plates commonly used in lightweight structures or in high-strength steel structures. Detailed finite element models were created and verified against eight experimental tests conducted by Yam and Cheng (1993) with good agreement. A comprehensive parametric study consisting of 108 FE models was conducted covering a wide range of parameters, including plate thickness, material properties, gusset plate thickness and dimensions, bolt spacing, and arrangements. Also, the effects of initial imperfection and material strain hardening were studied.

MODELING USING GENETIC PROGRAMMING

Genetic programming (GP), introduced by Koza (1992), is one of the most powerful machine learning techniques, which can be used to find relationships between variables in a dataset. In this technique, computer programs are encoded and evolved to solve or approximately solve problems using an evolutionary algorithm. Due to its superiority over traditional statistical models, GP has been gaining popularity among researchers in the past two decades. GP tools, which rely primarily on a valid database, have been used by a number of researchers to derive empirical predictive models for various structural engineering problems, including steel structures (e.g., Cevik, 2007a, 2007b). GP-based models can be very useful when the relationship between variables is quite complex or when mechanics-based equations become erroneous due to significant uncertainty. In this research, gene expression programming (GEP), which is an extended version of GP, is implemented to derive a relationship between compressive capacity and key properties of corner gusset plates.

Model Development

In order to develop an accurate predictive model, both geometrical variables and material properties of gusset plates were considered. A careful review of past experimental and numerical studies, as well as a sensitivity analysis of the database, revealed that the most important parameters affecting the compressive behavior of gusset plates are as follows: material yield strength, F_y; plate thickness, t; plate buckling length, L; plate cantilever length, C; connection length, L_c; and fastener distance perpendicular to the brace axis, S. The geometric variables used in the models are shown in Figure 2. It should be recognized that the compressive capacity of gusset plates is also affected by other factors, such as initial imperfection and brace inclination angle. However, because the initial imperfections for the majority of specimens were not reported and because the out-of-plumbness

of the brace (and the gusset itself) is typically unknown before fabrication, the initial imperfection was accounted for implicitly. Also, Yam and Cheng (2002) reported that the brace angle had negligible effect on the ultimate capacity of the gussets. This was also confirmed with a sensitivity analysis of the database. Figure 3 shows histograms of different variables used in developing the GEP model.

Based on the preceding discussion, the ultimate compressive capacity of the corner gusset plates was considered to be a function of six parameters as follows:

$$P_u = f(F_y, t, L, C, L_c, S) \tag{1}$$

For model development purposes, the database was randomly divided into three categories: (1) learning data set, (2) validation data set, and (3) testing data set. The learning and validation data sets, referred to as training data, were used to develop the model, and the testing data set, referred to as unseen data, was used to evaluate the performance of the model with a set of data that was not used in the modeling process. Of the 205 data sets, 143, 31, and 31 data sets were used for learning, validation, and testing, respectively. To minimize the influence of random selection, three different combinations were generated for these categories. The genetic programming algorithms were implemented in GeneXproTools software (GEPSOFT, 2013).

The most important parameters affecting the GEP predictive models are the number of programs (chromosomes), the number of terms or sub-ETs (genes), and the head size of the genes. These parameters, which determine the size, complexity, and precision of the models, were selected on the basis of trial and error and recommendation from previous researchers. It is recognized that due to the random nature of the GP algorithms, the optimum model is not typically achieved with a single run (Gandomi et al., 2011). As such, to achieve a model with minimal errors, numerous runs were carried out by varying key parameters and criteria used in the algorithms. Table 1 presents a summary of the parameters used in the algorithms.

In order to select the best predictive model, the following objective function, which considers the performance of the models for both the learning and validation data sets, was defined (Gandomi et al., 2011) as:

$$OBJ = \left(\frac{n_L - n_V}{n_T}\right)\left(\frac{MAE_L}{R_L^2}\right) + \left(\frac{2n_V}{n_T}\right)\left(\frac{MAE_V}{R_V^2}\right) \tag{2}$$

where n_L, n_T, and n_V are the number of learning, training, and validation data sets, respectively. MAE_L and MAE_V are, respectively, the mean absolute error for learning and validation data sets, and R is the correlation coefficient, which can be calculated as follows:

$$MAE = \frac{\sum_{i=1}^{n}|u_i - t_i|}{n} \tag{3}$$

$$R = \frac{\sum_{i=1}^{n}(u_i - \overline{u}_i)(t_i - \overline{t}_i)}{\sqrt{\sum_{i=1}^{n}(u_i - \overline{u}_i)^2 \sum_{i=1}^{n}(t_i - \overline{t}_i)^2}} \tag{4}$$

where n is the number of samples, and u_i and t_i are the actual and computed values for the ith outputs, respectively. The average of the actual output values is $\overline{u}_i$, and the average of computed output values is $\overline{t}_i$. The best GEP model results in minimal value for the objective function, taking into account both the correlation coefficients and mean absolute errors. It should be noted that the R value alone is not a sufficient measure for evaluating the validity of the models. The outcome of the GEP algorithm is an expression tree (ET), which can be expressed as an empirical equation. In the model development and selection process, in addition to providing the best fitness values for the learning and validation data sets, attempts were made to avoid highly complex

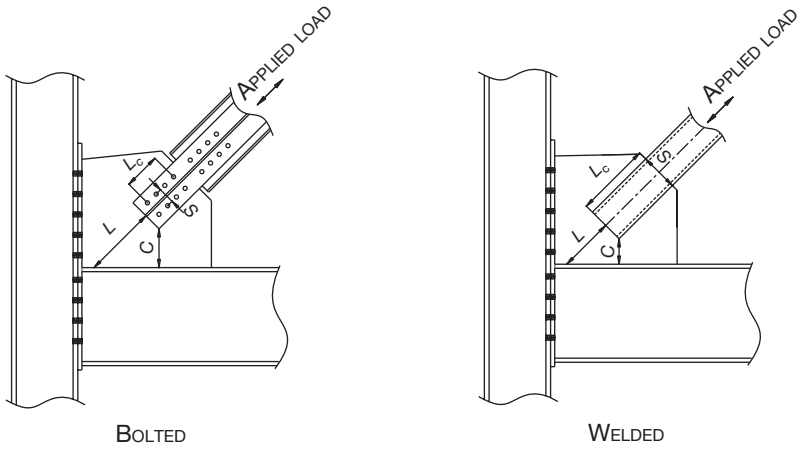

Fig. 2. Geometrical variables used in modeling process.

models. Figure 4 shows the expression tree (ET) for the best GEP model selected among all runs. The model consists of two sub-ETs, which are linked by the multiplication function. By substituting the terms into the model, the resulting empirical equation for estimating the compressive capacity of gusset plates takes the following formats in U.S. customary units and metric units, respectively:

$$P_u = \frac{(151.1t - 1.2)\sqrt{F_y L_c (2.94S^{1/3} + 5.04L^{1/2} + 2.63F_y^{1/2} - 14.43)}}{\left(8.98 + \frac{C}{t} + \frac{L_c}{L}\right)} \quad (5)$$

$$P_u = \frac{(2t - 0.4)\sqrt{F_y L_c (S^{1/3} + L^{1/2} + F_y^{1/2} - 14.43)}}{\left(8.98 + \frac{C}{t} + \frac{L_c}{L}\right)} \quad (5M)$$

where P_u is the nominal compressive strength of the gusset plate and all other terms were defined previously. The units of dimensions and yield strength are inches and ksi in Equation 5, and millimeters and MPa in Equation 5M. It is important to note that the preceding expressions are valid for the ranges of variables used in the training phase

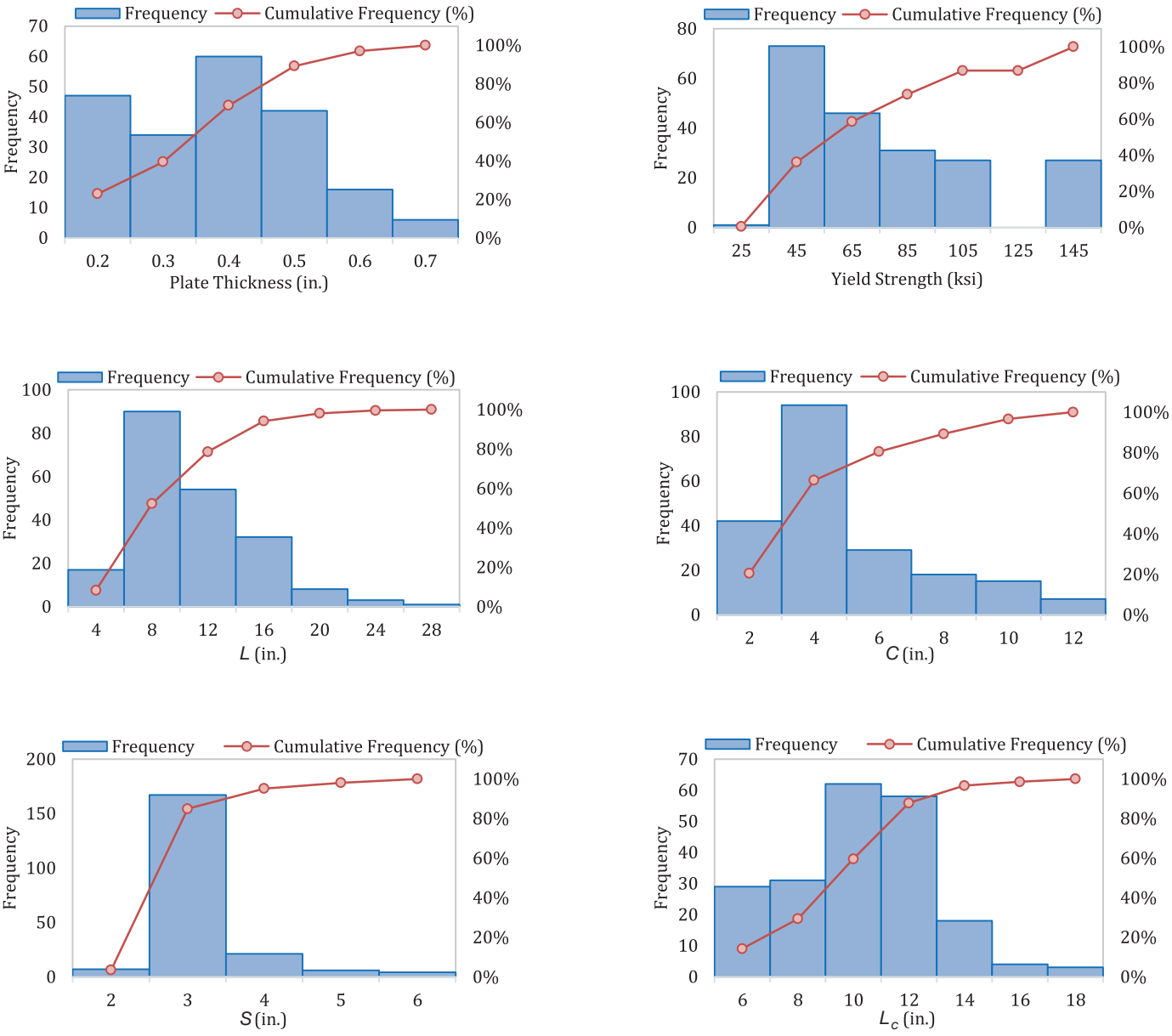

Fig. 3. Histograms of geometric and material properties of 205 gusset plate connections.

Table 1. Parameters and Criteria Used in the GEP Algorithms	
Parameter	**Settings**
Number of sub-ETs (genes)	1, 2, 3
Linking function	Addition, multiplication
Chromosomes	30, 50, 100
Head size	8, 9, 10, 12
Function set	+, –, ×, ÷, $\sqrt[2]{\ }$, $\sqrt[3]{\ }$, $\sqrt[4]{\ }$, ^2, ^3
Lower bound	–10
Upper bound	10
Number of variables	6
Gene size	26
Fitness function	RMSE

Table 2. Performance Comparison of the Proposed GEP Model and Effective Length Factor Method						
Model	**R^2**	**MAE**	**MAPE (%)**	**RMSE**	**Mean $P_u/P_{calc.}$**	**STD $P_u/P_{calc.}$**
GEP model	0.97	26.16	11.89	34.97	1.024	0.152
Thornton method (K = 0.65)	0.82	75.68	30.50	97.30	1.346	0.574
Thornton method (K = 0.5)	0.80	73.59	27.77	100.09	1.202	0.343
Dowswell (2006)	0.83	72.33	29.68	92.77	1.618	1.641

illustrated in Figure 3. These empirical equations allow for prediction of the compressive capacity of new gusset plate designs based on previously published test results via hand calculations. As such, they are recommended to be used in predesign and preliminary stages or in conjunction with the existing design methods.

Model Validation and Performance Evaluation

The accuracy of the predictive expression derived using the GEP technique was evaluated by several performance measures, including the coefficient of determination, R^2; mean absolute error, MAE; and root mean squared error, RMSE. Figure 5 shows the relationship between the estimated compressive strengths of gusset plates using Equation 5 and the actual experimental and FE values. As shown, R^2 and error values are quite close for the three categories of data sets, especially for the validation and testing data sets, indicating a good generalization capability of the empirical expression. The resulting high coefficients of determination, which are close to unity for all three sets of data, reveal a fairly good correlation between the estimated values and target compressive capacities.

Figure 6 shows the prediction performance of the GEP-based model together with the results of effective length factor method for 31 gusset plates considered as testing (or unseen) data sets, which were not used in developing the model. The gusset plates used for testing purpose are a random selection of test specimens and finite element models. The vertical axis represents the target-to-predicted ratio of the compressive strengths, where the target values are the buckling capacity of gusset plates used for testing.

For comparison purpose, the compressive capacities of gusset plates were calculated using the column analogy method with effective length factors of 0.5 and 0.65 as well as those recommended by Dowswell (2006). As shown, the higher accuracy of the presented expression in predicting the target values is clearly illustrated in these graphs.

Figure 7 shows the correlation between the estimated and actual compressive strengths for all gusset plates considered in this study (whole sets of data) using the two approaches. The comparison indicates that the coefficient of determination for the proposed expression is significantly higher than those of the column analogy method with the different values of K factor considered in this research. Also, for the whole sets of data, both the mean absolute error and the root mean squared error for the GEP-based model are considerably less than those of the latter method.

Table 2 presents a summary of values for the performance measures used for model validation. As shown, the mean value of compressive strength to predicted strength ratios for the derived expression is very close to unity (1.024), with

a standard deviation of 0.152, while, as reported by previous researchers, the predicted values of the column analogy method are conservative for the majority of specimens. The best R^2 factor based on the column analogy method was 0.83 achieved using the recommended K factors from Dowswell (2006). The significantly lower error values and standard deviations, as well as the higher correlation coefficient of the predicted buckling capacities using the presented empirical equation compared with the results of existing methods, indicate that this model is capable of predicting the ultimate strength of gusset plates with acceptable precision.

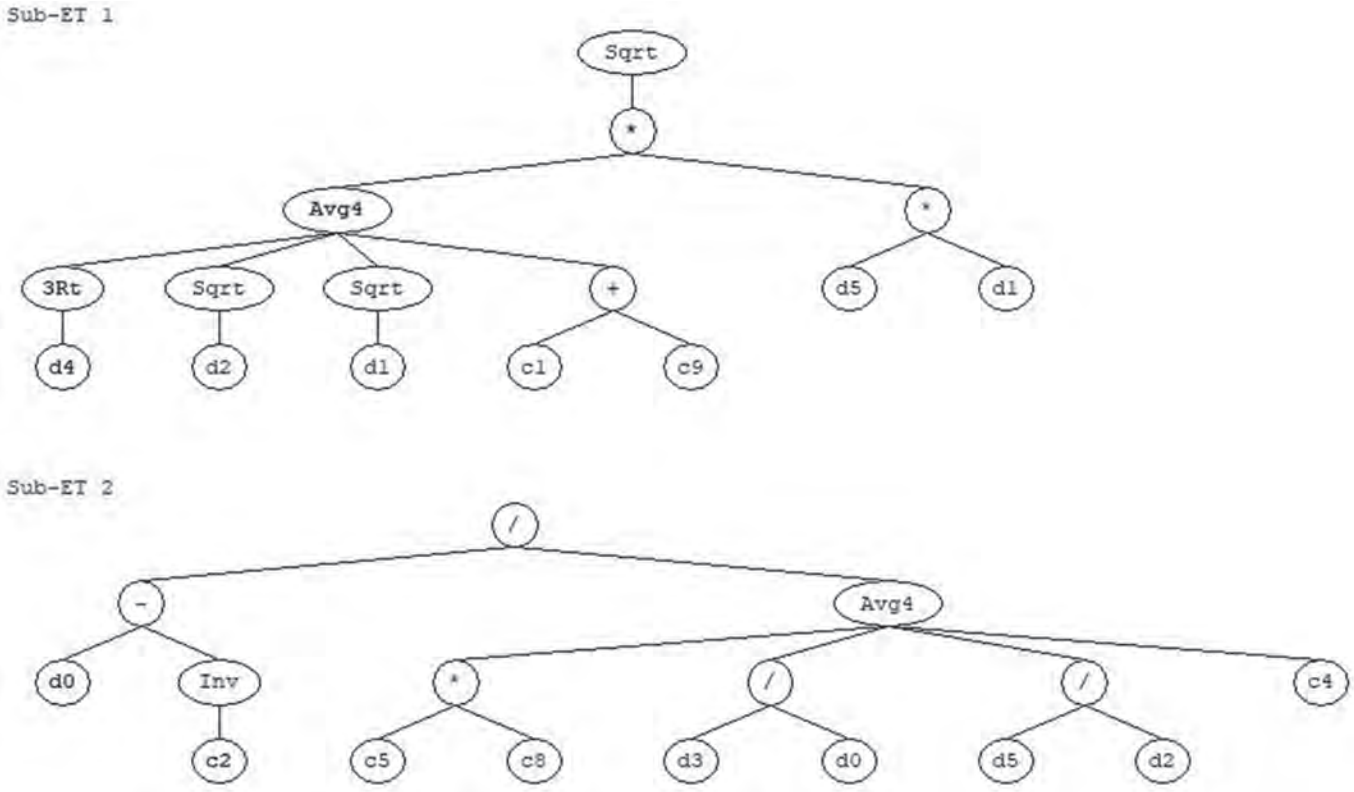

Fig. 4. Expression tree of the predictive model.

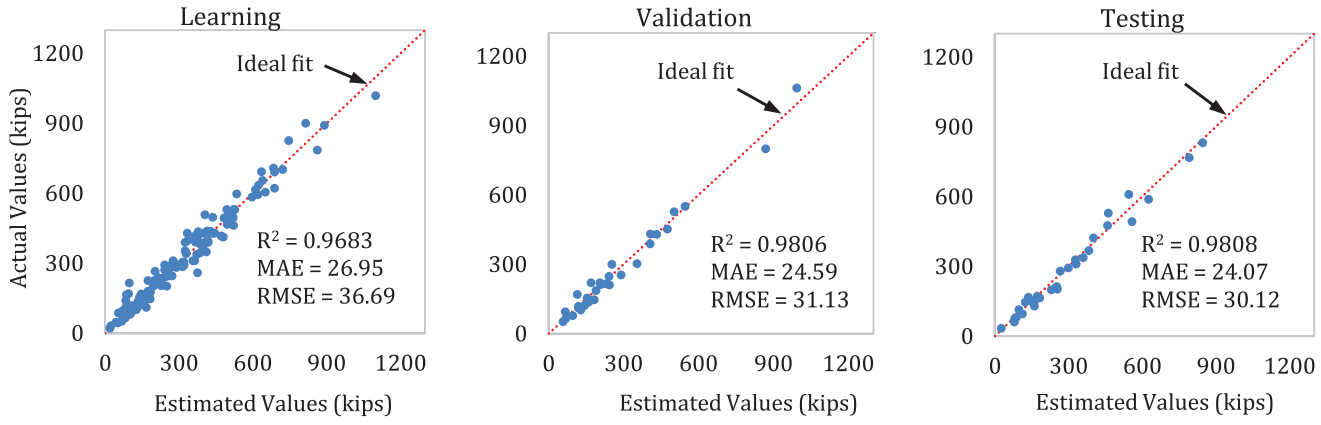

Fig. 5. Estimated compressive strength versus experimental/FE values for learning, validation, and testing data sets.

SUMMARY AND CONCLUSIONS

In this study, an evolutionary computing technique, called gene expression programming (GEP), was used to derive an empirical expression for predicting the compressive capacity of corner gusset plates. A simple yet accurate equation was derived based on a comprehensive database from past experimental and numerical research. For comparison purposes, the predicted values from this equation were compared with the results of the effective length factor method (Thornton method) commonly used in current design practice. The compressive strength of the gusset plates was separately calculated using effective length factors of 0.5, 0.65, and those recommended by Dowswell (2006). In comparison with the latter method, the proposed GEP-based model has a significantly better correlation with the experimental and FE data, and results in more consistent test-to-predicted ratios, with the mean value being 1.024 (STD = 0.152). For the 205 data sets used, the mean absolute percentage errors (MAPE) for the GEP-based formulation and Thornton method were, respectively, 11.9% and 27.8%, indicating a better prediction performance of the presented equation. However, because the expression derived using the GEP algorithm is based purely on data, as in other empirical predictive models, it should be used only in the variable ranges studied in this paper. As such, it is not intended to replace the current design approach based on the column analogy method, but rather to serve as a cross check on the results of existing methods because it allows the designers to examine if their predicted values are consistent with the previously published test results and FE data. The proposed model can be a useful tool for assessing the compressive strength of gusset plates in preliminary and pre-design stages via hand calculation.

ACKNOWLEDGMENTS

This research program was funded by the C.W. Carry Chair in Steel Structures and the department of Civil and Environmental Engineering at the University of Alberta. The authors wish to thank Prof. Cheng Fang of Tongji University for providing their research database.

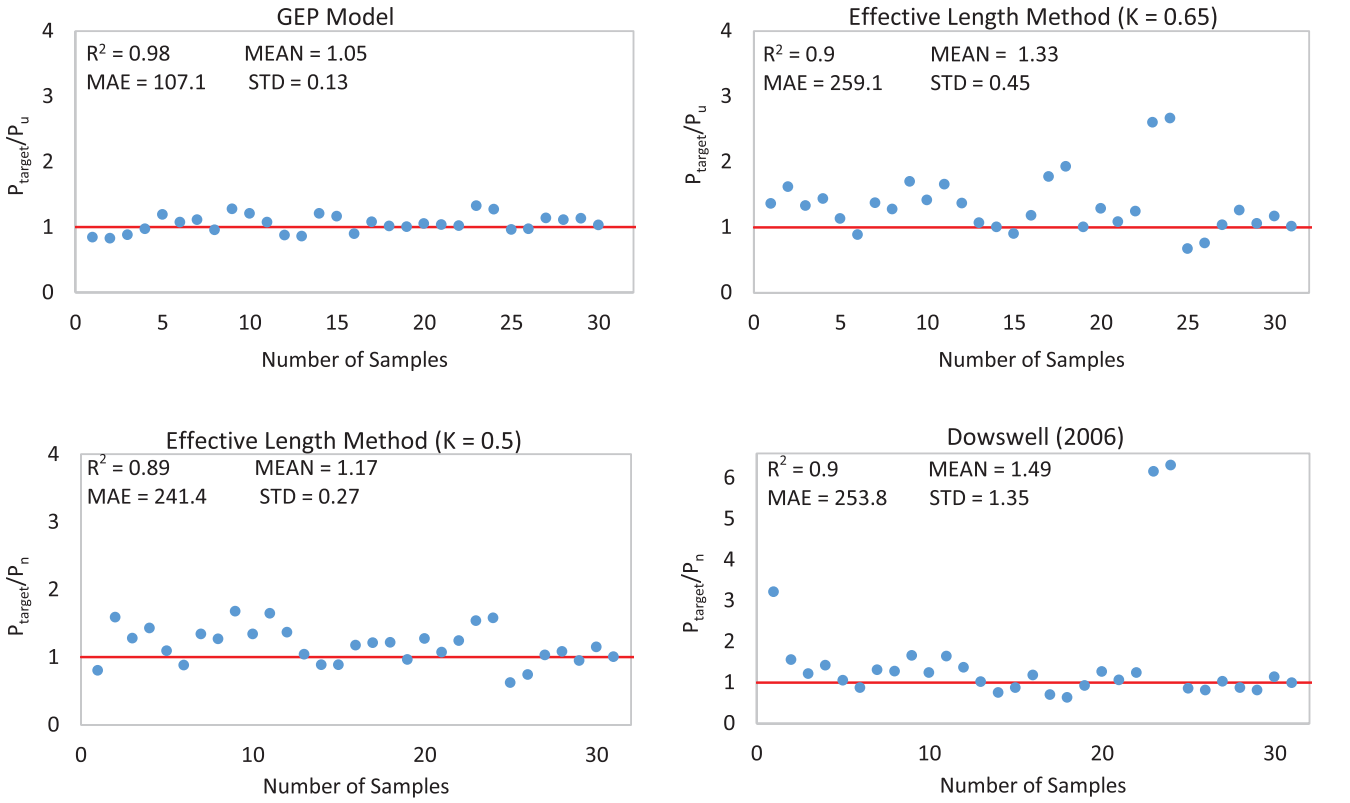

Fig. 6. Prediction performance of GEP-based expression for testing data sets and comparison with the effective length factor method.

REFERENCES

Brown, V.L. (1988), "Stability of Gusseted Connections in Steel Structures," PhD Dissertation, University of Delaware, Newark, Del.

Chakrabarti, S.K. (1987), "Inelastic Buckling of Gusset Plates," PhD Dissertation, University of Arizona, Tucson, Ariz.

Cevik, A. (2007a), "A New Formulation for Longitudinally Stiffened Webs Subjected to Patch Loading," *Journal of Constructional Steel Research*, Vol. 63, pp. 1,328–1,340.

Cevik, A. (2007b), "Genetic Programming Based Formulation of Rotation Capacity of Wide Flange Beams," *Journal of Constructional Steel Research*, Vol. 63, pp. 884–893.

Chen, S.-J. and Chang, C.-C. (2012), "Experimental Study of Low Yield Point Steel Gusset Plate Connections," *Thin-Walled Structures*, Vol. 57, pp. 62–69.

Cheng, J.J.R. and Hu, S.Z. (1987), "Comprehensive Tests of Gusset Plate Connections," *Proceedings of the 1987 Annual Technical Session*, Structural Stability Research Council, pp. 191–205.

Cheng, J.J.R., Yam, M.C.H., and Hu, S. (1994), "Elastic Buckling Strength of Gusset Plate Connections," *Journal of Structural Engineering*, American Society of Civil Engineers, Vol. 120, No. 2, pp. 538–559.

Dowswell, B. (2006), "Effective Length Factors for Gusset Plate Buckling," *Engineering Journal*, AISC, Vol. 43, No. 2, pp. 91–102.

Fang, C., Yam, M.C.H., Zhou, X., and Zhang, Y. (2015), "Post-Buckling Resistance of Gusset Plate Connections: Behavior, Strength, and Design Considerations," *Engineering Structures*, Vol. 99, pp. 9–27.

Ferreira, C. (2006), *Gene Expression Programming: Mathematical Modelling by an Artificial Intelligence*, 2nd Ed. Springer-Verlag, Germany.

FHWA (2009), *Guidelines for Design and Rating of Gusset-Plate Connections for Steel Truss Bridges*, Federal Highway Administration, U.S. Department of Transportation, McLean, Va.

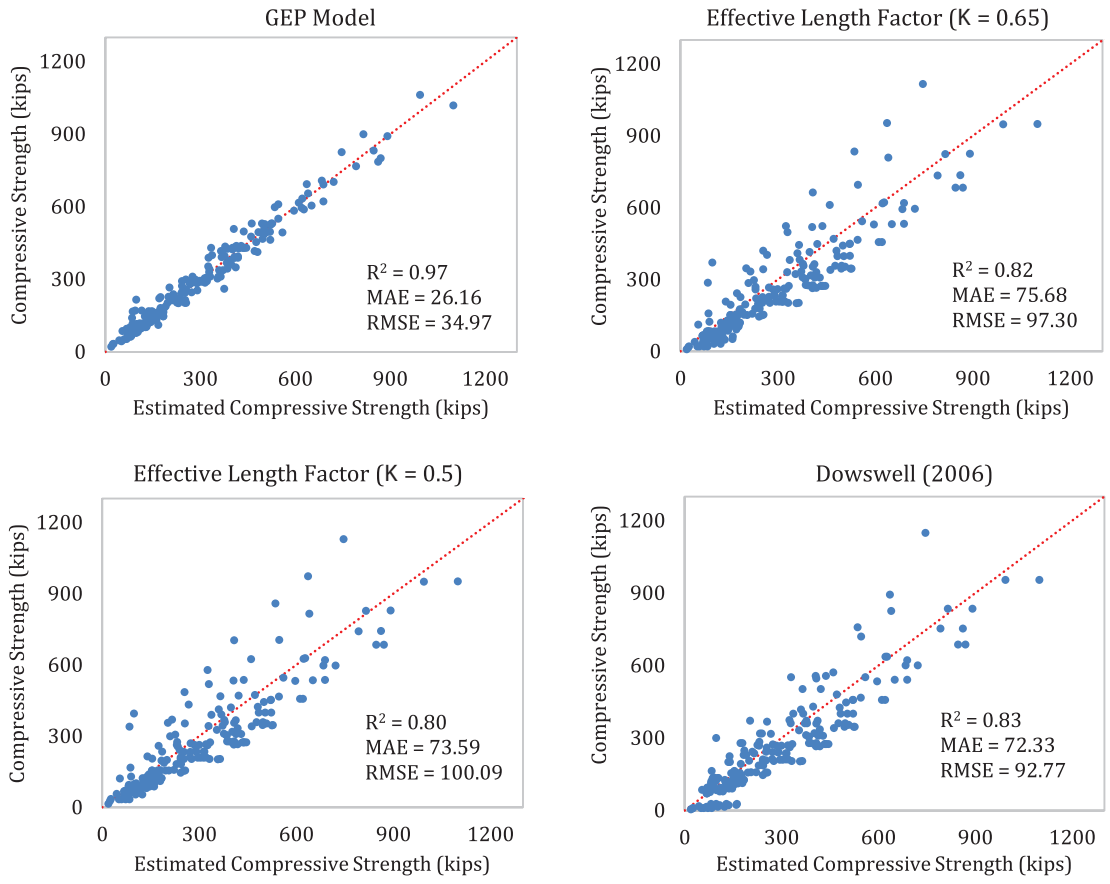

Fig. 7. Correlation of estimated and actual values of compressive capacity for the whole data.

Gandomi, A.H., Tabatabaei, S.M., Moradian, M.H., Radfar, A., and Alavi, A.H. (2011), "A New Prediction Model for the Load Capacity of Castellated Steel Beams," *Journal of Constructional Steel Research*, Vol. 67, pp. 1,096–1,105.

GEPSOFT (2013), GeneXproTools, Version 5.0.

Gross, J.L. and Cheok, G. (1988), "Experimental Study of Gusseted Connections for Laterally Braced Steel Buildings," National Institute of Standards and Technology, Gaithersburg, Md., November.

Koza, JR. (1992), *Genetic Programming: On the Programming of Computers by Means of Natural Selection*. MIT Press, Cambridge, Mass.

Naghipour, M., Abdollahzadeh, G., and Shokri, M. (2013), "Analysis and Design Procedure of Corner Gusset Plate Connections in BRBFs," *Iranica Journal of Energy and Environment*, Vol. 4, pp. 271–282.

Nast, T.E., Grondin, G.Y., and Cheng, J.J.R. (1999), "Cyclic Behavior of Stiffened Gusset Plate Brace Member Assemblies," Structural Engineering Report No. 229, University of Alberta, Department of Civil and Environmental Engineering, Edmonton, Canada, December.

Rabinovitch, J. and Cheng, J.J.R. (1993), "Cyclic Behavior of Steel Gusset Plate Connections," *Structural Engineering Report No. 191*, University of Alberta, Department of Civil and Environmental Engineering, Edmonton, Canada, August.

Sheng, N., Yam, M.C.H., and Iu, V.P. (2002), "Analytical Investigation and the Design of the Compressive Strength of Steel Gusset Plate Connections," *Journal of Constructional Steel Research*, Vol. 58, pp. 1,473–1,493.

Thornton, W.A. (1984), "Bracing Connections for Heavy Construction," *Engineering Journal*, AISC, Vol. 21, No. 3, pp. 139–148.

Walbridge, S.S., Grondin, G.Y., and Cheng, J.J.R. (1998), "An Analysis of the Cyclic Behavior of Steel Gusset Plate Connections," Structural Engineering Report No. 225, University of Alberta, Department of Civil and Environmental Engineering, Edmonton, Canada, September.

Whitmore, R.E. (1952), "Experimental Investigation of Stresses in Gusset Plates," Bulletin No. 16, University of Tennessee Engineering Experiment Station, Knoxville, Tenn., May.

Yam, M.C.H., and Cheng, J.J.R. (1993), "Experimental Investigation of the Compressive Behavior of Gusset Plate Connections," *Structural Engineering Report No. 194*, University of Alberta, Department of Civil Engineering, Edmonton, Canada, September.

Yam, M.C.H., and Cheng, J.J.R. (2002), "Behavior and Design of Gusset Plate Connections in Compression," *Journal of Constructional Steel Research*, Vol. 58, No. 5, pp. 1,143–1,159.

APPENDIX

Reference	ID	F_y (MPa)	t (mm)	L (mm)	C (mm)	L_c (mm)	S (mm)	P_u (kN)	P_T (kN)	P_{GEP} (kN)
Chakrabarti (1987)	1	248	6.35	203	72	102	76	305.59	281.81	418.23
	2	248	6.35	232	77	102	76	312.71	290.79	414.083
	3	248	6.35	203	74	102	76	317.6	295.08	412.00
Cheng and Hu (1987)	C1-Free	505	6.7	275	147	375	135	441.7	1642.99	956.17
	C2-Free	240	3.11	275	147	375	135	122.4	90.19	144.74
	C3-Free	505	6.7	487	297	375	135	380.1	1271.94	621.21
	C4-Free	240	3.11	487	297	375	135	89.6	34.26	88.26
Gross and Cheok (1988)	1A	321.99	6.35	171	25	102	76	515.99	359.83	752.98
	1B	321.99	6.35	171	25	102	76	427.03	359.83	752.98
	2A	321.99	6.35	178	27	102	76	613.85	379.85	741.76
	2B	321.99	6.35	178	27	102	76	658.34	379.85	741.76
	3B	321.99	6.35	199	30	102	76	391.44	375.32	733.21
Brown (1988)	1	330.95	6.38	146	32	114	102	800.68	476.12	736.14
	2	311.64	4.98	81	22	191	0	533.79	331.98	517.76
	3	311.64	5.03	146	32	114	102	444.82	335.15	504.98
	9	311.64	4.88	68	27	191	0	354.08	314.18	446.67
	10	311.64	5	84	23	191	0	487.08	333.65	520.19
	11	330.95	6.35	133	42	114	102	737.96	473.25	649.11
	13	330.95	6.3	105	47	114	102	620.08	469.25	584.58
	14	330.95	6.3	29	0	191	0	598.73	455.99	596.15
	15	330.95	6.35	121	34	114	102	685.92	474.80	689.64
	16	330.95	6.35	68	26	191	0	654.33	456.35	674.89
	17	311.64	4.93	147	32	114	102	533.79	326.02	491.27
	18	330.95	6.38	94	31	191	0	687.25	457.88	718.50
	20	310.26	9.55	72	37	191	0	783.33	649.55	1002.98
Rabinovitch and Cheng (1993)	A1	449	9.32	172	69	280	70	1682	1621.68	1759.24
	A2	443	6.18	172	69	280	70	1128	1001.62	945.17
	A5	449	9.32	336	185	280	70	907	1537.26	1178.62
Nast et al. (1999)	T2	424	9.61	166	53	280	70	1690	1584.85	1929.10
Yam and Cheng (1993; 2002)	GP1	295	13.3	167	66	210	68	1956	1212.64	1906.80
	GP2	305	9.8	167	66	210	68	1356	917.00	1281.83
	GP3	275	6.5	167	66	210	68	742	526.06	650.13
	SP1	295	13.3	452	267	350	68	1606	1815.16	1495.94
	SP2	305	9.8	452	267	350	68	1010	1316.22	903.35
	AP1	295	13.3	192	75	210	68	1720	1228.72	1887.65
	AP2	305	9.8	192	75	210	68	1210	929.96	1255.53
	AP3	275	6.5	192	75	210	68	728	536.09	628.18
	MP1	295	13.3	167	66	210	68	1933	1212.64	1906.80
	MP2	305	9.8	167	66	210	68	1316	917.00	1281.83

Reference	ID	F_y (MPa)	t (mm)	L (mm)	C (mm)	L_c (mm)	S (mm)	P_u (kN)	P_T (kN)	P_{GEP} (kN)
Yam and Cheng (1993; 2002)	MP3	275	6.5	167	66	210	68	721	526.06	650.13
	MP3A	275	6.5	167	66	210	68	819	526.06	650.13
	MP3B	275	6.5	167	66	210	68	821	526.06	650.13
Walbridge et al. (1998)	GP1B1	300	6	172	69	280	70	688	668.75	682.47
	GP1B3	300	6	172	69	280	70	692	668.75	682.47
	GP2B7	300	9	172	69	280	70	1292	1049.39	1252.49
	GP3B11	300	12	172	69	280	70	1793	1409.84	1876.12
Sheng et al. (2002)	1	295	13.3	237	115	140	68	1626	895.20	1377.94
	2	295	13.3	167	66	210	68	1987	1212.50	1906.80
	3	295	13.3	97	16	280	68	2349	1533.34	2352.94
	4	295	13.3	237	115	140	68	1595	889.59	1377.94
	5	295	13.3	167	66	210	68	1949	1209.39	1906.80
	6	295	13.3	97	16	280	68	2335	1530.07	2352.94
	7	305	9.87	237	115	140	68	1143	673.72	893.62
	8	305	9.87	167	66	210	68	1432	923.35	1294.82
	9	305	9.87	97	16	280	68	1867	1175.08	1726.17
	10	305	9.87	237	115	140	68	1122	666.39	893.62
	11	305	9.87	167	66	210	68	1402	915.30	1294.82
	12	305	9.87	97	16	280	68	1814	1166.58	1726.17
	13	275	6.5	237	115	140	68	509	360.65	421.88
	14	275	6.5	167	66	210	68	696	526.61	650.13
	15	275	6.5	97	16	280	68	989	693.35	978.90
	16	275	6.5	237	115	140	68	498	347.94	421.88
	17	275	6.5	167	66	210	68	666	504.96	650.13
	18	275	6.5	97	16	280	68	920	669.61	978.90
	19	295	13.3	237	115	140	68	1480	895.20	1377.94
	20	295	13.3	167	66	210	68	1793	1212.50	1377.94
	21	295	13.3	97	16	280	68	2208	1533.34	2352.94
	22	295	13.3	237	115	140	68	1232	895.22	1377.94
	23	295	13.3	167	66	210	68	1490	1212.50	1906.80
	24	295	13.3	97	16	280	68	2061	1509.76	2352.94
	25	305	9.87	237	115	140	68	878	673.76	893.62
	26	305	9.87	167	66	210	68	1082	923.35	1294.82
	27	305	9.87	97	16	280	68	1454	1156.93	1726.17
	28	275	6.5	237	115	140	68	404	360.77	421.88
	29	275	6.5	167	66	210	68	560	526.61	650.13
	30	275	6.5	97	16	280	68	765	682.36	978.90
Chen and Chang (2012)	E8t	100	17	300	141	240	100	1084	642.19	1205.972
Naghipour et al. (2013)	Test	300	8	377	196	140	90	403.3	546.12	488.942
	1	300	4	377	196	140	90	112.72	67.71	138.232

Reference	ID	F_y (MPa)	t (mm)	L (mm)	C (mm)	L_c (mm)	S (mm)	P_u (kN)	P_T (kN)	P_{GEP} (kN)
Naghipour et al. (2013)	2	300	4	307	146	210	90	201.07	173.29	206.282
	3	300	4	237	97	280	90	368.75	368.48	305.592
	4	300	4	167	47	350	90	750.64	574.12	486.302
	5	300	8	519	296	140	90	247.11	492.29	379.68
	6	300	8	449	246	210	90	391.43	699.10	520.71
	7	300	8	379	197	280	90	625.45	921.35	682.21
	8	300	8	309	147	350	90	1032.25	1148.49	886.56
	9	300	8	239	98	420	90	1677.35	1369.60	1151.31
	10	300	12	499	204	140	90	893.18	869.06	1004.03
	11	300	12	429	164	210	90	1428.89	1162.80	1357.01
	12	300	12	359	124	280	90	1867.46	1463.94	1746.60
	13	300	12	289	84	350	90	2156.27	1766.18	2196.34
	14	300	12	219	44	420	90	2433.37	2066.45	2708.55
	15	300	16	673	304	140	90	1219.83	1179.57	1326.19
	16	300	16	603	264	210	90	1819.91	1564.75	1735.36
	17	300	16	533	224	280	90	2228.95	1957.76	2150.58
	18	300	16	463	184	350	90	2657.41	2352.69	2591.89
	19	300	16	393	144	420	90	3069.46	2748.29	3071.10
Fang et al. (2015)	G1T4P48S355	355	4	205	92	192	68	318.47	200.89	288.05
	G1T4P48S460	460	4	205	92	192	68	372.58	210.52	346.12
	G1T4P48S690	690	4	205	92	192	68	488.45	209.79	462.36
	G1T4P48S960	960	4	205	92	192	68	612.44	209.79	586.36
	G1T4P55S355	355	4	167	65	220	68	388.977	301.36	370.44
	G1T4P55S460	460	4	167	65	220	68	456.721	345.19	446.60
	G1T4P55S690	690	4	167	65	220	68	606.764	395.22	599.34
	G1T4P55S960	960	4	167	65	220	68	772.8	401.02	762.56
	G1T4P65S355	355	4	127	37	260	68	601.914	438.74	506.47
	G1T4P65S460	460	4	127	37	260	68	686.954	539.86	613.36
	G1T4P65S690	690	4	127	37	260	68	853.758	723.08	828.21
	G1T4P65S960	960	4	127	37	260	68	1069.83	880.76	1058.23
	G1T8P48S355	355	8	205	92	192	68	1027.31	787.47	908.47
	G1T8P48S460	460	8	205	92	192	68	1216.44	1006.93	1091.61
	G1T8P48S690	690	8	205	92	192	68	1465.9	1467.13	1458.21
	G1T8P48S960	960	8	205	92	192	68	1629.49	1972.76	1849.28
	G1T8P55S355	355	8	167	65	220	68	1083.01	890.96	1095.39
	G1T8P55S460	460	8	167	65	220	68	1274.1	1145.62	1320.60
	G1T8P55S690	690	8	167	65	220	68	1504	1689.66	1772.25
	G1T8P55S960	960	8	167	65	220	68	1810.3	2304.70	2254.865
	G1T8P65S355	355	8	127	37	260	68	1400.82	1033.76	1346.36
	G1T8P65S460	460	8	127	37	260	68	1711.59	1335.20	1630.51
	G1T8P65S690	690	8	127	37	260	68	2320.42	1988.67	2201.63
	G1T8P65S960	960	8	127	37	260	68	2772	2743.95	2813.11

Reference	ID	F_y (MPa)	t (mm)	L (mm)	C (mm)	L_c (mm)	S (mm)	P_u (kN)	P_T (kN)	P_{GEP} (kN)
Fang et al. (2015)	G1T12P48S355	355	12	205	92	192	68	1747.31	1224.50	1673.79
	G1T12P48S460	460	12	205	92	192	68	2124.58	1582.52	2011.21
	G1T12P48S690	690	12	205	92	192	68	2900.86	2360.20	2686.65
	G1T12P48S960	960	12	205	92	192	68	3529.45	3261.70	3407.17
	G1T12P55S355	355	12	167	65	220	68	1846.1	1364.68	1942.53
	G1T12P55S460	460	12	167	65	220	68	2244.68	1765.62	2341.90
	G1T12P55S690	690	12	167	65	220	68	3047.47	2639.62	3142.84
	G1T12P55S960	960	12	167	65	220	68	3630.5	3658.17	3998.69
	G1T12P65S355	355	12	127	37	260	68	2236.09	1564.30	2259.10
	G1T12P65S460	460	12	127	37	260	68	2722.38	2025.69	2735.88
	G1T12P65S690	690	12	127	37	260	68	3772.88	3034.28	3694.175
	G1T12P65S960	960	12	127	37	260	68	4425.8	4214.69	4720.22
	G2T4P48S355	355	4	369	208	240	68	234.093	85.80	189.56
	G2T4P48S460	460	4	369	208	240	68	267.511	85.80	225.70
	G2T4P48S690	690	4	369	208	240	68	326.182	85.80	297.60
	G2T4P48S960	960	4	369	208	240	68	378.112	85.80	373.84
	G2T4P55S355	355	4	324	176	275	68	305.734	138.34	227.19
	G2T4P55S3460	460	4	324	176	275	68	359.391	138.34	271.04
	G2T4P55S690	690	4	324	176	275	68	462.057	138.34	358.40
	G2T4P55S960	960	4	324	176	275	68	555.734	138.34	451.17
	G2T4P65S355	355	4	274	141	325	68	367.881	269.91	284.62
	G2T4P65S460	460	4	274	141	325	68	438.521	271.84	340.43
	G2T4P65S690	690	4	274	141	325	68	582.854	271.84	451.82
	G2T4P65S960	960	4	274	141	325	68	724.178	271.84	570.33
	G2T8P48S355	355	8	369	208	240	68	689.756	859.94	672.81
	G2T8P48S460	460	8	369	208	240	68	779.976	1072.10	801.09
	G2T8P48S690	690	8	369	208	240	68	963.185	1477.79	1056.27
	G2T8P48S960	960	8	369	208	240	68	1137.19	1861.80	1326.91
	G2T8P55S355	355	8	324	176	275	68	826.217	1001.34	788.43
	G2T8P55S460	460	8	324	176	275	68	936.766	1263.22	940.59
	G2T8P55S690	690	8	324	176	275	68	1193.58	1786.87	1243.74
	G2T8P55S960	960	8	324	176	275	68	1450.62	2320.64	1565.70
	G2T8P65S355	355	8	274	141	325	68	1034.62	1193.31	954.44
	G2T8P65S460	460	8	274	141	325	68	1140.27	1522.27	1141.59
	G2T8P65S690	690	8	274	141	325	68	1470.6	2206.49	1515.12
	G2T8P65S960	960	8	274	141	325	68	1819.72	2948.87	1912.51
	G2T12P48S355	355	12	369	208	240	68	1579.45	1432.30	1344.85
	G2T12P48S460	460	12	369	208	240	68	1774.92	1841.85	1601.26
	G2T12P48S690	690	12	369	208	240	68	2051.31	2717.02	2111.33
	G2T12P48S960	960	12	369	208	240	68	2385.87	3706.81	2652.29
	G2T12P55S355	355	12	324	176	275	68	1838.42	1615.21	1549.66
	G2T12P55S460	460	12	324	176	275	68	2101.79	2081.91	1848.73

Reference	ID	F_y (MPa)	t (mm)	L (mm)	C (mm)	L_c (mm)	S (mm)	P_u (kN)	P_T (kN)	P_{GEP} (kN)
Fang et al. (2015)	G2T12P55S690	690	12	324	176	275	68	2437.76	3086.881	2444.57
	G2T12P55S960	960	12	324	176	275	68	2833.76	4236.761	3077.39
	G2T12P65S355	355	12	274	141	325	68	2141.99	1867.57	1830.77
	G2T12P65S460	460	12	274	141	325	68	2494.34	2412.48	2189.74
	G2T12P65S690	690	12	274	141	325	68	2852.31	3594.31	2906.23
	G2T12P65S960	960	12	274	141	325	68	3324.18	4961.21	3668.48
	G3T4P48S355	355	4	233	91	192	68	371.034	212.18	297.24
	G3T4P48S460	460	4	233	91	192	68	437.266	225.97	356.43
	G3T4P48S690	690	4	233	91	192	68	575.427	227.08	474.77
	G3T4P48S960	960	4	233	91	192	68	719.009	227.08	600.87
	G3T4P55S355	355	4	195	72	220	68	397.926	316.73	358.28
	G3T4P55S3460	460	4	195	72	220	68	470.737	368.18	430.85
	G3T4P55S690	690	4	195	72	220	68	629.87	435.35	576.19
	G3T4P55S960	960	4	195	72	220	68	801.044	455.37	731.30
	G3T4P65S355	355	4	155	52	260	68	568.928	456.12	446.89
	G3T4P65S460	460	4	155	52	260	68	646.998	567.72	539.43
	G3T4P65S690	690	4	155	52	260	68	820.584	779.77	725.13
	G3T4P65S960	960	4	155	52	260	68	1044.14	978.29	923.67
	G3T8P48S355	355	8	233	91	192	68	1088.63	790.16	937.53
	G3T8P48S460	460	8	233	91	192	68	1300.07	1011.40	1124.22
	G3T8P48S690	690	8	233	91	192	68	1659.82	1476.91	1497.46
	G3T8P48S960	960	8	233	91	192	68	1879.22	1991.07	1895.17
	G3T8P55S355	355	8	195	72	220	68	1127.05	893.73	1081.45
	G3T8P55S3460	460	8	195	72	220	68	1338.31	1150.24	1300.51
	G3T8P55S690	690	8	195	72	220	68	1640	1699.91	1739.22
	G3T8P55S960	960	8	195	72	220	68	1950.7	2324.17	2207.41
	G3T8P65S355	355	8	155	52	260	68	1407.39	1036.27	1264.41
	G3T8P65S460	460	8	155	52	260	68	1718.7	1339.41	1526.23
	G3T8P65S690	690	8	155	52	260	68	2324.81	1998.08	2051.64
	G3T8P65S960	960	8	155	52	260	68	2793.99	2762.02	2613.39
	G3T12P48S355	355	12	233	91	192	68	1819.98	1225.33	1727.41
	G3T12P48S460	460	12	233	91	192	68	2214.06	1583.91	2071.39
	G3T12P48S690	690	12	233	91	192	68	3069.19	2363.30	2759.11
	G3T12P48S960	960	12	233	91	192	68	3838.68	3267.65	3491.89
	G3T12P55S355	355	12	195	72	220	68	1913.44	1365.52	1940.52
	G3T12P55S460	460	12	195	72	220	68	2326.19	1767.03	2333.59
	G3T12P55S690	690	12	195	72	220	68	3214.68	2642.77	3120.80
	G3T12P55S960	960	12	195	72	220	68	3969.37	3664.25	3960.91
	G3T12P65S355	355	12	155	52	260	68	2262.95	1565.05	2189.05
	G3T12P65S460	460	12	155	52	260	68	2765.05	2026.95	2642.34
	G3T12P65S690	690	12	155	52	260	68	3875.47	3037.11	3551.98
	G3T12P65S960	960	12	155	52	260	68	4892.97	4220.16	4524.53

Steel Structures Research Update

Advances in Design with Hollow Structural Steel Members

JUDY LIU

INTRODUCTION

Recent advances in design of steel-frame systems with hollow structural steel (HSS) members are highlighted. The featured work includes new and updated design guides that are co-authored by Jeffrey Packer and Jason McCormick. Jeffrey Packer is the Bahen/Tanenbaum Professor of Civil Engineering at the University of Toronto. Dr. Packer has been named a Fellow of the Canadian Academy of Engineering and five other engineering institutes or societies. His accolades include the AISC Special Achievement Award and the American Society of Civil Engineers Shortridge Hardesty Award. Jason McCormick is the Arthur F. Thurnau Associate Professor in the Department of Civil and Environmental Engineering at the University of Michigan. Dr. McCormick's work has been recognized with numerous awards, including the AISC Milek Fellowship, the AISC Early Career Faculty Award, and the National Science Foundation CAREER Award.

Dr. Packer's research interests include static, fatigue, impact, blast, and seismic behavior of HSS members, connections, trusses, and frames. Recent work includes publications on experiments, finite element modeling, parametric studies, and design of welds to branch members in hollow section connections (Tousignant and Packer, 2018). Dr. Packer's experimental, numerical, and analytical research informs the design of HSS for various loading conditions, with a bias toward code/specification-related issues and guidance for practicing engineers (as exemplified in the design guides described in the next section).

Dr. McCormick's research on HSS members and connections ranges from research on steel HSS-based seismic moment frames (Wei and McCormick, 2018; Fadden and McCormick, 2014) to the use of innovative materials (e.g., polymer foam) to control the structural response of HSS members under seismic and wind loads. He has also investigated the cyclic behavior of HSS columns under combined large axial loads and bending moments. Dr. McCormick's research serves to fill gaps in knowledge with regard to HSS behavior, improve design methods, and enhance the performance of systems with HSS members under seismic and wind loads.

Selected studies are featured along with a preview of the new design guides. Research on HSS columns under axial and lateral loads fills knowledge gaps in seismic behavior and design. Foam-filled brace and bending member experiments show improved seismic performance with a light-weight polyurethane fill. Field tests, laboratory experiments, and numerical modeling are used to study behavior and develop design methods for hollow and concrete-filled HSS subject to blast and impact loading. Research on single-sided fillet welds of HSS members leads to improved design recommendations. Improved design procedures are also recommended based on research on HSS connections that are in branch compression, near chord ends, or offset laterally.

DESIGN GUIDES

AISC Design Guide 24, *Hollow Structural Section Connections*, by Packer et al. (2010), was first published a decade ago. A second updated and expanded edition by Packer and McCormick is expected to be published in 2020. Considering that the content of AISC *Specification* Chapter K was significantly reduced in the 2016 edition (AISC, 2016a), this guide will be of immense help to engineers applying AISC *Specification* Chapters J and K to HSS connections. The second edition is planned to be more than 50% longer than the first edition; contains more design examples; and most importantly, adds new chapters on limit states for HSS connections and seismic connections.

Packer and McCormick are also contributors to the next HSS design guide by the Comité International pour le Développement et l'Étude de la Construction Tubulaire (CIDECT) (Zhao et al., 2019). This *Design Guide for Concrete-Filled Hollow Section Columns under Static, Impact, Blast, Seismic and Fire Loading* is the 10th in a series of design guides by CIDECT. Round and rectangular HSS composite columns are covered, with/without rebar, and also concrete-filled double-skin tubes (a tube-in-tube concept where the

Judy Liu, PhD, Research Editor of the AISC Engineering Journal, Professor, Oregon State University, School of Civil and Construction Engineering, Corvallis, Ore. Email: judy.liu@oregonstate.edu

annulus between the tubes is filled with concrete or grout). Design procedures for the five loading conditions are summarized, reviewing the methods in the United States, Europe, Australia, and China. Design examples are given for all loading criteria, including the AISC *Specification* for static loads, the AISC *Seismic Provisions* (AISC, 2016b) for seismic loads, and ASCE 59-11 (ASCE, 2011) for blast.

HSS COLUMNS UNDER AXIAL AND LATERAL LOADS

There is interest in using rectangular and square HSS for columns, but knowledge about their behavior under large axial loads and bending moments is lacking. HSS columns can be effective for multi-axis loading and have lower weak-axis slenderness ratios than comparable-weight W-shapes. To address the knowledge gap and to evaluate current guidelines, validated finite element models were used to study the collapse behavior of HSS columns under combined axial and lateral loading (Sediek et al., 2019).

Finite element models of rectangular HSS columns were validated against experiments of HSS beams undergoing cyclic bending up to rotations of 8% (Fadden and McCormick, 2012) for use in a parametric study. Comparisons of the computational model and the physical test results show good agreement in the cyclic responses, including moment capacity, strength degradation, and local buckling (Figure 1). The ASTM A500 Grade B HSS columns investigated in this study represented a range of local and global slenderness ratios. Global slenderness ratios, L/r, ranged from 60.7 to 80.1. In the absence of a highly ductile limit for HSS webs under combined compression and flexure, the limit for built-up box sections was used. The axial compressive load was constant in the analysis; one of two lateral displacement histories was then applied. The first loading history was the symmetric cyclic (SC) loading with increasing displacements specified in the AISC *Seismic Provisions*. The second loading protocol was a cyclic ratcheting (CR) drift history developed by Wu et al. (2018) to simulate more realistic first-story column displacements (Sediek at al., 2019).

The HSS columns were evaluated using the critical constant axial load ratio (CCALR), the maximum axial load ratio for which the column is able to reach 4% drift for both loading protocols without axial failure. The analysis results revealed effects of element width-to-thickness ratios, axial load levels, and loading protocols. The results also suggested potential revisions to current design specifications. Increasing the axial load level reduced the ductility of the HSS columns. The same HSS column that reached 6% drift with an initial axial load level of $0.2P_y$, or 20% of the nominal yield strength of the column, failed at 4% drift under an axial load level of $0.4P_y$. Of the loading protocols, the SC load history was more severe; CCALR values were typically lower for the SC protocol than for the CR loading protocol. The CCALR was not sensitive to the global slenderness ratio but decreased by 46% when the web width-to-thickness ratio, h/t, increased from 10.4 to 24.6. Results indicated that columns that qualified as highly ductile for h/t but were subjected to axial load levels higher than $0.7P_y$ were unable to sustain the loading to 4% drift. On the other hand, an HSS column that was not highly ductile for the flange width-to-thickness ratio, b/t, was able to reach to 4% drift under a

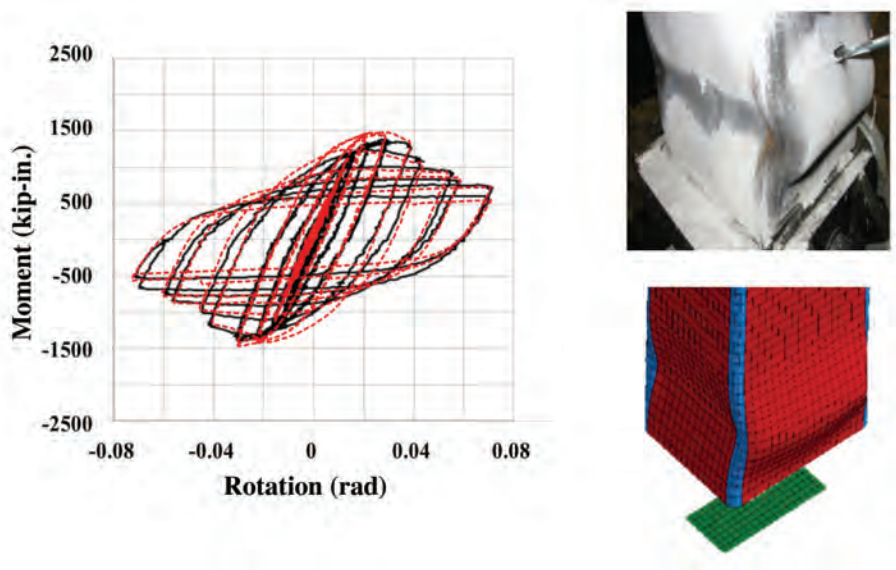

Fig. 1. FE model of HSS beam validated with results from Fadden and McCormick (2012).

typical gravity load of $0.25P_y$. Some revisions to the highly ductile limits for HSS columns should be considered.

FOAM-FILLED BRACES AND BENDING MEMBERS

A pourable, expanding, closed-cell polyurethane foam is explored as an alternative fill in hollow structural section (HSS) braces and beams. The foam is lightweight and commonly used in insulation, for flotation, and in impact protection in automobiles. Starting as a two-equal-part liquid mixture, the foam expands into a rigid solid with approximately four times its liquid volume. The foam fill is used to delay local buckling and increase energy dissipation in the HSS braces and beams while limiting increases in strength that could influence a capacity-based design approach. Furthermore, the foam's advantages over concrete fill include lower mass for seismic demands and ability to be used as an in-situ retrofit strategy.

Foam-Filled Braces

Filling HSS braces with foam provides a lightweight method to limit local buckling and improve fracture life. Under cyclic inelastic loading, HSS braces yield in tension and buckle in compression. The braces can exhibit local buckling followed by premature fracture. A study has been undertaken to evaluate the effectiveness of a polyurethane foam fill in improving the seismic performance of round HSS braces. Another research objective was to explore whether diameter-to-thickness, D/t, limits can be less stringent for filled steel braces in seismic design (Ammons et al., 2018).

Foam-Filled Brace Test Specimens, Loading, and Test Set-Up

Four 62-in. brace specimens were tested to investigate the effectiveness of the foam fill and the potential to relax the D/t limits for seismic design with foam-filled braces. The two unfilled brace (UB) specimens and two filled brace (FB) specimens used cold-formed circular sections of Japanese STK400 steel. The steel had specified minimum yield stress and tensile strength of 34 ksi and 58 ksi, respectively. The specimens with the 3.51-in.-diameter round HSS satisfied the highly ductile limits from the AISC *Seismic Provisions*, while the 4.50-in.-diameter round HSS qualified as moderately ductile. The UB and FB specimens were designated by their diameter and thickness in millimeters—for example, UB11445 and FB11445 for the moderately ductile, 4.5 mm thick, 114-mm-diameter round HSS.

The test specimens were placed in a four-pin frame and subjected to quasi-static cyclic loading at increasing displacements. The specimens were oriented at 45°, and pin connections at each end allowed for buckling in the plane of the frame (Figure 2). The loading history consisted of two cycles each of displacements ranging from 0.1 to 4% story drift. Cycles then continued at 4% drift until brace fracture occurred.

Foam-Filled Brace Test Results

The cyclic inelastic behavior of the filled and unfilled brace specimens was similar until local buckling and fracture. The elastic stiffnesses and yield strengths of the filled braces were comparable (within 3%) to those of the unfilled braces. Yielding and global buckling was followed by the initial

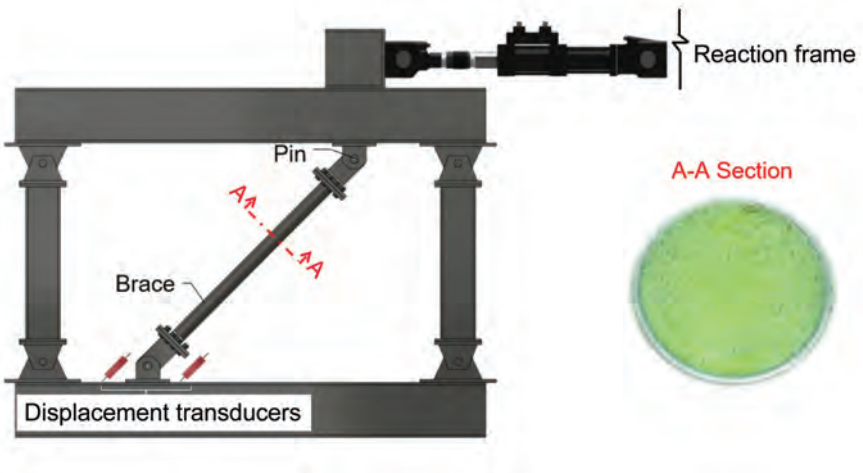

Fig. 2. Test set-up for unfilled and filled brace specimens.

formation of a plastic hinge at mid-length. The first instance of global buckling for Specimen FB11445 was delayed to the first 0.75% compressive cycle, compared to the first 0.5% cycle for Specimen UB11445. Local buckling was therefore also delayed. In both foam-filled braces, the local buckling and strength degradation were less severe than for the unfilled specimens. Figure 3 visually compares the plastic hinge regions in Specimens UB11445 and FB11445. Figure 4 confirms the lower strains at brace mid-length for FB11445. Meanwhile, with the foam fill, both sizes of braces were able to undergo an additional cycle of loading before fracture, and the cumulative energy dissipation increased by approximately 25%. Further testing is ongoing at the University of Michigan with round HSS that have D/t ratios beyond the moderately ductile requirement.

Foam-Filled Bending Members

Foam fill provides similar benefits for HSS bending members. The use of HSS beams in seismic applications may be limited by width-to-thickness and depth-to-thickness limits. Full-scale tests on empty and foam-filled HSS beams were conducted to evaluate the benefits of the foam fill, including the potential to inhibit local buckling in their plastic hinge region (Carreras et al., 2018).

Foam-Filled Bending Member Test Specimens, Loading, and Test Set-Up

The testing program was designed for evaluation of overall moment-rotation behavior, degradation of moment capacity, local buckling, and energy dissipation. The 60.5-in. beams were tested as vertical cantilevers with a fixed support at the base and lateral load applied at the top (Figure 5), following the loading protocol for qualifying connections (AISC, 2016b). The full-scale specimens were fabricated with U.S. cold-formed ASTM A500 Gr. B/C steel. The six section sizes allowed evaluation of different width-thickness and depth-thickness ratios in addition to the behavior of empty and filled HSS beams. One of the HSS satisfied the highly ductile limits from the AISC *Seismic Provisions*; four sections met the moderately ductile limit for the flange, and one was outside the moderately ductile limit. The foam fill was placed at the fixed-end connection to a depth of 1.5 times the theoretical plastic hinge length of the HSS.

Foam-Filled Bending Member Test Results

The foam fill was beneficial in limiting local buckling and reducing the degree of moment degradation. Comparisons of the empty and filled beams showed comparable moment capacity, initial stiffness and unloading stiffness. All specimens did experience local buckling and strength degradation. However, even at 0.06 radian, there was restraint of the local buckling in the filled specimen (Figure 6), and the degradation in moment was less severe. Degradation at the first positive 0.04-rad cycle ranged from 4.8% to 5.1% for the filled beams as compared to 7.8% to 23.9% for the empty beams. The degradation was the most severe for the empty HSS beam with the largest flange width-to-thickness ratio, b/t, of 31.3. The web flange-to-thickness ratio, h/t, had a lesser effect but did contribute to the moment degradation. This effect was evidenced by the two specimens with the same b/t and moment degradation of 10.5% for an h/t of 39.9 as compared to 7.8% for an h/t of 31.3. As a result, the influence of the foam fill is most significant for members with larger element slenderness ratios. Meanwhile, the increase in energy dissipation due to the foam fill ranged from 21.1% to 34.2%. One reason for the increased energy dissipation is the reduction in local buckling. Another reason is the crushing of the foam and dissipation of energy once local buckling does occur.

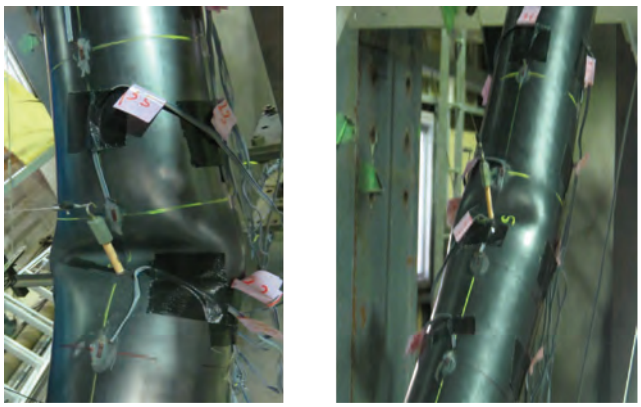

(a) empty braces *(b) filled braces*

Fig. 3. Local buckling.

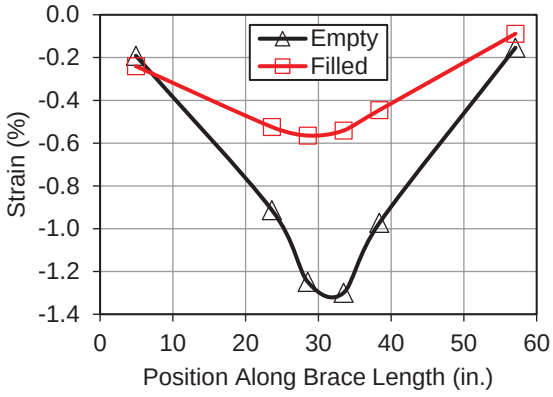

Fig. 4. Comparison of strain over brace length for empty and filled braces.

Conclusions and Future Work on Foam-Filled Braces and Bending Members

From the tests on the foam-filled braces, the foam delayed the local buckling and improved the energy dissipation. The effect of the lightweight foam fill on the elastic stiffness and yield strength was negligible. As such, the foam need not be considered in determination of loads, drift, or nominal capacity. The initial test results suggested that current element slenderness limits could be less stringent for foam-filled braces. Additional tests and detailed finite element studies for a broader inventory of braces are being conducted for development of revised element slenderness limits.

The results for the HSS beams filled with the polyurethane-based foam were similar. The filled HSS beams exhibited less moment capacity degradation and dissipated more energy. The foam fill helped to inhibit local buckling in the member. As with the foam-filled braces, the results for the HSS beam tests suggested that the use of the foam fill could result in a "relaxation of current slenderness requirements." (Carreras et al., 2018). A large-scale parametric study is being conducted to quantify the potential slenderness limits for foam-filled beams.

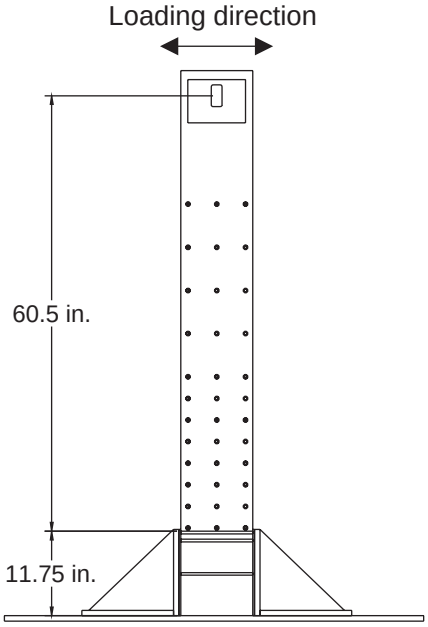

(a) test set-up drawing

(b) test of specimen

Fig. 5. Bending member testing.

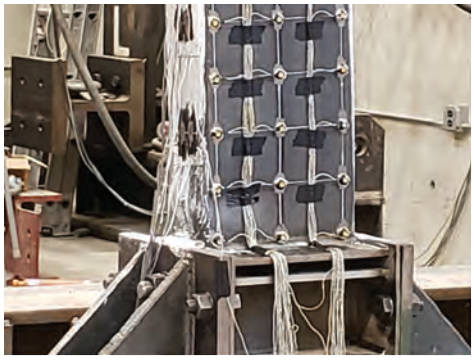

(a) unfilled

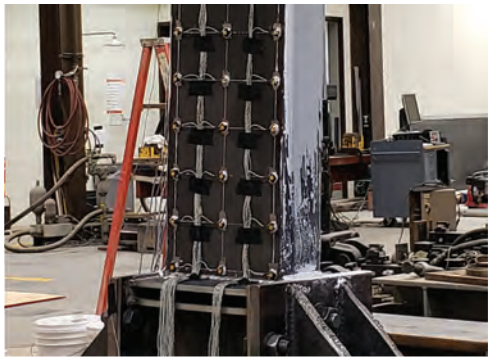

(b) filled HSS beams

Fig. 6. Local buckling.

BLAST RESPONSE OF STEEL AND COMPOSITE MEMBERS

Interest in research on the effects of blast loading on structural and other elements has led to the creation of the Centre for Resilience of Critical Infrastructure (CRCI) at the University of Toronto. The work emphasizes short-duration, impulsive loading and includes experimentation and numerical modeling of the behavior of the components under blast and impact. Structural elements and materials studied include architectural and blast-resistant glazing, steel HSS and wide-flange shapes, concrete-filled tubes, energy-dissipating steel connectors, historic masonry façades, and neo-classical columns. "Ongoing research in this area will continue to help develop design methods and best-practice approaches" for blast and impact loading on buildings (Seica et al., 2019). The work on the steel HSS and concrete-filled tubes, including concrete-filled double-skin HSS, will be briefly highlighted.

Hollow and Concrete-Filled HSS under Blast and Impact Loading

Field blast testing, laboratory testing, and numerical modeling of hollow and concrete-filled rectangular HSS has been conducted with the goal of developing blast design procedures. The field blast testing was conducted on 16 square HSS members, half of the specimens filled with a cementitious grout. HSS with 4.72-in. outside dimensions and 0.197-in. or 0.315-in. thickness were used. Duplicate pairs of the 10.7-ft span, simply supported, vertical flexural members were covered by steel cladding. The specimens were subjected to TNT explosive charges up to 2,200 lb. Pressures, displacements, and strains were measured. Figure 7 shows HSS specimens before and after the field blast test. Laboratory tests included material property static tests, "post-test 'autopsies' … on the concrete-filled RHS to evaluate the composite action and to measure the average bond stress," split Hopkinson pressure bar (SHPB) tests to evaluate high-strain-rate behavior of the HSS material, and Charpy V-notch tests to evaluate notch toughness of the HSS (Seica et al., 2019). Numerical modeling included comparisons of single-degree-of-freedom (SDOF) analysis and finite element (FE) analysis using LS-DYNA, displaying the blast response modeling capabilities of the FE analysis (Figure 8). Related work includes Ritchie et al. (2017a, 2017b, 2018a, 2018b) for far-field air-blast loading (characterized by member global failure) and Grisaro et al. (2019) for close-in blast loading (characterized by member local or cross-section failure).

Concrete-Filled Double-Skin HSS under Blast and Impact Loading

Concrete-filled, double-skin steel tubes (CFDST) were also studied. In these CFDST, an outer square HSS had 4.72-in. outside dimensions and 0.236 in. thickness. For the inner tube, a square HSS of 2.36- or 3.15-in. outside dimensions and 0.118-in. thickness was used, as illustrated in Figure 9. After field blast tests, sections cut from the centers of the

(a) HSS test specimens in concrete reaction structure

(b) HSS members after field test, with displacement transducers, illustrating global failure of members due to far-field air-blast

Fig. 7. HSS test specimens before and after field blast test.

test specimens showed no noticeable damage for the CFDST with the smaller inner tube (2.36 in.), but crushing of the cementitious grout and local buckling of the inner tube was observed for the specimen with the 3.15-in. HSS. In the laboratory, four-point bending tests were conducted to inform the numerical modeling. SDOF and FE analyses were again conducted. The FE analysis was able to represent the blast response with higher accuracy than the SDOF analysis.

WELDING OF HSS

Experimental and numerical research on fillet welds to round and rectangular HSS members (which are inherently single-sided), joined to rigid (plate) landing surfaces, has led to clarification of the application of the directional strength-increase factor (which accounts for direction of loading relative to the weld axis) for single-sided fillet welds (Packer et al., 2016; Tousignant and Packer, 2017b, 2019). Thus, for fillet welds to square and rectangular—but not round—HSS branches, it has been proposed that the directional strength-increase factor be disallowed in the 2022 edition of AISC *Specification* Chapter J for branch elements in tension, which tend to cause opening of the fillet weld at the root.

Other research on round-to-round HSS weld-critical connections, where the weld is joined to a flexible (HSS) landing surface, has led to design recommendations for weld effective lengths in such connections. The weld around the perimeter of a round HSS can have a highly nonuniform stress and be prone to weld "unzipping," but no specifications exist currently for weld effective length (e.g., in AISC *Specification* Section K5). Experimental and numerical research on welds in round-to-round HSS connections has addressed questions about the weld behavior (Tousignant and Packer, 2017a, 2018). Synthesis of the results has produced weld effective length recommendations for round HSS cross-, T-, and Y-connections (Tousignant and Packer, 2019). For fillet welds in such connections these recommendations are shown to provide adequate structural reliability in conjunction with the use of the directional strength-increase factor.

The research providing the basis for the new recommendations included 12 large-scale laboratory tests on round-to-round HSS connections (Tousignant and Packer, 2017a). The A500 Grade B/C specimens had HSS10.75×0.500 or HSS16.00×0.500 chord members and branches at 60° or 90° with 0.25 to 0.47 branch-to-chord width ratios. Quasi-static axial tension forces were applied to the ends of the branches [Figure 10(a)], causing brittle fractures in all fillet welds [as shown for a 90° connection in Figure 10(b)]. Measured strain distributions around the welds, a numerical parametric study (Tousignant and Packer, 2018), and a

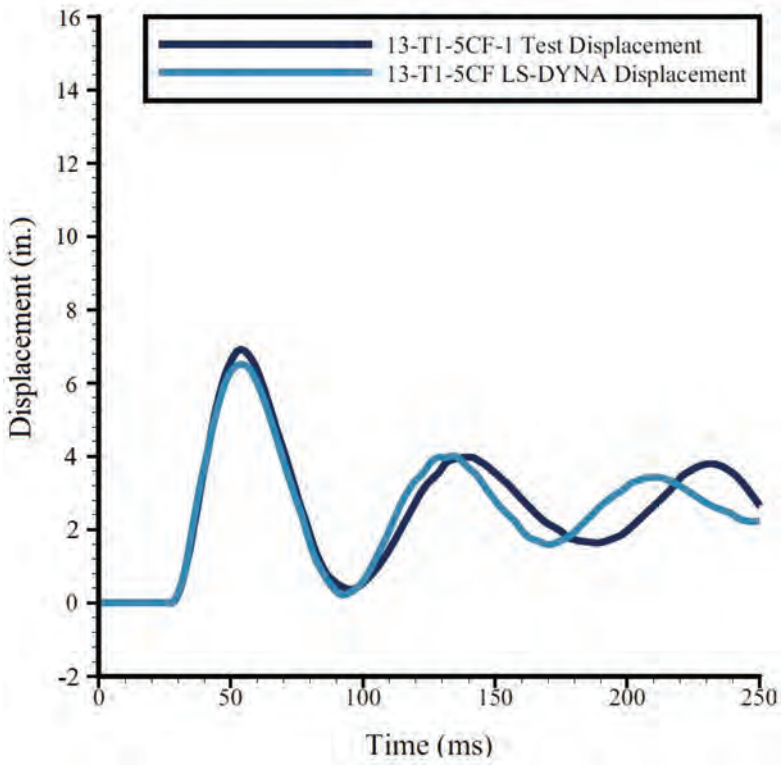

Fig. 8. Mid-span displacement vs. time (measured vs. predicted by LS-DYNA).

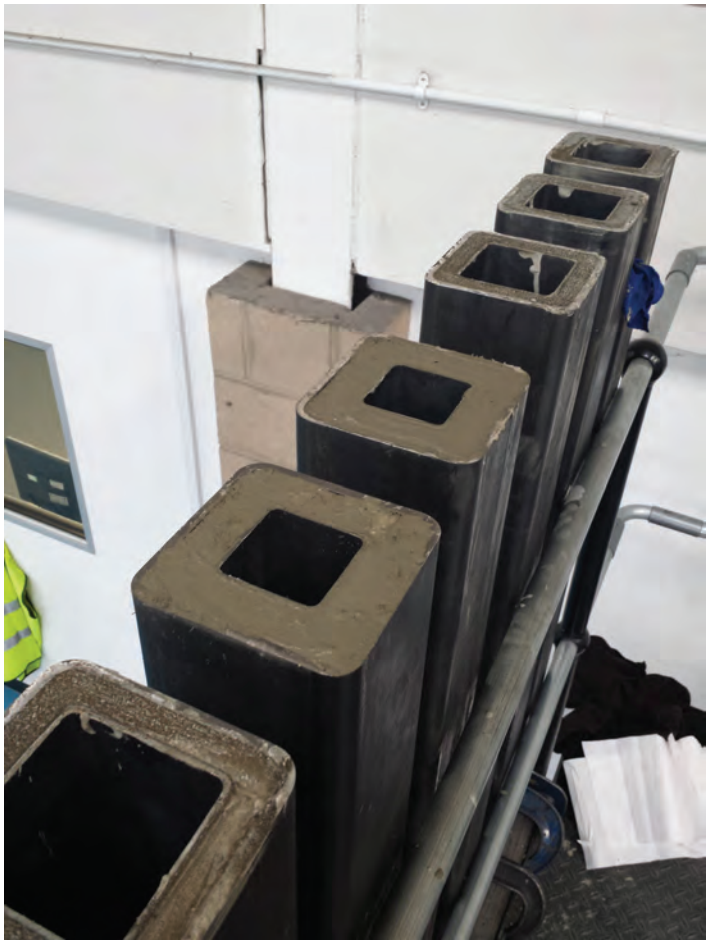

Fig. 9. CFDST test specimens under fabrication.

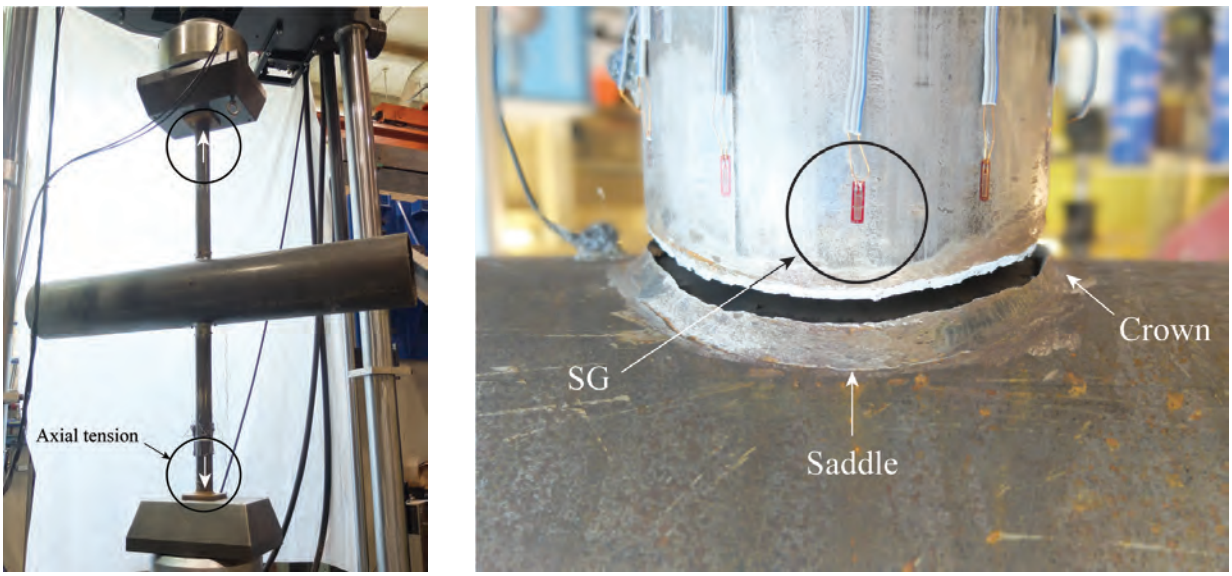

(a) test set-up *(b) weld fracture in a 90° cross section*

Fig. 10. Round-to-round HSS testing.

reliability analysis were considered in the development of the new design recommendations presented to AISC (Tousignant and Packer, 2019).

The recommendation for weld effective length in a round-to-round HSS cross-, T-, or Y-connection is a function of the branch-to-chord member angle, θ; the branch-to-chord diameter ratio, D_b/D; and the chord wall slenderness, D/t. As shown in Figure 11, the effective length, l_e, considers two arcs around the saddle regions of the weld. Additional details and a design example can be found in Tousignant and Packer (2019).

STATIC STRENGTH OF HSS CONNECTIONS

Several issues are currently being explored for statically loaded rectangular HSS-to-HSS connections. The first involves connections where the branch is near an open chord end. As may be expected, the connection strength is reduced for a small "end distance," so there is a minimum distance from an open chord end in order to achieve full connection capacity. A requirement for this minimum end distance, l_{end}, was incorporated in AISC *Specification* Table K3.2A (AISC, 2016a) based on the work of Fan and Packer (2017). This end distance was based only on a flexural yield-line mechanism in the chord connecting face, which presumes a chord plastification limit state, so research is currently in progress to generate an end distance requirement that applies to all potential limit states.

Another recent study has evaluated the case of loading across the full width of a rectangular HSS in compression, engaging both webs. Possible limit states include web local yielding, web local crippling, and web compression buckling. However, the AISC *Specification* (AISC, 2016a) is based on the behavior of I-shaped sections with a single web. Extensive experimental and numerical research has revealed that for matched-width rectangular HSS cross-connections with a chord sidewall slenderness (H/t) up to 50, web local yielding will govern if the bearing length is ≤0.25H (where H is the chord depth), web local crippling will not control, and web compression buckling will govern if the bearing length >0.25H (Kuhn et al., 2019). Wei and Packer (2019) have shown that the web compression buckling failure load is well-predicted by treating each HSS sidewall as a fixed-ended column and designing in accordance with AISC *Specification* Chapter E.

A third topic currently under study deals with rectangular HSS-to-HSS connections in which the branch is laterally offset to be flush with one sidewall of the chord. This is sometimes done in practice for ease of attaching cladding to the side of an HSS truss or frame. All HSS connection design recommendations, however, internationally, only cater to the case of a branch (or branches) aligned with the centerline of the chord. Laboratory experiments (Figure 12) and numerical studies—to expand the connection geometric database and consider different loading situations—are currently under way. Under branch axial compression, the connection capacity is determined by a combination of buckling of one chord sidewall and chord face plastification. The aim of this study is to derive design recommendations for HSS connections with laterally offset branches based on the existing set of limit states (and design equations) pertaining to connections with coincident branch and chord centerlines.

SUMMARY AND FUTURE WORK

Recent advances in design of HSS members and connections have been highlighted. Research on HSS columns under axial and lateral loads has contributed knowledge about seismic behavior and revealed a need for revisions to the highly ductile limits for HSS columns. In foam-filled brace and

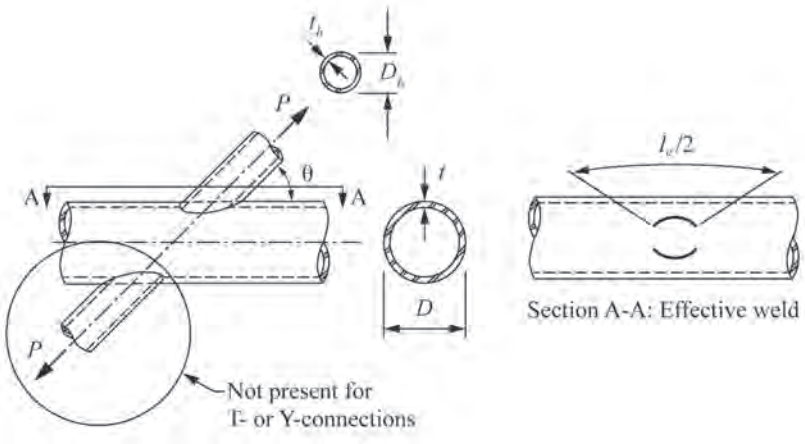

Fig. 11. Weld effective length for round-to-round cross, T-, and Y-connections.

bending member experiments, the lightweight polyurethane foam improved seismic performance by delaying local buckling, reducing strength degradation, and increasing energy dissipation. The database is being expanded with additional tests and detailed finite element studies on a broader inventory of braces for development of revised element slenderness limits. A large-scale parametric study, under way, is exploring potential slenderness limits for foam-filled beams. Design methods for hollow and concrete-filled HSS subject to blast and impact loading are being informed by field tests, laboratory experiments, and numerical modeling. Finally, a substantial amount of research on HSS connections has resulted in improved design procedures for single-sided fillet welds to HSS members, connections in compression, connections near chord ends, and connections that are offset laterally.

ACKNOWLEDGMENTS

Special thanks to Jason McCormick and Jeffrey Packer for all of the materials, coordination, edits, and other feedback and contributions. The work of their numerous research assistants is also appreciated.

The researchers would like to acknowledge their sponsors: the Explora Foundation; the Natural Sciences and Engineering Research Council of Canada (NSERC); the Steel Structures Education Foundation (SSEF)/Canadian Institute of Steel Construction (CISC); the American Institute of Steel Construction (AISC); the Thornton Tomasetti Foundation; the Lyon Sachs Research Fund; Atlas Tube; Walters Inc.; the National Science Foundation (CMMI–1334272, CMMI–1350605); U.S. NSF East Asia and Pacific Summer Institutes (EAPSI) Fellowship and Japan Society for the Promotion of Science (JSPS) Award No. 1713850; the University of Michigan; and the U.S. Department of Commerce, National Institute of Standards and Technology. Any findings, recommendations, or other material within are those of the researchers and do not necessarily reflect the views of the sponsors.

REFERENCES

AISC (2016a), *Specification for Structural Steel Buildings,* ANSI/AISC 360-16, American Institute of Steel Construction, Chicago, Ill.

AISC (2016b), *Seismic Provisions for Structural Steel Buildings*, ANSI/AISC 341-16, American Institute of Steel Construction, Chicago, Ill.

ASCE (2011), *Blast Protection of Buildings*, ASCE/SEI 59-11, American Society of Civil Engineers, Reston, Va.

Ammons, M., Shimada, H. Marzano, G., Kurata, M., and McCormick, J. (2018), "Seismic Performance of Foam Filled Tubular Steel Braces," *Proceedings of the Eleventh U.S. National Conference on Earthquake Engineering, Integrating Science, Engineering & Policy*, Los Angeles, Calif., June 25–29.

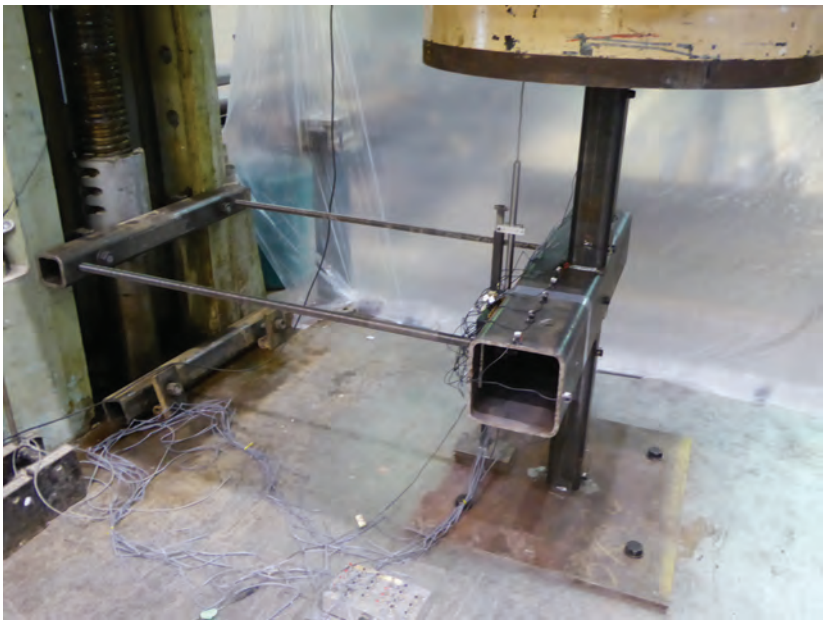

Fig. 12. Test set-up for rectangular HSS cross-connections with laterally offset branches.

Carreras, C.F., Alfaro, L., Wei, D., and McCormick, J. (2018), "Improvement of the Cyclic Bending Behavior of HSS Members through Foam Fill," *Proceedings of the Eleventh U.S. National Conference on Earthquake Engineering Integrating Science, Engineering & Policy*, Los Angeles, Calif., June 25–29.

Fadden, M. and McCormick, J. (2012), "Cyclic Quasi-Static Testing of Hollow Structural Section Beam Members." *Journal of Structural Engineering*, ASCE, Vol. 138, pp. 561–570. 10.1061/(ASCE)ST.1943-541X.0000506.

Fadden, M. and McCormick, J. (2014), "HSS-to-HSS Seismic Moment Connection Performance and Design," *Journal of Constructional Steel Research*, Vol. 101, pp. 373–384.

Fan, Y. and Packer, J.A. (2017), "RHS-to-RHS Axially Loaded X-Connections Near an Open Chord End," *Canadian Journal of Civil Engineering*, Vol. 44, pp. 881–892.

Grisaro, H.Y., Packer, J.A., and Seica, M.V. (2019), "Weak Axis Response of Steel I-Sections subjected to Close-In Detonations," *Journal of Constructional Steel Research*, Vol. 160, pp. 189–206.

Kuhn, J., Packer, J.A., and Fan, Y. (2019), "RHS Webs under Transverse Compression," *Canadian Journal of Civil Engineering*, Vol. 46, in Press.

Packer, J.A., Sherman, D., and Lecce, M. (2010), *Hollow Structural Section Connections*, Design Guide 24, AISC, Chicago, Ill.

Packer, J.A., Sun, M., and Tousignant, K. (2016), "Experimental Evaluation of Design Procedures for Fillet Welds to Hollow Structural Sections," *Journal of Structural Engineering*, ASCE, Vol. 142, No. 5, pp. 1–12.

Ritchie, C.B., Gow, M.I., Packer, J.A., and Heidarpour, A. (2017a), "Influence of Elevated Strain Rate on the Mechanical Properties of Hollow Structural Sections," *International Journal of Protective Structures*, Vol. 8, No. 3, pp. 325–351.

Ritchie, C.B., Packer, J.A., Seica, M.V., and Zhao, X.L. (2017b), "Behavior of Steel Rectangular Hollow Sections subject to Blast Loading," *Journal of Structural Engineering*, ASCE, Vol. 143, No. 12, pp. 115.

Ritchie, C.B., Packer, J.A., Seica, M.V. and Zhao, X.L. (2018a), "Behaviour and Analysis of Concrete-Filled Rectangular Hollow Sections Subject to Blast Loading," *Journal of Constructional Steel Research*, Vol. 147, pp. 340–359.

Ritchie, C.B., Packer, J.A., Seica, M.V. and Zhao, X.L. (2018b), "Flexural Behavior of Concrete-Filled Double-Skin Tubes Subject to Blast Loading," *Journal of Structural Engineering*, ASCE, Vol. 144, No. 7, pp. 1–19.

Seica, M.V., Packer, J.A., and Yankelevsky, D.Z. (2019), "Blast and Impact Loading Effects on Glass and Steel Elements and Materials," *Thin-Walled Structures*, Vol. 134, pp. 384–394.

Sediek, O.A., Wu, T.-Y., McCormick, J. and El-Tawil, S. (2019), "Seismic Behavior of HSS Columns under Lateral Loading," International Conference in Commemoration of 20th Anniversary of the 1999 Chi-Chi Earthquake, Taipei, Taiwan, September 15–19.

Tousignant, K., and Packer, J.A. (2017a), "Fillet Weld Effective Lengths in CHS X-Connections. I: Experimentation," *Journal of Constructional Steel Research*, Vol. 138, pp, 420–431.

Tousignant, K. and Packer, J.A. (2017b), "Numerical Investigation of Fillet Welds in HSS-to-Rigid End-Plate Connections," *Journal of Structural Engineering*, ASCE, Vol. 143, No. 12, pp. 1–16.

Tousignant, K. and Packer, J.A. (2018), "Fillet Weld Effective Lengths in CHS X-Connections. II: Finite Element Modelling, Parametric Study and Design," *Journal of Constructional Steel Research*, Vol. 141, pp. 77–90.

Tousignant, K. and Packer, J.A. (2019), "Weld Effective Lengths for Round HSS Cross-Connections under Branch Axial Loading," *Engineering Journal*, AISC, Vol. 56, No. 3, pp. 173–186.

Wei, D. and McCormick, J. (2018), "Experimental Testing of Tube-Based Seismic Collar Connections under Cyclic Loads," *Tubular Structures XVI*, Heidarpour and Zhao (Eds), Taylor & Francis Group, London.

Wei, F. and Packer, J.A. (2019), "AISC Provisions for HSS Web Stability Under Local Compression," *Engineering Journal*, AISC, submitted.

Wu, T.-Y, El-Tawil, S., and McCormick, J. (2018), "Highly Ductile Limits for Deep Steel Columns." *Journal of Structural Engineering.* 10.1061/(ASCE)ST.1943-541X.0002002, 04018016.

Zhao, X.L., Packer, J.A., Wang, Y.C., and McCormick, J.P. (2019), *Design Guide for Concrete-Filled Hollow Section Columns under Static, Impact, Blast, Seismic and Fire Loading*, Design Guide No. 10, CIDECT, Geneva, Switzerland.

Guide for Authors

Scope

Engineering Journal is dedicated to the improvement and advancement of steel construction. Its pages are open to all who wish to report on new developments or techniques in steel design, research, the design and/or construction of new projects, steel fabrication methods, or new products of significance to the uses of steel in construction. Only original papers should be submitted.

General

Papers intended for publication should be submitted by email Margaret Matthew, editor, at **matthew@aisc.org**.

The articles published in the *Engineering Journal* undergo peer review before publication for (1) originality of contribution; (2) technical value to the steel construction community; (3) proper credit to others working in the same area; (4) prior publication of the material; and (5) justification of the conclusion based on the report.

All papers within the scope outlined above will be reviewed by engineers selected from among AISC, industry, design firms, and universities. The standard review process includes outside review by an average of three reviewers, who are experts in their respective technical area, and volunteers in the program. Papers not accepted will not be returned to the author. Published papers become the property of the American Institute of Steel Construction and are protected by appropriate copyrights. No proofs will be sent to authors. Each author receives three copies of the issue in which his contribution appears.

Manuscripts

Manuscripts must be provided in Microsoft Word format. Include a PDF with your submittal so we may verify fonts, equations and figures. View our complete author guidelines at **aisc.org/ej**.

Smarter. Stronger. Steel.

American Institute of Steel Construction
130 E Randolph St, Ste 2000, Chicago, IL 60601
312.670.2400 | aisc.org/ej